University of Novi Sad
FACULTY OF TECHNICAL SCIENCES
DEPARTMENT OF PRODUCTION ENGINEERING
21000 NOVI SAD, Trg Dositeja Obradovica 6, SERBIA

UDK 621 ISSN 1821-4932

JOURNAL OF

PRODUCTION ENGINEERING

Volume 16 Number 2

Novi Sad, December 2013

Journal of Production Engineering, Vol.16 (2013), Number 2

Publisher: FACULTY OF TECHNICAL SCIENCES
DEPARTMENT OF PRODUCTION ENGINEERING
21000 NOVI SAD, Trg Dositeja Obradovica 6
SERBIA

Manuscript submitted for publication: December 10, 2013.
Printing: 1st
Circulation: 300 copies

CIP classification:

CIP – Катаголизација у публикацији
Библиотека Матице српске, Нови Сад

621

JOURNAL of Production Engineering / editor in chief Pavel Kovač. – Vol. 12, No. 1 (2009)- . – Novi Sad : Faculty of Technical Sciences, Department for Production Engineering, 2009-. – 30 cm

Dva puta godišnje (2012-). Je nastavak: Časopis proizvodno mašinstvo = ISSN
0354-6446
ISSN 1821-4932

Printing by: FTN, Graphic Center ***GRID,*** *Novi Sad*

ISSN: 1821-4932

INTERNATIONAL EDITORIAL BOARD

Editorial

The ***Journal of Production Engineering*** *dates back to 1984, when the first issue of the* ***Proceedings of the Institute of Production Engineering*** *was published in order to present its accomplishments. In 1994, after a decade of successful publication, the Proceedings changed the name into Production Engineering, with a basic idea of becoming a Yugoslav journal which publishes original scientific papers in this area.*

In 2009 year, our Journal finally acquires its present title - ***Journal of Production Engineering****. To meet the Ministry requirements for becoming an international journal, a new international editorial board was formed of renowned domestic and foreign scientists, refereeing is now international, while the papers are published exclusively in English. From the year 2011 Journal is in the data base COBISS and KoBSON presented.*

The Journal is distributed to a large number of recipients home and abroad, and is also open to foreign authors. In this way we wanted to heighten the quality of papers and at the same time alleviate the lack of reputable international and domestic journals in this area.

In this journal are published, reviewed papers from 11th Conference MMA 2012 Advanced Production Technologies in Novi Sad, Serbia and from "4rd International Conference of Sustainable Life In Manufacturing (SLIM 2013)", which was in the Fiesa-Piran in Slovenia and from International Conference "ETIKUM 2013" which was in Novi Sad, Serbia, and certain number of new scientific papers as well.

Editor in Chief

Professor Pavel Kovač, PhD,

Journal of Production Engineering
Vol.16 No.2

Contents

REVIEW PAPER

Kovac, P., Gostimirovic, M., Mankova, I., Soos, Lj., Savkovic, B.
OVERVIEW OF EXPERIMENTAL INVESTIGATION OF CUTTING PROCESS DYNAMIC 1

ORIGINAL SCIENTIFIC PAPER

Čerče, L., Pušavec, F., Dugar, J., Kopač, J.
FURTHER DEVELOPMENT OF THE SPATIAL CUTTING TOOL WEAR MEASUREMENT SYSTEM 5

Tanveer Hosssain Bhuiyan, Imtiaz Ahmed.
OPTIMIZATION OF CUTTING PARAMETERS IN TURNING PROCESS 11

Aweda, E. O., Dagwa, I.M., Dauda, M., Dauda, E.T.
EFFECTS OF CONTINUOUS COOLING ON HARDNESS AND MICROSTRUCTURAL PROPERTIES OF LOW CARBON STEEL WELDED PLATE 20

Savković, B., Kovač, P., Gerić, K., Sekulić, M., Rokosz, K.
APPLICATION OF NEURAL NETWORK FOR DETERMINATION OF CUTTING FORCE CHANGES VERSUS INSTANTANEOUS ANGLE IN FACE MILLING 25

Tratar, J., Kopač, J.
ROBOT MILLING OF WELDED STRUCTURES 29

Murčinková, Z., Vasilko, K.
THE REAL SHAPE OF THE WORKPIECE AFTER TURNING AND MILLING 33

Pucovsky, V., Kramar, D., Sekulić, M.
HIGH-PRESSURE JET ASSISTED TURNING PROCESS MODELLED WITH EVOLUTIONARY ALGORITHM 37

Duspara, M., Kosec, B., Stoić, M., Kramar, D., Stoić, A.
APPLICATION OF VORTEX TUBE FOR TOOL COOLING 41

Zabkar, B., Kopač, J.
AN INVESTIGATION INTO ROLLER BURNISHING PROCESS 45

Matin, I., Potran, M., Hadžistevic, M., Hodolič, J., Vukelić, Đ., Puškar, T., Drstvenšek, I., Vrba, I.
DEVELOPMENT OF THE SIMULATION MODEL FOR CASTING OF METAL SUBSTRUCTURE OF METAL-CERAMIC CROWN 49

Vrba, I., Palenčar, R., Hadžistević, M., Štrbac, B., Hodolič, J.
THE INFLUENCE OF THE SAMPLING STRATEGY AND THE EVALUATION METHOD ON THE CYLINDRICITY ERROR ON A COORDINATE MEASUREMENT MACHINE 53

Blanuša, V., Štrbac, B., Živković, A., Hadžistević, M.
MODELING DIAGNOSIS THERMAL SOURCE ON CNC MACHINE TOOLS USING INFRARED THERMOGRAPHY 57

Kosec, B., Soković, M., Karpe, B., Gojić, M., Nagode, A., Kosec, G.
FAILURE ANALYSIS OF DIES FOR ALUMINIUM ALLOYS DIE-CASTING AS THE KEY TO THE QUALITY 61

Škorić, B., Schrittwieser, R., Cavaleiro, A.
NANOSCALE DIMENSIONAL METROLOGY AND PHYSICAL CHARACTERIZATION 65

Narayan C. Nayak, Antaryami Mishra
DEVELOPMENT AND MECHANICAL CHARACTERIZATION OF PALMYRA FRUIT FIBER REINFORCED EPOXY COMPOSITES 69

Abhimanu Singh, Datta, C. K.
LOSS MINIMIZATION POLICY FOR A PRODUCTION LINE WITH IMMEDIATE FEEDBACK AND MULTI SERVER FACILITY AT ALL PROCESSING UNITS 73

PRELIMINARY NOTE

Senderská, K., Ižol, P., Mareš, A.
DIGITAL MILING LABORATORY 77

Šebo, J., Fedorčáková, M.
ECONOMIC OPTIMIZATION OF RECYCLING ORIENTED DISASSEMBLY OF CONSUMER ELECTRONICS: THE CASE STUDY OF MOBILE PHONE 81

Fedorčáková, M., Šebo, J.
THE RESULTS OF APPLICATION OF WASTEWATER BY NEW DEVELOPING ELECTROLYTIC FLOTATION METHODS 86

INSTRUCTION FOR CONTRIBUTORS 89

Journal of Production Engineering
Vol.16 No.2

Review Paper

Kovac, P., Gostimirovic, M., Mankova, I., Soos, Lj., Savkovic, B.

OVERVIEW OF EXPERIMENTAL INVESTIGATION OF CUTTING PROCESS DYNAMIC

Received: 29 September 2013 / Accepted: 28 October 2013

Abstract: *This paper reviews experimental investigations and modeling of chatter vibrations in metal cutting. The dynamic modeling and chatter stability of turning, milling and drilling process is presented. Various stability models are compared against experimentally validated time domain simulation model results. Influence of chatter stability on surface roughness, chip thickness is presented. The influence of amplitude in amplitude frequency spectra of cutting force versus tool wear parameters is determined.*
Key words: *Dynamic, cutting, experimental*

Pregled eksperimentalnih istraživanja pri dinamičkom procesu rezanja. *Ovaj rad razmatra eksperimentalno istraživanje i modelovanje pod dejstvom vibracija u rezanju metala. Dinamično modelovanje i praćenje stabilnosti procesa pod dejstvom vibracija je prikazano kod struganja, glodanja i bušenja. Razni modeli stabilnosti su upoređeni sa eksperimentalno dobijenim rezultatima uz pomoć simulacije modela. Uticaj vibracije na stabilnost hrapavosti površine, debljine korena strugotine je predstavljen.Oderđen je uticaj amplitude za rezličite frekvencije spektara amplitudeu na silu rezanja odnoso na parametar habanja alata.*
Ključne reči: *dinamičko, rezanje, eksperimentalno*

1. INTRODUCTION

Dynamics of metal cutting process have been a focus area of manufacturing research long time. Professor J. Tlusty contributed significantly to the understanding and engineering of dynamic cutting, stability and avoidance of chatter vibrations in machine tools. This article is compiled to review the current state of the knowledge in dynamic cutting, and in the research challenges in this area.

Tlusty presented the overview of dynamic cutting in the paper [1]. He focused extensively on the modelling and measurement of dynamic cutting coefficients, and their influence on the chatter stability in single point metal cutting processes.

With the advances in computer, sensor and high-speed machine tool technology, there have been new methods in predicting and avoiding chatter vibrations on the production floor.

Paper reviews the dynamics and research challenges in predicting both forced and self excited, chatter vibrations in machining operations.

Finite Element method based metal cutting process simulation models are most common in analysing the plastic deformation trends at the cutting edge, mechanistic models are mainly used in predicting cutting forces exciting machine tool vibrations [2, 3]. Tlusty [4] and Tobias [5] independently formulated the following absolute chatter stability law which has been widely used since 1950s:

$$a_{\lim} = \frac{-1}{2K_r G(\omega)} \qquad (1)$$

The stability equation leads to positive real depth of cut only when the real part $G(\omega)$ of the transfer function between the tool and workpiece is negative. Eq. (1) gives only absolute depth of cut when the minimum value of $G(\omega)$ is considered as shown in Figure 1[5].

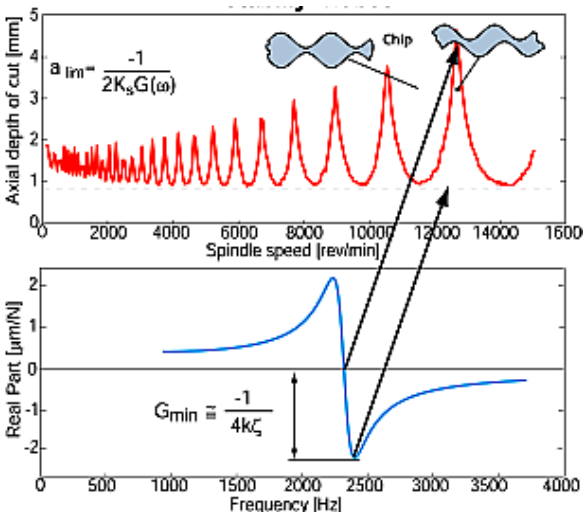

Fig. 1. Stability lobes based on orthogonal chatter theory.

2. STABILITY OF TURNING PROCESS

The general overview of a turning process is given in Figure 2 where the tool generates cutting action by moving in the feed direction towards the workpiece which rotates around its axis. The surfaces generated in stable and unstable cuts are also shown in Figure 2. It can easily be seen that chatter results in very poor surface quality.

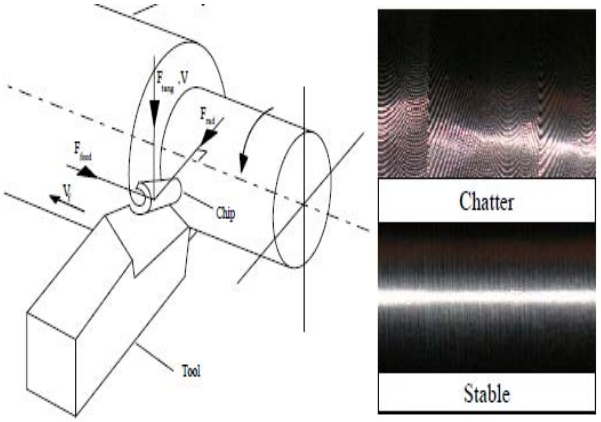

Fig. 2. Geometry of turning process and the surfaces generated in stable and unstable cuts.

The predicted stability lobes and experimental results are given in Figure 3.c where a sample finished surface after a stable and unstable operation can be seen. Also, the measured chatter sound for 1400 rpm is given in Figure 3.b. Reasonable agreement is observed between the experimental and analytical results [6].

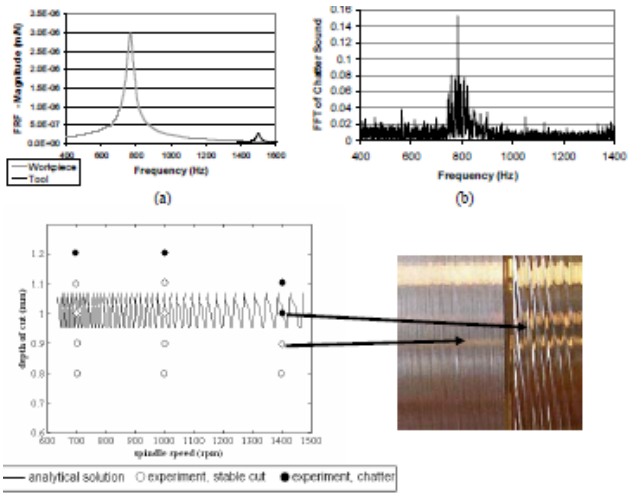

Fig. 3. (a) Transfer functions of the tool and the workpiece, (b) chatter sound measurement results for 1400 rpm tests, and (c)chatter test results for model verification and the surface finish of a stable vs. unstable cut.

3. MODELING OF DYNAMIC MILLING

The dynamic chip thickness considers relative vibrations between the tool and workpiece. Tlusty's research group pioneered the discrete time domain simulation of dynamic milling [7, 8]. They digitized the dynamic chip thickness at discrete angular intervals $d\varphi = \Omega \Delta t$ where $\Omega(rad / s)$ is the angular velocity of the spindle and Δt is the sampling interval which needs to be selected 8-10 times smaller than any natural mode period in order to capture vibrations. The time domain simulation of milling proposed by Tlusty is adopted by a number of researchers for process planning, evaluation of machine tool dynamics and different cutter geometries [9].

Altintas's group developed the true kinematic model of dynamic milling, and included the structural dynamic models of both work piece and cutter at the cutting edge - finish surface contact zones [10, 11], see Figure 4. For example, a point on the cutting edge has coordinates, which are dependent on spindle speed, feed, tool geometry, radial immersion and depth of cut:

Details of the complete mathematical model of dynamic milling can be found in [11]. Once the oscillatory chip thickness is evaluated, the dynamic milling forces ($Fx(t)$, $Fy(t)$) are predicted. The structural vibrations of the work piece and cutter are predicted by applying cutting forces to each structure at discrete time intervals:

$$\left.\begin{aligned} m_x \ddot{x}(t) + c_x \dot{x}(t) + k_x x(t) &= \sum_{j=1}^{N} F_{x_j}(t) \\ m_y \ddot{y}(t) + c_y \dot{y}(t) + k_y y(t) &= \sum_{j=1}^{N} F_{y_j}(t) \end{aligned}\right\} \quad (2)$$

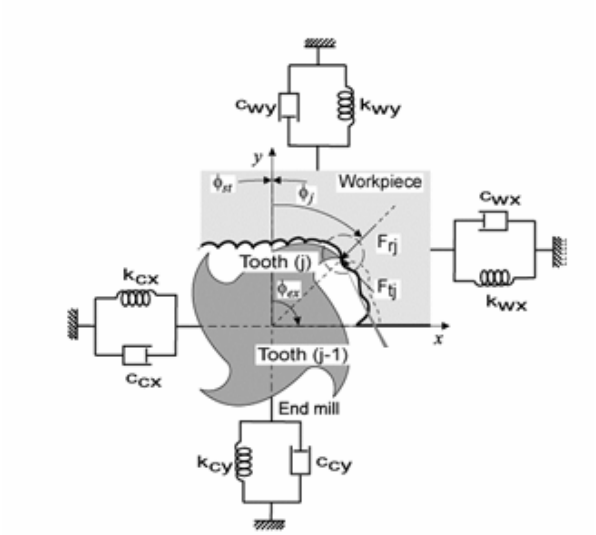

Fig. 4. Surface and chip load evaluation using true kinematics of dynamic milling.

The physical mechanism behind the stability lobe is illustrated in Figure 5. with the following example. If we consider a milling operation which chatters at frequency fc [Hz], while cutting at a spindle speed of n[rev / min].

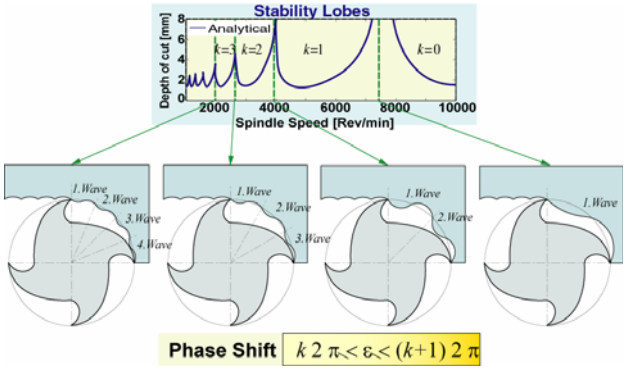

Fig. 5. The stability pockets correspond to having integer number of waves between the tooth periods in milling [12]

When the tooth passing and chatter frequencies match, exactly one vibration wave is left at each tooth period, which corresponds, to the lobe number one (i.e. *k=1).* Hence highest depth of cut is possible at this high speed. The peaks of the successive lobes correspond to integer divisions of chatter frequency, and produce integer numbers of full vibration waves at each tooth period. The lowest axial depth of cut corresponds to having worst regenerative phase shift (-180 degree) that leaves a half vibration wave at the end of each tooth period. Due to largest regeneration at this speed, where the inner and outer waves have opposite phase, the dynamic chip thickness grows and becomes largest during chatter.

4. DRILLING PROCESS

When drilling a full hole, a vibration of slightly less than 3 cycles per revolution is obtained, so this is a backward whirling motion. When cutting, rubbing and process damping forces at the chisel edge are removed from the model, thus simulating the drilling of a piloted hole, the least stable mode is found to be a little less than 7 cycles per revolution, which is also a backward whirl. Bayly's results are illustrated in Figure 6, along with experimental measurement of one revolution for each case.

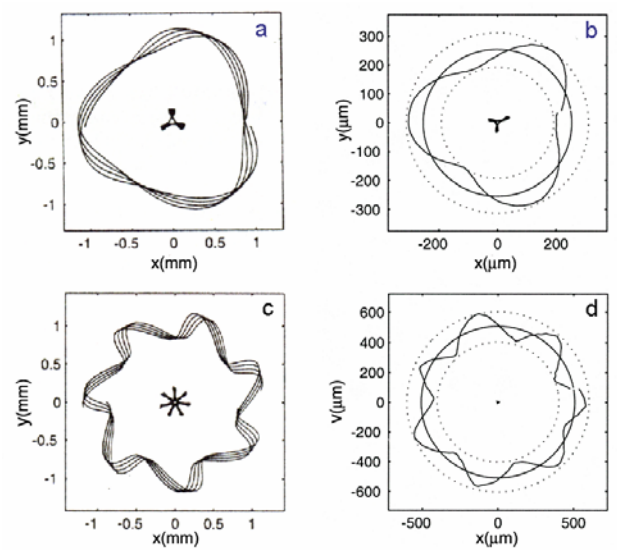

Fig. 6. Simulated and experimental hole profile; (a),(b): full hole (3 sided); (c),(d): piloted hole (7 sided), after Bayly et al. [13]

Figure 7 shows amplitude in amplitude frequency spectra of cutting force versus tool wear [14]. In the figure it is possible to notice width of flank wear land is influenced by dominating amplitudes until certain value of tool wear and id the area of catastrophic tool wear amplitudes are decreasing.

The test setup prepared for measuring acceleration of tool versus dimension of holder and direction of vibration of forces in direction of cutting speed and feed. The setup is prepared for measuring of turning process. It consists of accelerometer, amplifier, AD convertor, notebook PC with user software applications. By use of computer software signal processing was provided.

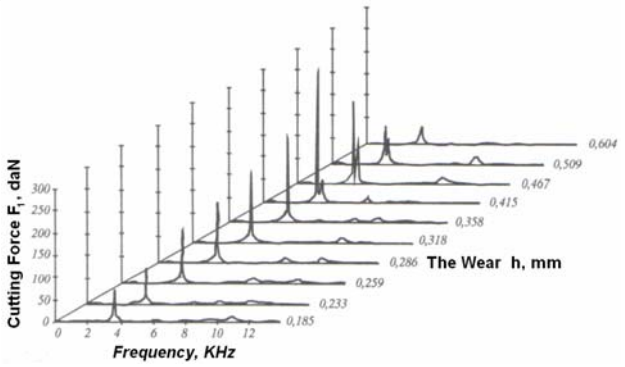

Fig. 7. Amplitude characteristic for the different values of the frequency and width of flank wear land

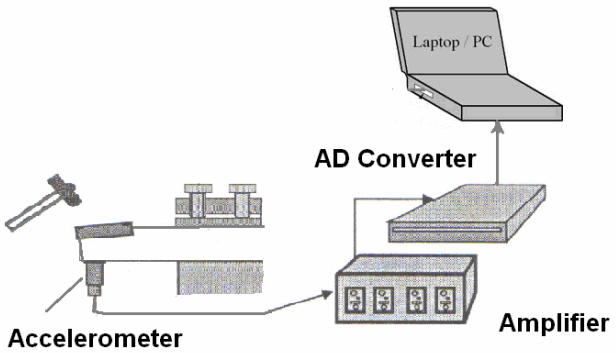

Fig. 8. Measuring set up with position of accelerometer

Figure 9 shows graph of experimental signal with correlation curves [15].

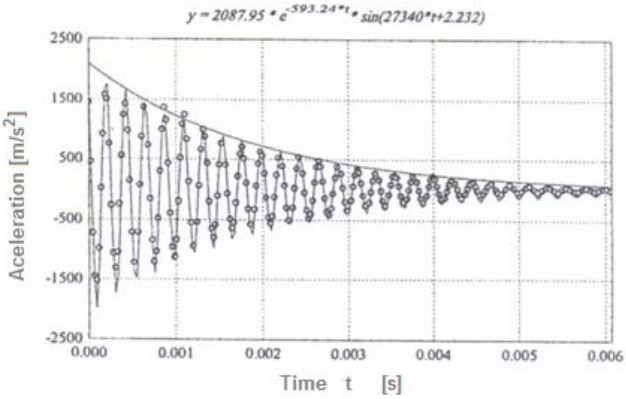

Fig. 9. Graph of experimental signal with correlation curves [15]

5. CONCLUSION

High productivity and quality in machining strongly depend on the process dynamics and stability. Rigidity of machine tools and selection of process parameters are two main factors in dynamic behavior of cutting operations. In this paper, methods that can be used for analysis and modeling of machine tool structures and cutting process stability are reviewed. These methods can be used to analyze as well as improve the dynamic behavior of machining processes.

The significant progress has been made in modeling

machining processes. The frequency domain chatter stability laws in high speed milling have been well developed and used in industry effectively. Significant research efforts have been reported in time domain modeling of turning, boring and milling operations which allow the analysis of dynamic machining when the machine tool and workpiece stiffness, work material, tool geometry and cutting conditions are varied.

6. REFERENCES

[1] Tlusty, J., 1978, Analysis of the State of Research in Cutting Dynamics, Annals of the CIRP, 2:583-589.

[2] Altintas, Y., 2000, Manufacturing Automation: Principles of Metal Cutting and machine Tool Vibrations, Cambridge University Press.

[3] Kovač, P., Mankova, I., Gostimirovic, M., Sekulic, M., Savković, B.: A REVIEW OF MACHINING MONITORING SYSTEMS, Journal of production engineering, Vol. 14, No 1, 2011, pp 1-6.

[4] Tlusty, J., Polacek, M, 1957, Besipiele der behandlung der selbsterregten Schwingung der Werkzeugmaschinen, FoKoMa, Hanser Verlag, Munchen.

[5] Tobias, S.A., Fiswick, W., 1958, Theory of Regenerative Machine Tool Chatter, Engineering, London, 258.

[6] Erhan Budak,: Machining stability and machine tool dynamics, 11th International Research/Expert Conference "Trends in the Development of Machinery and Associated Technology" TMT 2007, Hammamet, Tunisia, 05-09. September, 2007 II 1-29.

[7] Smith, S., Tlusty, J., 1993, Efficient Simulation Programs for Chatter in Milling, Annals of the CIRP, 42/1, 463-466.

[8] Tlusty, J. and Ismail, F., 1981, Basic Nonlinearity in Machining Chatter, Annals of the CIRP, 30:21-25.

[9] Ehman, K.F., Kapoor, S.G., DeVor, R.E. and Lazoglu, I., 1997, 'Machining Process Modeling: A Review', J. of Manufacturing Science and Engineering, Trans. of ASME, 119:655-663.

[10] Campomanes, M. L., Altintas, Y., 2003, An Improved Time Domain Simulation for Dynamic Milling at Small Radial Immersions, Trans. ASME, Manufacturing and Engineering and Science, 125:416-422.

[11] Montgomery, D., Altintas, Y. 1991, Mechanism of Cutting Force and Surface Generation in Dynamic Milling, Trans. ASME Journal of Engineering for Industry, 113:160-168.

[12] Y. Altintas, M. Weck, Chatter Stability of Metal Cutting and Grinding, Annals of the CIRP, 53/2, 2004, 619-642.

[13] Bayly, P.V., Lamar, M.T., Calvert, S.G., 2002, - Low-frequency Regenerative Vibration and the Formation of Lobed Holes in Drilling, Trans. ASME Journal of Manufacturing Science and Engineering, 124:275-285.

[14] Lee,L. C., Lee, K. S., Gan, C. S.,On the Correlation Between Dynamic Cutting Force and Tool Wear, International Journal of Machine Tools and Manufacture, Vol 29, No 3, 1989.

[15] Nedic B., Dinamika procesa rezanja, Monografija, Univerzitet u Kragujevcu, Masinski Fakultet, 2006.

Authors: **Prof. Pavel Kovac PhD, Prof. Dr. Marin Gostimirovic PhD, Prof Ildiko Mankova PhD[1], Prof. Ljubomir Soos PhD[2],, Assist. Borislav Savkovic, M.Sc.,** University of Novi Sad, Faculty of Technical Sciences, Institute for Production Engineering, Trg Dositeja Obradovica 6, 21000 Novi Sad, Serbia, Phone.: +381 21 450-366, Fax: +381 21 454-495.

[1]Technical University of Košice, Department of Technology and Materials, Fac. of Mechanical engineering, Masiarska, 04001 Kosice 74, Slovakia
Phone: +421-55-602 2013

[2]Slovak University of Technology in Bratislava, Faculty of Mechanical Engineering, ÚSETM, Nám. Slobody 17, 81231 Bratislava, Slovakia,
Phone.: +421 2 572 96 537, Fax: +421 2 524 97 809.E-mail:

kovacp@uns.ac.rs
maring@uns.ac.rs
ildiko.mankova@tuke.sk
lubomir.soos@stuba.sk
savkovic@uns.ac.rs

Note:
This paper presents a part of researching at the CEEPUS III project., and Bilateral project between Serbia and Slovakia.

Journal of Production Engineering
Vol.16 No.2

Original Scientific Paper

Čerče, L., Pušavec, F., Dugar, J., Kopač, J.

FURTHER DEVELOPMENT OF THE SPATIAL CUTTING TOOL WEAR MEASUREMENT SYSTEM

Received: 7 September 2013 / Accepted: 09 October 2013

Abstract: *The tool wear evaluation has a very strong impact on the product quality as well as efficiency of the manufacturing process. This paper presents the further development of an innovative and reliable direct measuring procedure for measuring spatial cutting tool wear. The influence of the orientation of measurement head according to the measurand was examined. Based on the analysis of measurements accuracy and the amount of captured reliable data, the optimal setup of the measuring system was defined. Further a special clamping system was designed to mount the measurement device on the machine tool.*
To test the measurement system tool life experiment were performed, where cutting tool wear was measured directly on machine tool. The results showed that novel tool wear diagnostic represent objective estimation, performed on a machine tool that provides higher productivity and quality of the machining process.
Key words: *spatial cutting tool wear, wear diagnostic on machine tool, optical triangulation*

Dalji razvoj volumetrijskog mernog sistema habanja reznog alata. *Određivanje pohabanosti reznog alata ima veliki uticaj na kvalitet proizvoda kao i na efikasnost proizvodnog procesa. Ovaj rad predstavlja dalji razvoj inovativnog i pouzdanog direktnog načina volumetrijskog merenja habanja reznog alata. Ispitivan je uticaj orijentacije merne glave u odnosu na merni predmet. Na osnovu analiza tačnosti merenja i broja izmerenih pouzdanih podataka, optimalno podešavanje sistema je definisano. Takođe je razvijen i specijalan sistem pribora za prihvatanje mernog uređaja na mašinu alatku.*
Radi testiranja mernog sistema sprovedeno je eksperimentalno ispitivanje habanja alata, gde je pohabanost alata merena direktno na mašini alataki. Rezultati su pokazali da moderno merenje habanja alata predstavlja objektivnu procenu a izvođenje na mašini alatki obezbeđuje povećanu proizvodnost i kvalitet proizvodnog procesa.
Ključne reči: *volumsko habanje reznog alata, dijagnostika pohabanosti na mašinama alatkama, optička trijangulacija*

1. INTRODUCTION

Machining performance of material is very important in terms of material processing and quality of final product. Based on the machining performance optimal machining parameters are usually determinate. The term machining performance refers to the ease with which a metal can be machined to an acceptable surface finish, and is hardly measured/evaluated. It is defined by the following criteria: cutting tool wear, cutting tool life, cutting forces, power consumption, chip formation, machined surface integrity and geometrical accuracy of the machined surface.
Criteria, such as cutting force, roughness, energy consumption, integrity and geometrical accuracy of the machined surface can be objectively determined by exact measurements, while cutting tool wear is in practice measured manually and on a subjective level [1]. Most frequently, cutting tool wear is measured with the use of toolmakers microscopes to help determine the range of wear (flank face). In addition to poor precision of this method, the problem is in three-dimensional nature of wear, which cannot be fully analyzed with 2D based measurements/measurement principles. It can be concluded that research on defining and analyzing tool wear in three dimensions is still of great significance.

A survey of the literature indicates that many different approaches have been applied for tool wear prediction [2-6], contrary direct measuring techniques make an assessment of tool wear by either evaluating the worn surface by optical methods (microscope), or measuring the tool material loss by radiometric techniques. Direct methods require to periodically interrupting the cutting process. Optical methods use optical equipment like the toolmaker's microscope, optical microscope, scanning electrical microscope, charged coupled devices (CCD cameras), white light interferometry etc. [7-11].

The main disadvantages of mentioned methods is the inability of measuring crater depth KT (spatial geometry) and/or needs to preform them off line of the machining process.
In one of our previous works [12] spatial tool wear measurement system has been presented which is able to measure crater depth KT on-line on the machine tool. In next chapters, optimisation of this measurement system and test on a case study will be presented.

2. MEASURING SYSTEM

The measuring system consists of a high-accuracy 2D profile laser displacement sensor Keyence LJ-G015 with proper controller Keyence LJ-G5001 [13] and

motorized linear translation stage Standa 8MT173-DCE2, as is seen on figure 1 and 2.
With movement of the profile sensor across the cutting tool and the support of developed software (LabVIEW application), the profile data are grabbed and prepared in a matrix form for further evaluation/analyses.

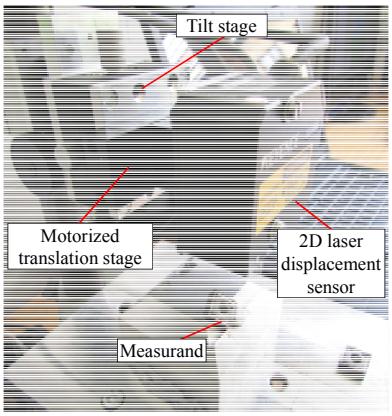

Fig. 1. Measuring system

Laser displacement sensor measure the distance from measurement head to the points projected on the measured object. In this way Z-coordinate of point cloud are measured. X-coordinate is defined by the specification of the laser displacement sensor [13], while Y-coordinate represents linear stage feed direction.

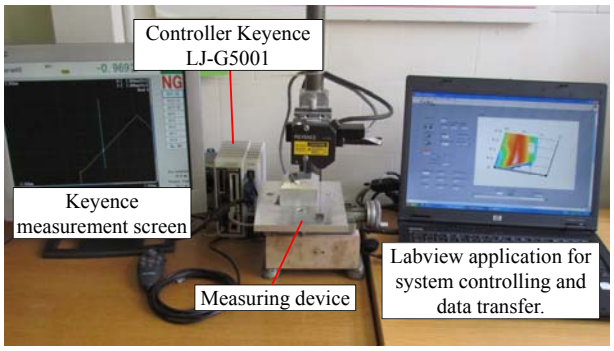

Fig. 2. Measuring interface and controller caption

3. EXPERIMENTAL WORK

In experimental work the influence of the orientation of measurement head according to the measurand was examined. The aim of the optimization is to find the optimal orientation of measurement head that capture as large amount of data from the rake face, cutting edge, and primary and secondary flank face.
For this proposes a special clamping system has been designed. Cutting insert is fixed on a prismatic holder and can be rotated about it axis for angle α. The prismatic holder can be rotated for angle γ. The measuring head was fixed on a tilt stage, which rotates for angle β (**Error! Reference source not found.**).
The extreme positions of the measuring system were experimentally defined on base of needed data quality. Cutting insert was rotated from 12° to 30° while prismatic holder from -25° to 15°. The measuring head was rotated from -5° to 5°.

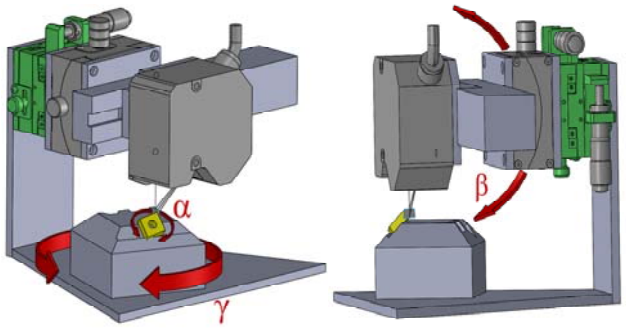

Fig. 3. Special clamping system

The general full factorial design consisted of 75 experimental runs, taken at 5 levels for angles α, γ and 3 levels for angle β. For each captured point cloud the surface was reconstructed, trimmed to the volume of 2.4 x 2.4 x 1mm.
The number of triangles in a single measurement presents an estimator of the quality of the measurements.

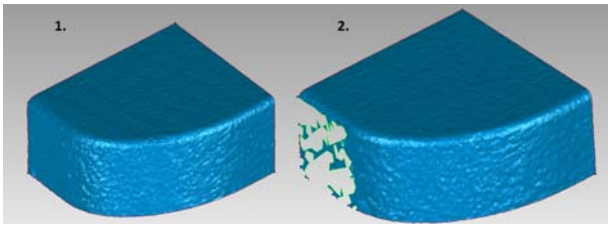

Fig. 4. Comparison of two measurement meshes

Error! Reference source not found. shows a comparison between two measurements. The first measurement was done under the conditions α= 12 °, β= -5° and γ= -15 ° while the second α= 12°, β = -5° and
γ= -5°. From the results we can assume that changing the angle γ for 10° drastically deteriorated measured surface on the secondary cutting edge. There are actually no measured points.

Because of the smaller incident angle there is scattering of laser beam, so the amount of captured data in this area is smaller.

All measurements were individually compared with the reference measurement, measured on a professional measuring device Alicona IF-Edge Master with 5µm lateral resolution. From the obtained deviation results following estimators were calculated (table 1):

- number of triangles
- maximal / minimal deviation,
- mean value of the deviation,
- mean value of the of negative deviations,
- mean value of the positive deviations and
- number of segments for which deviations are in the range of ± 0.008 mm in %.

Table 1 is presenting just 4 of 75 results. Based on input and output parameters the empirical regression models were developed. To analyse the quality of those models ANOVA has been performed and found out that significant correlation can be made only for

prediction of "Number of triangles" and "Part of deviations which are in the range of ± 0.008 mm".
Booth models have been used for optimization of the measurement head position. The optimization was based on overall desirability function [14], were each solution is valuated from 0 to 1, higher it is, better it is. The optimal combinations scored 0.638, with angles α=16°, β= -5° and γ= -21. In **Error! Reference source not found.**, result of geometrical comparison with referential measurement is shown. With the use of this setup 91.11% of measurements results are in the range of ± 0.008 mm, while the number of triangles is 45310.

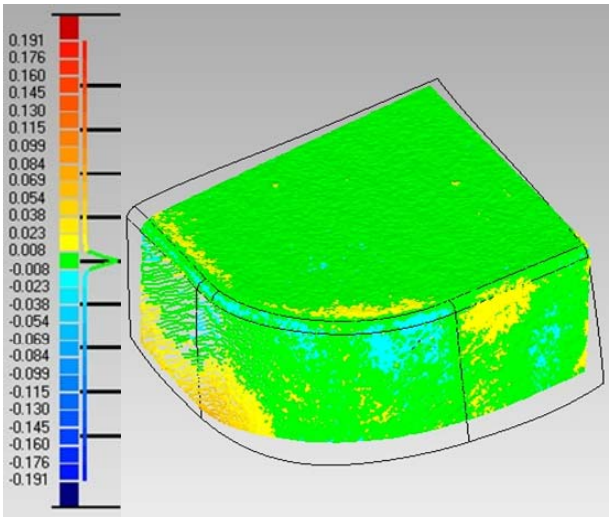

Fig. 5. 3D deviation results of the optimal setup (α=16°, β= -5° and γ= -21°, D=0.638)

4. CASE STUDY

The optimization procedure of the key parameters was tested in machining environment. For this purpose a special clamping system has been designed that simulate the previously obtained optimal setup and can be mounted on the machine tool. The measurement system is mounted on MORI SEIKI SL-153 CNC lathe as can be seen on **Error! Reference source not found.**. This provided a quick measurement of tool wear on the machine tool. It is ensured that the measuring device is placed in such a way, so that it is accessible and ready to implement measurements at any time (without removing cutting insert). At the same time the measuring device does not interfere with other processes, executed by the machine tool during its operation. In this way, we can implement the measurement that includes far more information about tool wear without having to take out the cutting tools, as it is necessary when it comes to the measurement with a toolmaker's microscope.

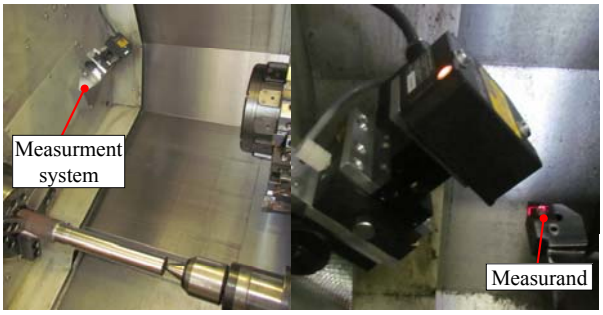

Fig. 6. Measurement system mounted on Mori Seiki machine tool

The presented measurement system has been tested by determining the machining performances of bearing steal material 100Cr6, which has been heat treated to a hardness of 63 HRc in the longitudinal turning. The initial workpiece diameter was 40 mm and length 310 mm. Machining tests were conducted on a Mori Seiki SL-153 turning center. Commercially available Walter CNMA120412-T02020 cutting inserts with grade WAK20 were used with PCLNR 2020K 12 tool-holder. The experiment was performed with no cooling/lubrication fluids.

The cutting parameters have been defined according to the producer recommendations and were a_p=0.7 mm, v_c=50 m/min and f_n=0.15 mm/rev. These parameters were defined based on maximizing the material removal rate with an industry acceptable tool life of 10-15 min.
The workpiece was machined longitudinally at intervals over a length of 20 mm. Resaults of correspodning tool wear is presented in figure 7.

Input				Output						
#	α [°]	β [°]	γ [°]	Number of triangles	Maximum deviation [mm]	Minimal deviation [mm]	Mean value of the deviation [mm]	Mean value of the positive deviations [mm]	Mean value of the of negative deviations [mm]	Part of deviations which are in the range of ± 0.008 mm [%]
1	12	-5	-25	42122	0,046	-0,309	-0,001	0,006	-0,007	74,57
2	12	-5	-15	38842	0,119	-0,194	0,000	0,004	-0,004	83,19
3	12	-5	-5	37385	0,089	-0,025	0,001	0,005	-0,004	82,10
4	12	-5	5	36966	0,249	-0,162	0,002	0,010	-0,006	74,02
…	….									

Table 1. Input and output parameters for statistical evaluation caption

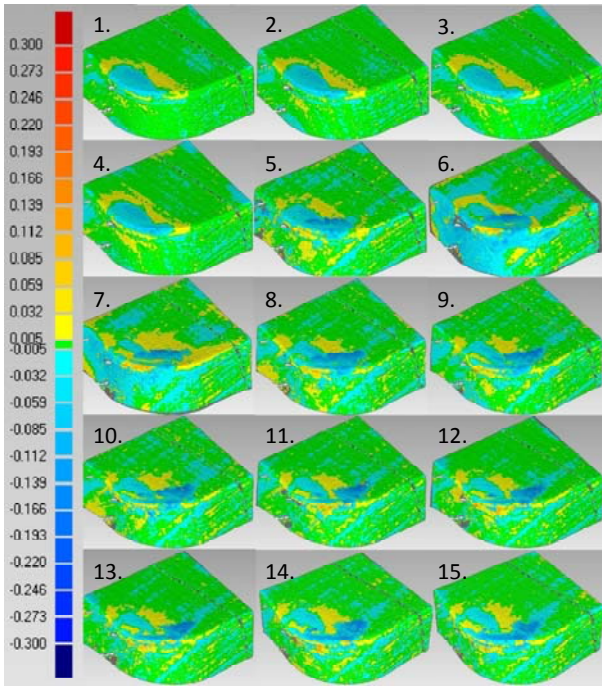

Fig. 7. 3D deviation results

After each operation, the measurement procedure is carried out in the following order:

1. Machine tool moves the cutting insert to the measuring area.
2. Machine tool operator starts the measurement on PC measuring interface.
3. Laser displacement sensor captures the first profile.
4. Motorized linear stage Standa 8MT173-DCE2 move the measurement head for predefined ΔY.
5. By repeating steps 3 and 4 gradually the system captured a large number of 2D profiles and stores theme in internal memory of Keyence LJ-G5001 controller.
6. When the last profile is measured, the system transfer data from the Keyence LJ-G5001 controller to PC and move the translation stage to zero position.
7. Machine tool moves the cutting insert to the working area.

The measurement itself is executed in approximately 20 seconds (at 3 mm length measurement and ΔY = 0.005mm).

A total of 15 repeated measurements were performed. **Error! Reference source not found.** is showing the progression of wear on flank and rake face, BUE and chipping of cutting edge. The increase of crater wear depth is evident with growing darker blue color.

The maximum crater wear depth KT after the last experiment was in a range between 0.021 mm and 0.086 mm (figure 8). From the results it is also clearly visible the progression of chipping on cutting edge.

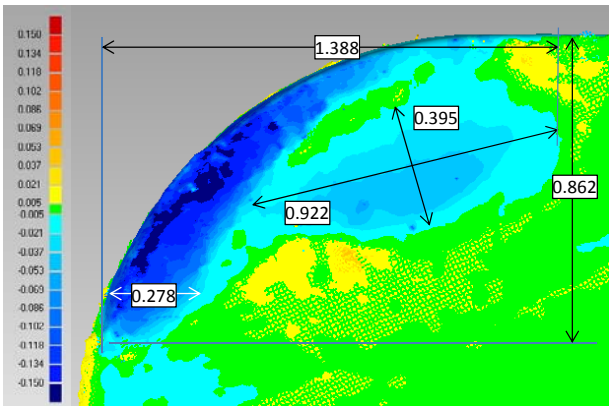

Fig. 8. Measurement of crater wear and chipping with spatial tool wear measurement system

Additionally, presented measurement of crater wear, obtained with spatial measurement system, was compared to the conventional measurement made with toolmakers microscope (figure 9).

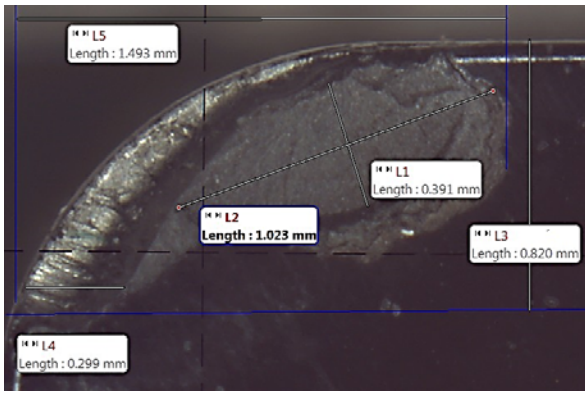

Fig. 9. Measurement of crater wear made with toolmakers microscope

From these measurements carried out with spatial tool wear measurement system (**Error! Reference source not found.**), it is evident that the length of crater wear is 0.922 mm, the crater wear width is 0.395 mm. With the use of toolmakers microscope the length of crater wear is 1.023 mm, the crater wear width is 0.391 mm. The results show a good correlation between the measurements carried out with spatial tool wear measurement system and toolmakers microscope. Some minor variations in measurements may be attributed to the subjective nature of measuring with toolmakers microscope. This error may also occur due to the precision of determining the lower limit of the wear formation, since the microscope image does not reveal the depth of wear.

Whit the use of spatial measurement system, the limit of the wear formation can be accurately determined. Depth of flank wear can be seen from the comparison of cutting inserts cross-sections (**Error! Reference source not found.**). From cross-sections becomes clear that the depth of flank wear (VB) where chipping occurs is in the area from 0 to 0.150 mm, and

the width of wear goes from approximately 0.3 mm to 0.1 mm.

Such critical tools wear negatively effect on roughness and tolerances of produced parts.

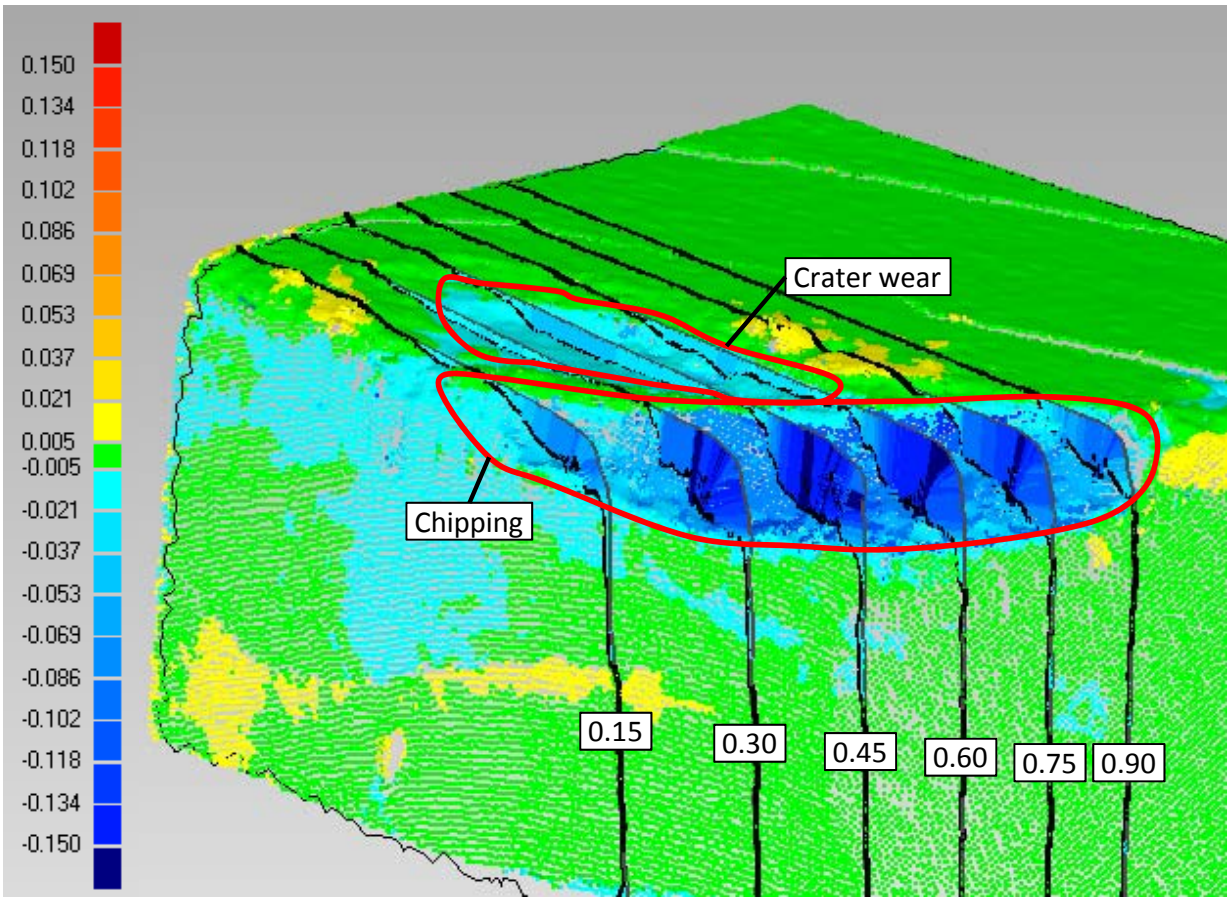

Fig. 10. Chipping, crater wear and cross sections parallel to secondary flank face

5. CONCLUSION

In this work further development of spatial tool wear evaluation system is presented. The influence of incident angles of the scanning process was examined. Based on the analysis of measurements accuracy and the amount of captured data, the optimal setup of the measuring system was defined. Further a special clamping system was designed to mount the measurement device on the machine tool.

To test the measurement system, machining experiment was done, where cutting tool was measured directly on the machine tool. The results had been compared with the result obtained with conventional measurement method, with the use of toolmakers microscope. From the results of the measurements we can say that the proposed spatial tool wear measurement system offers high resolution and accuracy 3D dimensional deviation measurement. It outperforms traditional 2D deviation methods both in accuracy, efficiency and reliability. Another huge benefit of this method is the fact that the measurement can be performed very quickly, without removing the cutting tool from the machine tool. Obtained measurement data are realistic 3D models of the cutting tool, where we can clearly see what the existing conditions of the cutting tool are.

Future work will be focused on developing computational procedures for the analysis of 3D deviation data provided. The objective is automatic diagnostics and early alert pointing to possible tool damage, excessive local tool wear, tool misalignment and other possible causes for tool breakage and stop of the process.

6. REFERENCES

[1] W. Grzesik, Advanced Machining Processes of Metallic Materials, Elsevier B.V., 2008.

[2] J. Kopač: Odrezavanje; Teoretične osnove in tehnološki napotki, 2008.

[3] K.C. Ee, A.K. Balaji, I.S. Jawahir, Progressive tool-wear mechanisms and their effects on chip-curl~chip-form in machining with grooved tools: an extended application of the equivalent toolface (ET) model, Wear, vol. 255, 2003, p. 1404-1413.

[4] G. Byrne, D. Dornfeld, I. Inasaki, G. Ketteler, W. Konig, R. Teti, Tool Condition Monitoring (TCM) - The Status of Research and Industrial Application, CIRP Annals - Manufacturing Technology, vol. 44, Issue 2, 1995, p. 541-567.

[5] E. Govekar, J. Gradišek, I. Grabec, Analysis of acoustic emission signals and monitoring of machining processes, Ultrasonics 38, vol. 1–8,

2000, p. 598–603.
[6] E. Dimla, Sensor signals for tool-wear monitoring in metal cutting operations--a review of methods, International Journal of Machine Tools and Manufacture, vol. 40, Issue 8, 2000, p. 1073-1098.
[7] S. Kurada, C. Bradley, A review of machine vision sensor for tool condition monitoring, Comput. Ind., vol 34, 1997, p. 52-72.
[8] J. Jurkovič, M. Korošec, J. Kopač, New approach in tool wear measuring technique using CCD vision system, International journal of machine tools & manufacture, vol. 45, 2005, p. 1023-1030.
[9] T. G. Dawson, Thomas R. Kurfess, Quantification of tool wear using white light interferometry and three-dimensional computational metrology, International Journal of Machine Tools and Manufacture, vol. 45, Issues 4-5, April 2005, p. 591-596.
[10] W.H. Wang, Y.S. Wong, G.S. Hong, 3D measurement of crater wear by phase shifting method, Wear, vol. 261, Issue 2, 31 Julij 2006, p. 164-171.
[11] A. Weckenmann, K. Nalbantic, Precision Measurement of Cutting Tools with two Matched Optical 3D-Sensors, CIRP Annals - Manufacturing Technology, vol. 52, Issue 1, 2003, p. 443-446.
[12] L. Čerče, F. Pušavec, J. Kopač, Spatial cutting tool wear evaluation, Journal of Production Engineering, Vol. 15, no. 2, p. 10 - 14, 2012.
[13] High-accuracy 2D Laser Displacement Sensor, LJ-G Series, User`s manual 2010.
[14] Raymond H. Myers, Douglas C. Montgomery, Christine M. Anderson-Cook, Response Surface Methodology: Process and Product Optimization Using Designed Experiments, 3rd Edition, 2009.

Authors: **L. Čerče, F. Pušavec, J. Dugar, and J. Kopač**, University of Ljubljana, Slovenia
E-mail: janez.kopac@fs.uni-lj.si

Journal of Production Engineering
Vol.16 No.2

Original Scientific Paper

Tanveer Hosssain Bhuiyan, Imtiaz Ahmed.

OPTIMIZATION OF CUTTING PARAMETERS IN TURNING PROCESS

Received: 7 April 2013 / Accepted: 09 May 2013

Abstract: *Predicting the main cutting force during turning is of great importance as it helps in setting the appropriate cutting parameters before machining starts.Again, optimization of cutting parameters is one of the most important elements in any process planning of metal parts as economy of machining operation plays a key role in gaining competitive advantage. This paper presents an experimental study of main cutting force in turning of AISI 1040 steel and developing a model of the main cutting force during turning using Response surface Methodology (RSM) as well as optimization of machining parameters using Genetic Algorithm (GA). The second order empirical model of the main cutting force in terms of machining parameters are developed based on experimental results. The experimentation is carried out considering three machining parameters: cutting speed, feed rate and depth of cut as independent variables and the main cutting force as the response variable. The formulated model is validated against new set of experimental values using Mean Absolute Percent Error (MAPE) method. The Genetic Algorithm approach is also used to optimize the cutting parameters to keep the main cutting force to a minimum.*
Keywords: *Response surface methodology, genetic algorithm, mean absolute percent error, main cutting force.*

Optimizacija parametara rezanja pri procesu struganja. Predviđanje glavne sile rezanja pri struganju je od velikog značaja jer pomaže u određivanju odgovarajućih parametra rezanja pre početka obrade. Optimizacija parametara rezanja je jedan od najvažnijih elemenata u svakom procesu planiranja obrade, ekonomičnost obrade koja igra ključnu ulogu u sticanju konkurentske prednosti. Ovaj rad predstavlja eksperimentalnu studiju glavne sile rezanja pri struganju čelika AISI 1040 i razvijanju modela glavne sile rezanja podržanog RSM (*metoda odzivne površine*) metodologijom, kao i optimizacija parametara rezanja korišćenjem genetskog algoritma (GA). Empirijski model glavne sile rezanja je razvijen na osnovu eksperimentalnih rezultata. Eksperimenti su vršeni s obzirom na tri parametra rezanja: brzina rezanja, pomak i dubina rezanja kao ulazne promenljive i glavna sile rezanja kao izlazna promenljiva. Dobijeni model je proveren pomoću seta novih eksperimentalnih vrednosti korišćenjem metode srednje apsolutne greške. Takođe, primena Genetskih algoritama se koristi za optimizaciju parametra rezanja da bi glavnu silu rezanja sveli na minimum.
Ključne reči: *Metoda odzivne površine, genetskoi algoritmi, metoda srednje apsolutne greške, glavna sila rezanja.*

1. INTRODUCTION

The most emerging needs of the modern metal cutting operation are to increase the material removal rate with better surface finish and high machining accuracy. These objectives can be achieved by reducing cutting temperature in the cutting zone. In metal cutting process, high cutting temperature and its detrimental effects are generally reduced by proper selection of process parameters. The selection of optimal cutting parameters is a very important issue for every machining process in order to enhance the quality of machined products, to reduce the machining costs and to increase the production rate. The cutting parameter optimization is also necessary in minimizing the cutting force during machining as the high cutting force can result many adverse conditions, like- reduction in tool life, high power consumption, greater surface roughness, poor surface finish etc.

Optimization of process parameters in machining operations has been an area of interest for many researchers since 1950 when Gilbert presented an analytical procedure for determining the optimum cutting speed in a single pass turning operation. The selection of optimal cutting parameters in machining is a difficult task which involves the development of machining models and optimization algorithm able to optimize these models. Several mathematical models have been developed to establish the relationship between the cutting performance and the cutting parameters. Optimization of cutting parameters in turning which will ultimately minimize the cutting force requires a model in terms of those parameters. Optimization of cutting parameters involves the use of optimization algorithms and other numerical optimization techniques to optimize the machining models. An optimization problem consists of optimizing one or multiple objective functions while satisfying several constraints. Those objectives are often conflicting and incomparable like- the increase of rate of feeding brings about the growth of the production rate but also increases the cost of the operation due to excessive tool wear and decreases the surface quality because of greater roughness. However

various optimization techniques for selecting process variables were developed. Vijayakumar et al. [1] used the ant colony algorithm for solving multi-pass turning optimization problems. The machining parameters are determined by minimizing the unit product cost, subject to various practical machining constraints. It has been established from this research that the ACO can obtain a near optimal solution in an extremely large solution space within a reasonable computation time.Saravanan et al. [2] applied simulated annealing (SA) and genetic algorithm (GA) to determine the optimal machining parameters for continuous profile machining with respect to the minimum production cost subject to a set of practical constraints. The constraints considered to this problem are cutting force, power constraints and tool tip temperature. It has shown that SA has performed slightly better than GA.

Sardiñas et al. [3] proposed a multi-objective optimization technique, based on genetic algorithmsto optimize the cutting parameters in turning processes: cutting depth, feed and speed. The proposed model used microgenetic algorithm in order to obtain the non-dominated points and build the Pareto front graph. Two conflictingobjectives, tool life and operation time, are simultaneously optimized in this research. This research also remarks the advantages of multi-objective optimization approach over the single –objective one. Kolahan and Abachizadeh [4] also developed a simulated annealing algorithm to optimize machining parameters in turning operation on cylindrical work pieces. The turning operation usually includes several passes of rough machining and a final pass of finishing. Seven different constraints are considered in a non-linear model where the goal is to achieve minimum total cost. The weighted total cost consists of machining cost, tooling cost and tool replacement cost. Their computational results show that the proposed optimization procedure has considerably improved total operation cost by optimally determining machining parameters. Srikanth and Kamala [5] proposed a real coded genetic algorithm (RCGA) and its advantages over the existing approach of binary coded genetic algorithm. The results obtained, conclude that RCGA is reliable and accurate for solving the cutting parameter optimization. Saha [6] used genetic algorithm (GA) to obtain the optimum cutting parameters by minimizing the unit production cost for a given amount of material removal for the multi-pass face milling process.The cutting parameters optimized were:cutting speed, feed and depth of cut. Car et al. [7] employed Genetic algorithm to obtain optimal cutting parameters in CNC turning that yield minimum machining time and minimum production cost. Ganesan et al.[8] applied Genetic Algorithm (GA) and Particle Swarm Optimization (PSO) to determine the optimal machining parameters with respect to the minimum production time for continuous profile machining. Theresults obtained from GA and PSO are compared and it was found that PSO generates better results than GA. Using this technique machining time can be further minimized. Xie and Guo [9] combines genetic algorithms (GAs) with a pass enumerating method in selecting the cutting parameters that will minimize the unit production cost (UC) in multi-pass turnings. In the passenumerating method, the number of all possible rough cuts is calculated in order to divide the whole complicated problem into several sub-problems. The results show that the optimization approach can find the better results than other algorithms proposed previouslyto significantly reduce the UC.

Sahoo [10] used Response Surface Methodology (RSM) to develop a predictive model of surface roughness in terms of machining parameters in turningbased on experimental results and then used Genetic algorithm (GA) to optimize the machining parameter that results minimum surface roughness. Sharma and Subbiah [11] used artificial neural network (ANN) to optimize cutting parameters for surface roughness prediction in CNC turning. This research also concluded that ANN is a reliable method and it can be readily applied to different metal cutting processes with greater confidence. Korat and Agarwal [12] used Taguchi techniquesto optimize the effects of cutting parameters on surface finish and MRR of EN24/AISI4340 work material in CNC turning. The orthogonal array, signal to noise ratio and analysis of variance were employed to study the performance characteristics in turning operation. This research concluded that it is possible to increase machine utilization and decrease production cost in an automated manufacturing environment. Savadamuthu et al. [13] proposed an optimal fuzzy control schemedesigned by the Taguchi-genetic method in optimizing cutting parameters in turning. The orthogonal array, the signal-to-noise ratio, and the analysis of variance are employed to study the performance characteristics in turning operations of AISI 1030 steel bars using TiN coated tools.An Adaptive NeuroFuzzy Inference System (ANFIS) is proposed inthis paperto control a constant cutting force turning process under various cutting conditions which consists of two parts: predictor and the fuzzy logic controller. The step size of the predictor and the scaling factors of the fuzzy controller are adjustedfor ensuring stability and obtaining optimal control performances.The genetic method is applied to search for the optimal controlparameters of both the predictor and the fuzzy controller. Pansare et al. [14] employed Ant colony optimization algorithm (ACO) to obtain optimum turning parameters for minimum surface

roughness valuein multipass turning operation. The cutting process had roughing and finishing stage andthe relationship between the parameters and the performance measures were determined using multiple linear regression, thismathematical model is used to determine the optimal parameters. The experimental results showed that the proposed technique is both effective and efficient. Davis et al. [15] optimized the cutting parameters (depth of cut, feed rate, spindle speed) in turning EN24 steel (0.4% C) with hardness 40+2 HRC by using Taguchi method. In this research turning operation werecarried out on EN24 steel by carbide P-30 cutting tool in dry condition.

The objective of this paper is to develop a model of main cutting force (P_z) in turning in terms of the cutting parameters: cutting speed (V_c), feed rate (S_0) and depth of cut (t)using the RSM method and then obtain the optimal value of the cutting parameters using a Genetic Algorithm (GA) approach. The optimal value of cutting parameters is so selected that will minimize the main cutting force required in turning and thus reduce the power consumption, tool wear, chatter and vibration and thus improves surface finish.The next section describes the methodology used for model formulation and optimization. The following section contains the formulated model of cutting force using RSM technique and then cutting parameters are optimized using GA in the next section. The last section involves the findings and conclusion of this research.

2. METHODOLOGY

This section is divided into two parts, section 2.1 describes the RSM methodology for developing the cutting force model and section 2.2 describes the GA approach for the optimization of cutting parameters.

2.1. Model formulation

To develop the model of the main cutting force (Pz) in terms of the cutting parameters: speed, feed rate and depth of cut in turning, Response Surface Methodology (RSM) is used in Minitab16 software in this research. Response surface method is found to be a successful technique to perform the trend analysis of cutting force with respect to various combinations of design variables including the cutting speed (Vc), feed rate (So) and depth of cut (t). It is a combination of experimental and regression analysis and statistical inferences. The concept of the response surface involves a dependent variable (Pz) called the response variable and several independent variables. If all of these variables are assumed to be measurable, the response surface can be expressed as:

$$Pz=f(Vc,S0,t)+e \quad (1)$$

Where, 'e' is the error which is normally distributed with zero mean according to the observed response.

Where, b_0 is the free term, the coefficients b_1, b_2... bk are linear terms, b_{11}, b_{22}...bkk are the quadratic terms, and b_{12}, b_{13}... b_{k-1}, kare the interactionterms. Replacing the general variables of the above equation by the conventional denotation and considering the interaction effect of the parameters along with main effects can be represented by:

$$Pz = b_0 + \sum_{i=1}^{k} b_i X_i + \sum_{i,j=1}^{k} b_{ij} X_i X_j + \sum_{i=1}^{k} b_{ii} X_i^2 \quad (2)$$

Where, b_0 is the free term, the coefficients b_1, b_2... b_k are linear terms, b11, b22...bkk are the quadratic terms, and b_{12}, b_{13}... b_{k-1}, kare the interactionterms. Replacing the general variables of the above equation by the conventional denotation and considering the interaction effect of the parameters along with main effects can be represented by:

$$P_z = b_0 + b_1V_c + b_2S_0 + b_3t + b_{12}V_cS_0 + b_{13}V_ct + b_{23}S_0t + b_{11}V_c^2 + b_{22}S_0^2 + b_{33}t^2 \quad (3)$$

Where, b_0 = constant, independent of all parameters which contains environmental factors, tool and workpiece material properties constant.

The data for main cutting force (P_z), cutting speed (V_c), feed rate (S_0) and depth of cut (t) have been collected from turning of a round bar of AISI-1040 steel having a diameter of 40 mm and length 30 cm in a lathe machine using uncoated carbide tool as the cutting tool in a dry machining environment.This operation have been performed in a lathe machine in which 20 feed rates are possible ranging from 0.029-0.412 mm/rev and the rpm ranges from 46-2000. The uncoated carbide insert used here has the following tool geometry:

- Back rake angle: -5^0
- Side rake angle: 0^0
- Principal cutting edge angle: 9^0
- Side cutting edge angle: 10^0
- End clearance angle: 8.5^0
- Side clearance angle: 10^0
- Nose radius: 2.5 mm

Four cutting speeds (V_c) and four feed rates have been used in this research which are given in the following table 1.

Table 1: Cutting speed and feed rate values

Cutting speed (V_c), m/min	Feed rate (S_0), mm/rev
66	0.12
85	0.16
110	0.20
144	0.24

These four values of cutting speed and feed rates are combined to generate sixteen combinations of experiments. Thesesixteen experiments have been performed and the corresponding main cutting forces (P_z) values are found. The experimental values have been used in the RSM method to estimate the values of the coefficients of equation (3). In this research, the depth of cut (t) has been kept fixed at 1.5mm. So, the main cutting force becomes the function of only the cutting speed (V_c) and feed rate (S_0). Thus, depth of cut (t) will not appear in the expression of the main cutting force.Again, after developing the model, validation of the model has been performed using different sets of cutting parameters values.

In the section 3, amodelfor the main cutting force (P_z) has been formulated and deviation of the model from the experimental values has also been computed using the Mean Absolute Percent Error (MAPE) method.

2.2. Computing methodology:Genetic Algorithm

GA is based on the mechanics of natural selection and genetics to search through decision space for optimal solutions. In GA, a string represents a set of decisions that is a potential solution to a problem. Each string is evaluated on its performance with respect to the objective function. The ones with better performance (fitness value) are more likely to survive than the ones with worse performance. Then the genetic information is exchanged between strings by crossover and perturbed by mutation. The result is a new generation with better survival abilities. This process is repeated until the strings in the new generation are identical, or certain termination conditions are met. GA is continued since the stopping criterion is reached.GAs are different from other search procedures in the three ways, firstly GAs consider many points in the search space simultaneously, rather than a single point; secondly GAs work directly with strings of characters representing the parameter set, not the parameters themselves and finally GAs use probabilistic rules to guide their search, not deterministic rules. Because GAs considers many points in the search space simultaneously there is a reduced chance of converging to local optima. In a conventional search, based on a decision rule, a single point is considered and that is unreliable in multimodal space. GAs consists of four main sections such as encoding, selection, reproduction, and termination [16, 17, 18, 19].

GA has been recently employed in the machining parameter optimization problem with success. The main motivations behind using GA in cutting parameter optimization are that it can quickly scan a vast solution set. Bad proposals do not affect the end solution negatively as they are simply discarded. The inductive nature of the GA means that it doesn't have to know any rules of the problem - it works by its own internal rules. This is very useful for complex or loosely defined problems and unconstrained optimization problem. Genetic algorithms search parallel from a population of points so it can effectively explore many different branches of the tree at once and when a certain branch turns out to be non-optimal, abandon that search proceeding with other more likely candidates. They do not tend to be easily trapped by local optima, due again to the parallelism of their approach. The unconstrained nature of the objective function of the model proposed in this paper indicates a vast solution set and makes GA an ideal approach to solve this kind of problem within a short time with favorable solutions compared to other techniques.

Following steps summarized the working procedure of GA to solve the problem described in this paper.

i. Generate initial random population of chromosomes (V_C, S_O).
ii. Evaluate the fitness f(x) of each chromosome x in the population.
iii. Create a new population by repeating following steps until it is complete.
iv. Select two parent chromosomes from a population according to their fitness.
v. Crossover the parents to form a new offspring with a probability.
vi. Mutate new offspring at each of its position in chromosome with a probability.
vii. Place new offspring in a new population.
viii. Use newly generated population for next run of algorithm.
ix. If the stopping criterion is satisfied or the generations are identical; stop the generation and return the best solution in current population.
x. Go to step ii.

The GA approach is depicted in Figure 1.

3. FORMULATED MODEL OF CUTTING FORCE AND ITS VALIDATION

The experimental values of the cutting speed, feed rate and main cutting force have been analyzed using the RSM technique to estimate the coefficients of the general expression of main cutting force (P_z), shown in equation (3).After the analysis of the experimental values, the estimated regression coefficients of the second order empirical models are found which are given in the following table 2.

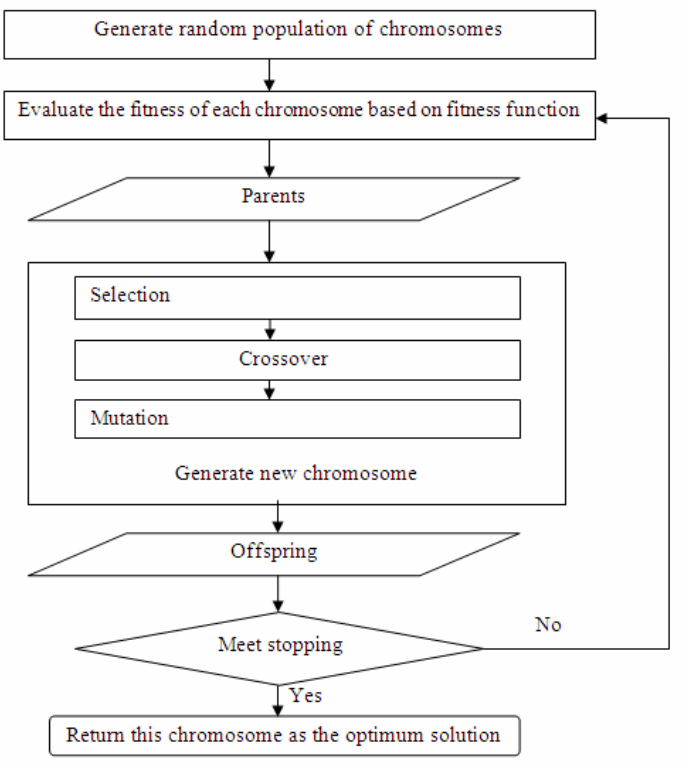

Figure 1: Genetic algorithm approach for optimization of cutting parameters

Table 2: Regression results for the second-order model

Term	Coefficient	SE Coefficient	T	P
Constant	610.43	93.09	6.557	0.000
V_c	-8.31	1.13	-7.367	0.000
S_0	4516.69	774.92	5.829	0.000
V_c*V_c	0.03	0.00	6.147	0.000
S_0*S_0	-1562.50	2026.18	-0.771	0.045
V_c*S_0	-6.07	2.48	-2.444	0.035

R-Sq = 99.66% R-Sq (pred) = 98.70% R-Sq(adj) = 99.49%

Putting these coefficients in the general expression of the main cutting force (P_z) the expression of P_z become:

$$P_z = 610.43 - 8.31V_c + 4516.69\,S_0 + 0.03\,V_c^2 - 1562.50\,S_0^2 - 6.07\,V_cS_0 \quad (4)$$

Figure 2 shows the estimated three dimensional surface which represents the changes of main cutting force (P_z) with respect to the cutting parameters: cutting speed (V_c) and feed rate (S_0).

It is seen from the above figurethat cutting force increases when cutting speed is decreased and feed rate is increased. If the cutting speed decreases keeping the feed rate constant, cutting force increases and vice-versa. Again, increase in feed rate keeping the cutting speed constant results an increase in the cutting force and vice-versa.

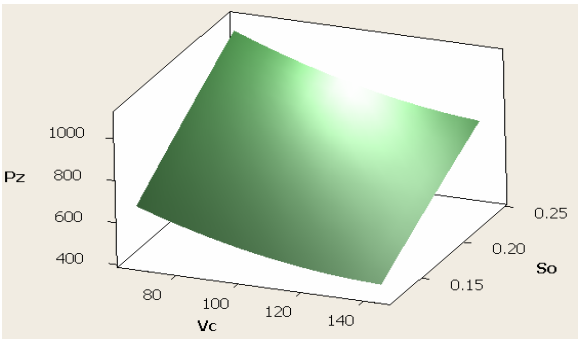

Figure 2:Surface plot for P_z with respect to cutting parameters

Now, the model has been validated against some testing data. In finding the deviation of the empirical values of the cutting force from the actual values, Mean Absolute Percent Error (MAPE) has been calculated. It is seen that, the MAPE during training is only 1.25 % and during testing it is found to be 22.83%. This difference occurs because during training, error calculations were performed using the actual values that were used in modeling but during testing error calculation was performed using new actual cutting forces values. The following table 3 presents the MAPE value during training and table 4 represents the MAPE value during testing.

Table 3: MAPE during training

Cutting speed, (V_c)	Feed rate, (S_0)	Main cutting force, P_z (Actual value)	Main cutting force, P_z (Empirical value)	Absolute % of Error
66	0.12	650	664.078	2.165907692
66	0.16	826	811.221	1.789200969
66	0.20	960	953.364	0.69125
66	0.24	1074	1090.51	1.536945996
85	0.12	578	578.419	0.072456747
85	0.16	718	720.948	0.410640669
85	0.20	874	858.478	1.77597254
85	0.24	998	991.008	0.700641283
110	0.12	504	498.709	1.04984127
110	0.16	628	635.168	1.141464968
110	0.20	756	766.628	1.405820106
110	0.24	888	893.088	0.572927928
144	0.12	460	450.483	2.068869565
144	0.16	564	578.688	2.604184397
144	0.20	696	701.892	0.846551724
144	0.24	830	820.096	1.193204819
			MAPE	1.251617542

Table 4: MAPE during testing

Cutting speed, ($V_{c)}$	Feed rate, (S_0)	Main cutting force, P_z (Actual value)	Main cutting force, P_z (Empirical value)	Absolute % of Error
66	0.14	608	738.275	21.42677632
66	0.22	825	1022.56	23.94671515
80	0.18	645	812.601	25.98468217
80	0.22	795	948.845	19.35154717
100	0.14	468	596.162	27.38495726
100	0.18	605	732.549	21.0825124
125	0.14	435	535.917	23.19921839
125	0.22	658	791.552	20.29662614
			MAPE	22.83412937

4. CUTTING PARAMETER OPTIMIZATION USING GA

To optimize the cutting force model depicted in equation 4, GA toolbox of MATLAB was utilized. Table 5 exhibits the major GA parameters selected in the toolbox for optimization.

During selection of parametres four parametres are considered (crossover fraction & function, mutation function & fraction) as most sensitive and different combinations of this four parametres are tried to determine the optimum values with a view to minimizing the objective function for different values of V_C and S_0 [20]. For other ones we took the suggested default values of the software (MATLAB). For other applications in another environment one has to determine the optimum values at first. As it is only one time adjustment for a particular environment and set values of different parametres, it will not cause any trouble to practitioners.

Optimal results were obtained after 54 iterations. A lower bound [5.78, 0.029] andan upper bound[251.33, 0.412] was used for two variables respectively cutting speed and feed rate. Optimized values of the cutting force function and other variables are summarized in Table 6. Figure 3 depicts the graphic presentation of the simulation process with GA and figure 4 presents the final result window.

Table 5: GA parameters selected for economic design

GA parameters	Selected option
Population type	Double Vector
Population size	20
Fitness scaling function	Rank
Fitness selection function	Stochastic uniform
Crossover function	Single point
Crossover probability	0.8
Mutation function	Constraint dependent
Migration fraction	0.2
Generation limit	100
Stall generation	50
Function tolerance	1e-6

Table 6: Optimized values of cutting force, cutting speed and feed rate

Optimized cutting force ($P_{Z,}$ N)	Cutting speed($V_{C,}$ m/min)	Feed rate (S_O, mm/rev)
140.246	142.284	0.029

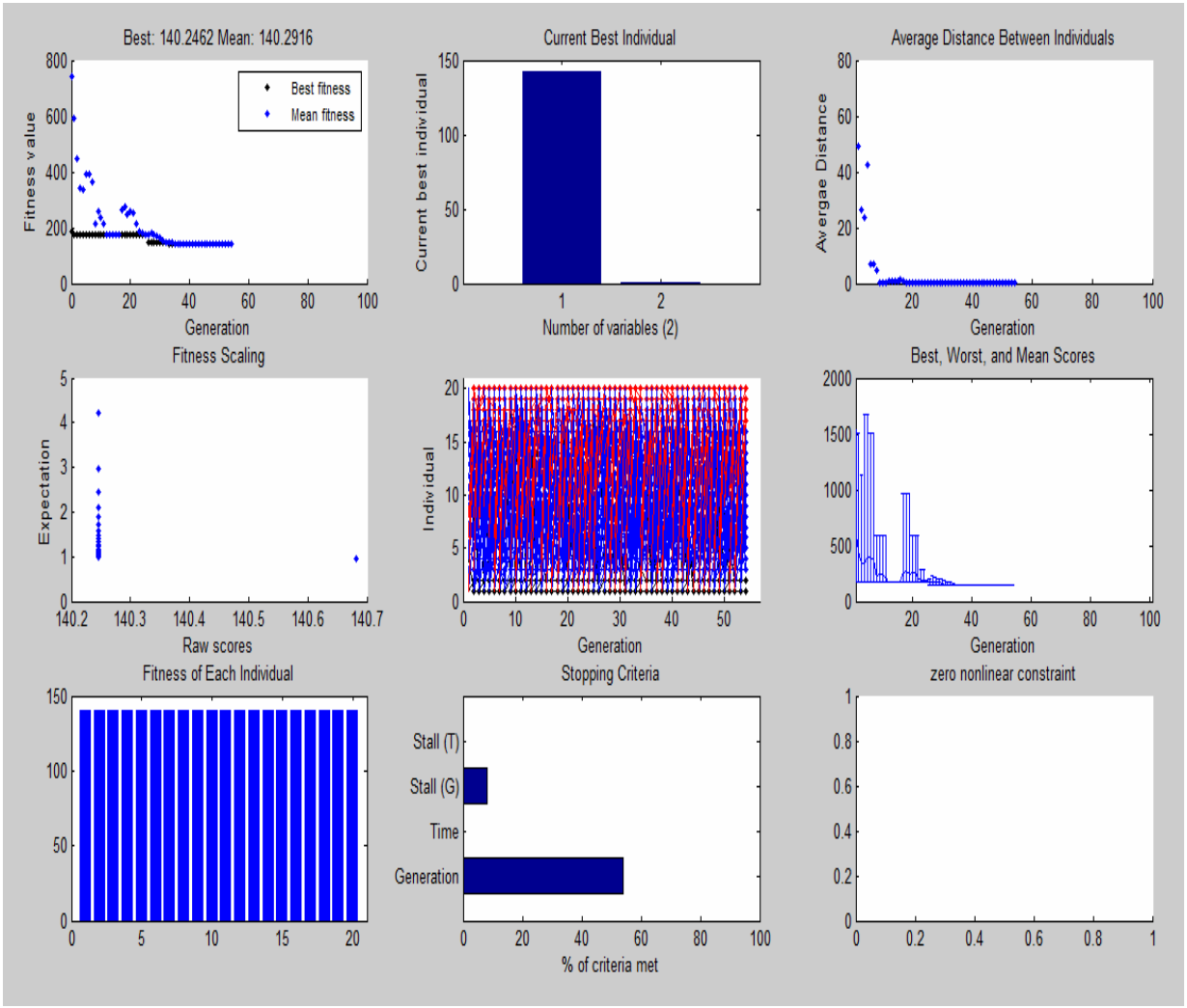

Figure 3: Graphic presentation of the simulation process with GA

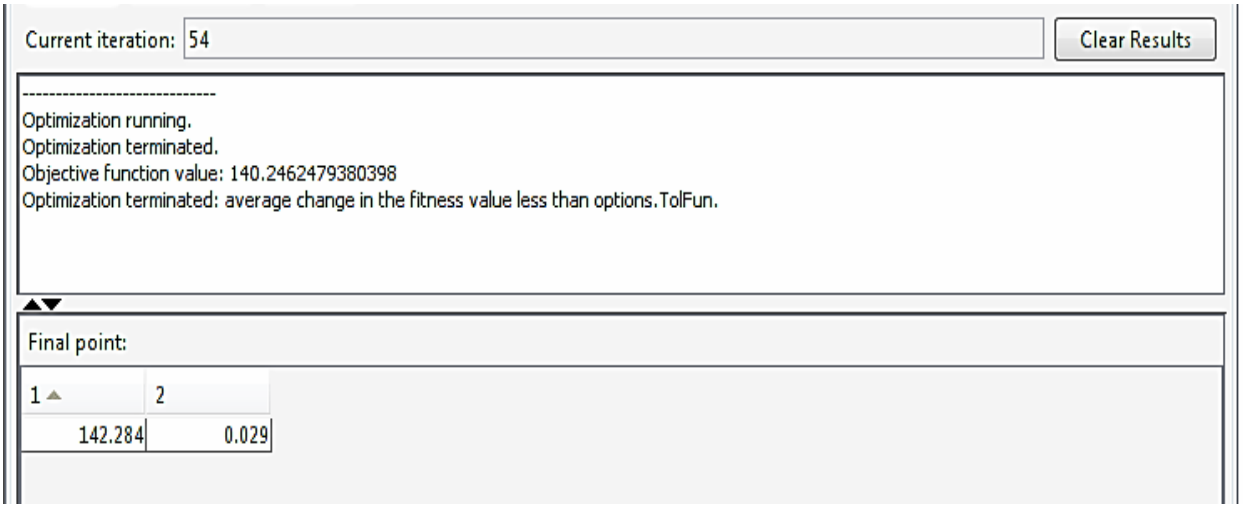

Figure 4: Final result window

5. CONCLUSION

Formulating a suitable cutting force model with respect to several criteria and constraints has been one of the most valued research topics for the researchers in the machining field for quite a long time. Again with recent advances in the field of expert systems it has become easier to optimize this model with the appropriate expert system. In this research, a model of the main cutting force (P_z) has been formulated during turning of AISI-1040 steel in dry machining condition, where the cutting force is considered as a function of the cutting speed (V_c) and feed rate (S_0). Using this model, the value of the cutting force can be predicted for a given set of cutting speed and feed rates. This will help in setting the machining parameters for a particular machining condition.It has been observed that, this model performs satisfactorily when tested against a new set of experimental data.Optimization of the cutting parameters has also been performed using GA to find the set of cutting parameters for which the cutting force value is minimum.However, in this research, depth of cut (t) is kept constant. But it may have significant effect on the main cutting force.This research can be extended by adding some significant machining variables and changing the machining conditions.Some promising opportunities for future research involve-

- Depth of cut can be incorporated as a machining variable rather than keeping fixed which will give better prediction of the cutting force.
- This research can be performed in a wet machining environment using a cooling medium where, the flow rate of coolant can be considered as another variable.
- Another model for predicting surface roughness can be developed and the parameters can be optimized for which the roughness will be minimum.

REFERENCES

[1] Vijayakumar, K., Prabhaharan, G., Asokan, P. and Saravanan, R., (2003), "Optimization of multi-pass turning operations using ant colony system", *International journal of machine tools and manufacture*, Vol. 43, No. 15, pp. 1633-1639.

[2] Saravanan, R., Asokan, P. and Vijayakumar, K., (2003), "Machining parameter optimization for turning cylindrical stock into a continuous finished profile using genetic algorithm and simulated annealing", *International journal of advanced manufacturing technology*, Vol. 21, No. 1, pp. 1-9.

[3] Sardiñas, R. Q., Santana, M. R. and Brindis, E. A., (2006), "Genetic algorithm-based multi-objective optimization of cutting parameters in turning processes", *Engineering Applications of Artificial Intelligence*, Vol. 19, No. 2, pp. 127-133

[4] Kolahan, F. and Abachizadeh, M., (2008), "Optimizing turning parameters for cylindrical parts using simulated annealing method", *proceedings of world academy of science, engineering and technology* , Vol. 36, ISSN 2070-3740.

[5] Srikanth, T. and Kamala, V., (2008), "A real coded genetc algorithm for optimization of cutting parameters in turning", *International journal of computer science and network security*, Vol. 8, No. 6, pp. 189-193.

[6] Saha, S.K., (2009), "Genetic Algorithm based optimization and post optimality analysis of multi-pass face milling", *hal-00355828*, version 1-25.

[7] Car, Z., Barisic, B. and Ikonic, M., (2009), "Ga Based CNC Turning Center Exploitation Process Parameters Optimization", *METABK*, Vol. 48, No. 1, pp. 47-50.

[8] Ganesan, H., Mohankumar, G., Ganesan, K. and Rameshkumar, K., (2011), "Optimization of Machining Parameters in Turning Process Using Genetic Algorithm and Particle Swarm Optimization with Experimental Verification", *International Journal of Engineering Science and Technology*, Vol. 3, No. 2, pp. 1091-1102.

[9] Xie, S. and Guo, Y., (2011), "Intelligent Selection of Machining Parameters in Multi-pass Turnings Using a GA-based Approach", *Journal of Computational Information Systems*, Vol. 7, No. 5, pp. 1714-1721.

[10] Sahoo, P., (2011), "Optimization of turning parameters for surface roughness using RSM and GA", *Advances in Production Engineering and Management*, Vol. 6, No. 3, pp. 197-208.

[11] Madhu, ch., Sharma, A., Gopichand, A., Pavan. and subbiah, V., (2012), "Optimization of cutting parameters for surface roughness prediction using artificial neural network in CNC turning", *Engineering Science and Technology: An International Journal*, Vol. 2, No. 2, pp. 207-214.

[12] Korat, M. and Agarwal, N., (2012), "Optimization of Different Machining Parameters of En24 Alloy Steel in CNC Turning by Use of Taguchi Method", *International Journal of Engineering Research and Applications*, Vol.2, No. 5, pp. 160-164.

[13] Savadamuthu, L., Muthu, S. and Vivekanandan, P., (2012), "Optimization of Cutting Parameters for Turning Process using Genetic Algorithm", *European Journal of Scientific Research*, Vol. 69, No. 1, pp. 64-71.

[14] Pansare, V. B. and Kavade, M. V., (2012), "Optimization Of Cutting Parameters In Multipass Turning Operation Using Ant Colony Algorithm", *International Journal Of Engineering Science and Advanced Technology*, Vol. 2, No. 4, pp. 955 – 960.

[15] Davis, R., Madhukar, J. S., Rana, V. S. and Singh, P., (2012), "Optimization of Cutting Parameters in Dry Turning Operation of EN24 Steel", *International Journal of Emerging Technology and and Advanced Engineering*, Vol. 2, No. 10, pp. 559-563.

[16] Gen, M., and Cheng, R. (2000), "Genetic algorithms and engineering optimization", New York: *John Wiley and Sons*.

[17] Goldberg, D.E., (1989), "Genetic algorithms in search, optimization and machine learning", Reading, MA: Addison-Wesley.

[18] Mitchell, M., (1996), "An introduction to genetic algorithms, Cambridge", MA: *MIT Press.*

[19] Holland, J.H., (1975), "Adaptation in natural and artificial systems: An introductory analysis with applications to biology, control and artificial intelligence", Ann Arbor, MI: *Univ. Michigan Press.*

[20] Kaya, I., and Engin, O. (2007), "A new approach to define sample size at attributes control chart in multistage processes: An application in engine piston manufacturing process", *Journal of Materials Processing Technology*, Vol. 183, No. 1, pp. 38–48.

Authors: **Tanveer Hosssain Bhuiyan and Imtiaz Ahmed,** Department of Industrial and Production Engineering Bangladesh University of Engineering and Technology (BUET) Dhaka -1000, Bangladesh.
Corresponding email: imtiazavi@ipe.buet.ac.bd

Journal of Production Engineering
Vol.16 No.2

Original Scientific Paper

Aweda, E. O., Dagwa, I.M., Dauda, M., Dauda, E.T.

EFFECTS OF CONTINUOUS COOLING ON HARDNESS AND MICROSTRUCTURAL PROPERTIES OF LOW CARBON STEEL WELDED PLATE

Received: 1 August 2013 / Accepted: 23 September 2013

Abstract: *In this study, the effects of continuous cooling on the hardness and microstructural properties of low carbon steel (LCS) plates using different coolants were investigated. The hardness was measured as well as the microstructural examination at distances; 10mm to 45mm in-steps of 5mm from the fusion zone. When hardness value of the control (unwelded) sample was compared with the welded samples that were cooled in air, water, and salty water, it was discovered that the hardness values increased by 3.18%, 4.40% and 10.5% respectively. The improvement in hardness values in air cooled samples was attributed to the transformation of austenite into pearlite in a ferrite matrix. While, for the water and salty water cooled samples, more martensite regions were observed at the grain boundaries of ferrite matrix with salty water having much more martensites.*

Key words: *Continuous cooling, hardness, micro structural studies, low carbon steel.*

Efekti kontiunalnog hlađenja na tvrdoću i mikrostrukturne osobine niskougljenične čelične zavarene ploče. U ovom radu ispitivani su efekti kontinuiranog hlađenja na čvrstoću i mikrostrukturna svojstava niskougljenične čelične ploče gde su korišćena različita sredstava za hlađenje. Merena je tvrdoća kao i ispitivanje mikrostrukture na rastojanjima: 10mm do 45mm u - koracima od 5mm od zone zavarivanja. Kontrolom vrednosti tvrdoće uzorka koji je poređen sa zavarenim uzorcima koji se hlade u vazduhu, vodi i slanoj vodi, otkriveno je da su vrednosti tvrdoće porasle za 3,18% , 4,40% i 10,5% respektivno. Poboljšanje vrednosti tvrdoće vazdušnim hlađenjem uzoraka je pripisano transformaciji austenita u perlit. Dok je za hlađenje vodom i slanom vodom uzoraka, ima više martenzitnih regiona na granicama zrna ferita odnosno korišćenjem slane vode dobija se martenzitna struktura.

Ključne reči: *Kontinualno hlađenje, tvrdoća, mikrostrukturna svojstva, niskougljenični čelik.*

1. INTRODUCTION

Low carbon (LC) steel materials are susceptible to hardness property change when they are welded depending on factors such as: cooling medium, rate of cooling, electrode type and composition, welding parameters, etc. The LC steel contain up to about 0.25 percent carbon and are used for general engineering construction work involving severe cold working especially in sheet form such as car bodies, furniture, tubing and magnetic materials[1]. The commonest method used in joining of LCS parts is the Shielded metal arc welding, (SMAW). Furthermore; it is used in the oil and gas sector. In the offshore environments it is used in the construction, building, repair and maintenance of ships, the surrounding water which is salty serves as a cooling medium. Studies [2] have shown that depending on the environment, welding can alter the carefully designed microstructure of steels as a result of heat affected zone thermal cycles that exceed the transformation temperature [3]. Depending upon the heating and cooling cycles involved, different types of microstructures are obtained in weld bead and the heat affected zone (HAZ).

This leads to varying mechanical properties such as hardness of different zones of a weldment [4]. Fukuoka et al [5] welded steel plates of sizes 2mm, 8mm, 14mm, 16mm and 19mm using gas shielded arc welding for both air and underwater welding. Cooling rate was observed to increase with increase in plate thickness with air weld recording a more consistent increase. From the results, it was observed that the hardness for underwater welding is almost twice that of the welding in air around weld metal and heat affected zone (HAZ), and remarkable differences were not observed between both welding processes in the base metal away from the weld zone. Currently [6], there is a strong interest in studying the effect of cooling rate on the mechanical properties and microstructure of industrial processed steels. Calik [6] has studied the effect of cooling rate on hardness and microstructure of AISI 1020, AISI 1040, and AISI 1060 steels and shown that the microstructure of these steels can be changed and significantly improved by varying the cooling rates. Adedayo and Oyatokun [7] studied the effect of saline water cooling on service quality of a welded AISI 1013 Carbon steel plate by varying the coolant flow rates.

Therefore, in this study the effect of simultaneous cooling (using different cooling media such as air, water and salty water (3.5percent salty in water)) and welding at varying distances from the weld fusion line on the hardness property and the microstructures of low carbon steel plates was investigated.

2. EXPERIMENTAL PROCEDURE

The elemental composition (see Table 1) of the low carbon steel was determined using X-Ray Fluorescence (XRF) at the Universal Steels, Ikeja, Lagos. The

cooling media used were: air, water and salty water (3.5 percent of sodium chloride in water)

2.1 Specimen Preparation

Fifty four samples were prepared for both hardness and microstructural tests from a 5mm thick plate. Eight (8) samples each were cooled with water and salty water. Hardness test and metallographic examination were carried out on the same samples. For each cooling position T1 to T8 (in steps of 5mm from 10mm to 45mm from the fusion zone), three samples were produced in order to obtain the average value. T1 was located at the furthest distance away from the weld joint, while, T8 was the closest to the weld joint. Nine (9) of the samples were used as control test samples. The effect of continuous cooling on hardness was observed at eight (8) different positions. Before the samples were butt welded, they were chamfered at angles 30^{o} creating a vee-groove and leaving a root face and a root gap of 2mm.

Element	Average content (%)	Element	Average content (%)
C	0.1460	Nb	0.0001
Si	0.297	Al	0.0001
Mn	0.285	B	0.0001
S	0.027	W	0.0001
P	0.021	Mo	0.0001
Cr	0.040	V	0.0001
Ni	0.018	Ti	0.007
Cu	0.028	Fe	99.131

Table 1. Average Content of Elements in theMaterial

2.2 Hardness Test

ASTM A370 standard was used to prepare hardness test samples. The hardness values of the fifty-four samples were obtained using Identec (Diamond Rockwell) Universal Hardness Testing Machine (Type 8187.5 LKV Model B) [Minor load= 10kgf, Total load= 60kgf, Scale= A, Indenter=diamond cone (120^{0})].

2.3 Welding Process

The shielded manual arc welding (SMAW) machine and E6013 electrode were used during the welding process. The welding parameter setting for the SMAW machine was set at: voltage; 18V, current; 250A, and average speed; 3.1mm/s; heat transfer efficiency factor f1 (for SMAW) was 0.65. Hence, the heat input was computed to be 1 453.06 J/mm. A constant mass flow rate of the coolant was set at 718.2 g/s throughout the work. The temperature at selected distances from the fusion zone was measured using a digital thermometer (TECPEL, DTM 307). The cooling process was aided by coolant flow guide.

2.4 Metallurgical Examination

Fifty-four (54) samples were ground and subsequently polished towards metallographic examination. An abrasive wheel was used to grind the weld joints. The grinding process was carried out using silicon carbide papers of various grits starting with the coarsest to the smoothest in the following order: 120, 240, 320, 400 and 600 grits sizes respectively. Coolant was applied intermittently in order to avoid the heating up of the sample which could alter its hardness property by annealing process as well as to wash away the particles that were removed from the surface. The polished surfaces were shinny and free of abrasive particles.

2.5 Etching and Microscopy

The polished surfaces of the samples were etched with Nital and examined under a metallurgical microscope. The microscope was used to study the microstructure of the polished surface under different conditions of welding and cooling. A magnification of ×100 was used.

3. RESULTS AND DISCUSSION

3.1 Cooling Curves

The cooling curves for the various cooling media air, water and salty water are presented as follows:

3.1.1 Air Cooled Samples

A rapid fall in temperature was observed from peak temperature (1200^{o}C) to 640^{o}C within 16s as shown in Fig. 1 which, is followed by a gradual fall to ambient temperature.

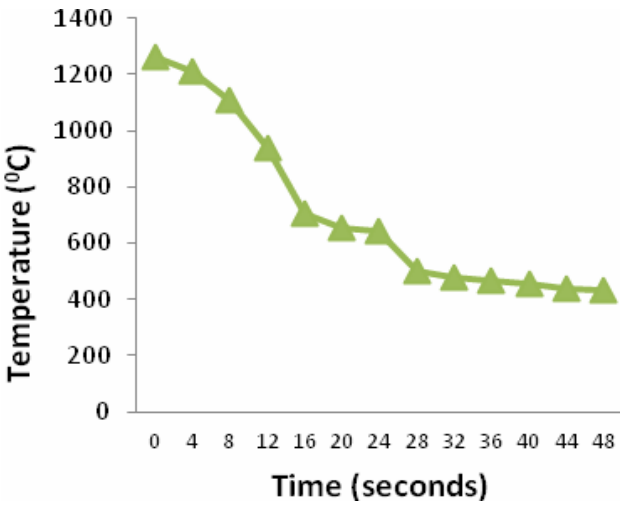

Fig.1. Cooling Curve for Air Cooled Sample

3.1.2 Water Cooled Samples

Figure 2 shows the cooling curve for the water cooled samples. It was observed that the closer the cooling position is to the weld zone, the faster the increased temperature drop because of the thermal gradient. The curve T1 is the farthest from the weldment while T8 is the closest to it.

The temperature dropped from 1200^{o}C to 600^{o}C within 8s. However, It took 52s for the sample's temperature to drop to the ambient temperature.

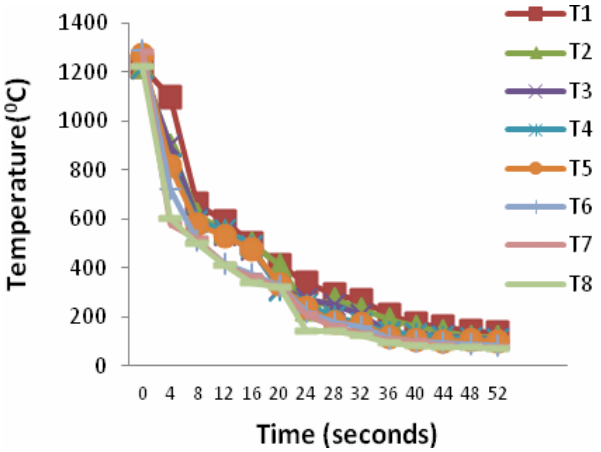

Fig.2. Cooling Curves of Water Cooled Samples

3.1.3 Cooling Curves for Salty Water Cooled Samples

The cooling curves for salty water cooled samples are shown in figure 3. It was observed that it took only 4s for the temperature to drop from 1200°C to 400°C. The cooling effect of salty water was observed to increase with decrease in cooling distance away from weld zone.

This cooling curve for salty-water cooling shows a more rapid cooling rate than air and water cooling. This rapid cooling experienced resulted in an increase in hardness of the samples that were cooled with salty water. Calik[6] has shown that the micro hardness of steels increases with the cooling rate and also carbon content.

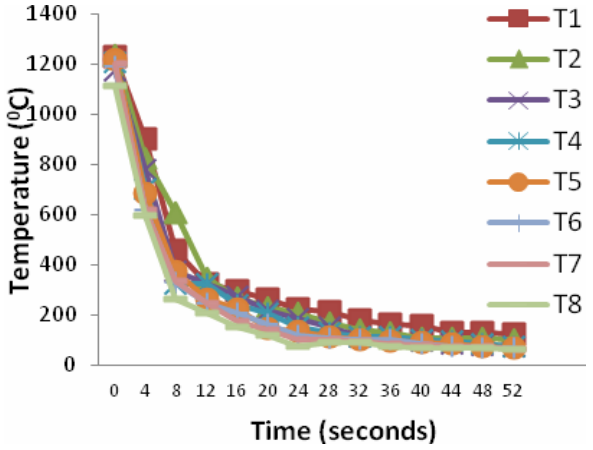

Fig.3. Cooling Curves of Salt Water Cooled Test Samples

3.2 Mechanical property:

3.2.1 Hardness

Rockwell Universal Hardness testing machine was used to carry out hardness tests on the welded samples. Figure 4 presents the results of water cooled (WC) and salty water cooled (SWC) samples. The control sample had a hardness of 45.7kgf.

The hardness values of water cooled samples have lower Rockwell hardness values compared to salty water cooled samples as presented in figure 4. This may be due to the faster cooling rate of salty water, which resulted in higher martensite formation. Also, the increased presence of fine dispersion of small particles in the pro-eutectoid ferrite and pearlitic ferrite, which will prevent the dislocation movement, may have also contributed to the higher Rockwell hardness number of the salty water cooled sample.

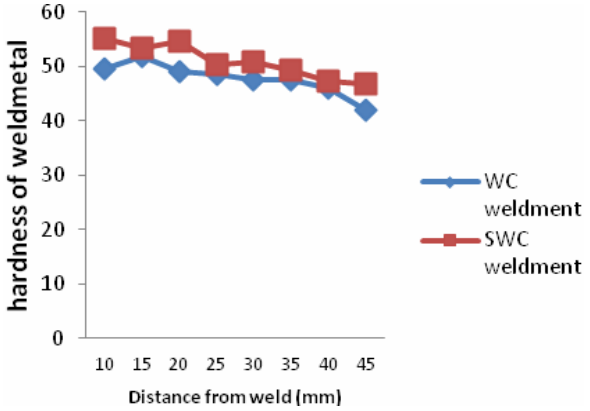

Fig.4. Weld Hardness (Water Cooled (WC) and Salty-Water Cooled (SWC) Samples)

Cooling medium	Minor Load (kgf)	Total Load (kgf)	Weldment (kgf)	HAZ (kgf)	Weldment (N)	HAZ (N)
Air	10.00	60.00	48.50	47.20	475.79	463.03

Table 2. Hardness Values of Air Cooled Sample

3.3 Microstructures

The microstructures of the samples cooled in air (control), water and salty water are presented in plates 1 to 6. Each of the plates has a magnification of ×100.

Plate 1: Control sample

(a) Air Weld

(b) Air HAZ

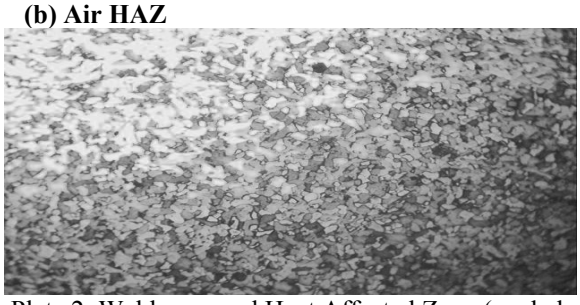

Plate 2: Weld zone and Heat Affected Zone (cooled under room temperature)

The control sample in plate 1 shows ferrite and pearlite layers because of the low carbon content in the material and the grain structure is coarse. The ferrites are the white areas while pearlites are the dark areas. Ferrite, which has a body centred cubic (bcc) structure transforms into austenite (a high temperature phase with face centred cubic (fcc) crystal structure). During the cooling cycle, the austenite transforms back into ferrite or other metastable phases as seen in plate 2.For low cooling rate as in the air cooled sample, the austenite was observed to transform into ferrite.

In plate 2a, the weld zone has fine grains whereas its heat affected zone as shown in plate 2b has coarse grains. This is attributed to the faster cooling rate at the weld zone. It was observed that there was no sufficient time for grain growth and nucleation in the weld zone.

3.3.1 Heat Affected Zone (Water)

Ibarra, et al, [8], observed in his work that due to the rapid cooling that occurs in wet weld, the heat affected zone of most welded mild steel are coarse-grained and martensitic. This was also observed in the heat affected zone micrographs shown in plates 3 and 4. The salty water cooled samples have more martensitic structures than water and air cooled samples.

15mm

45mm

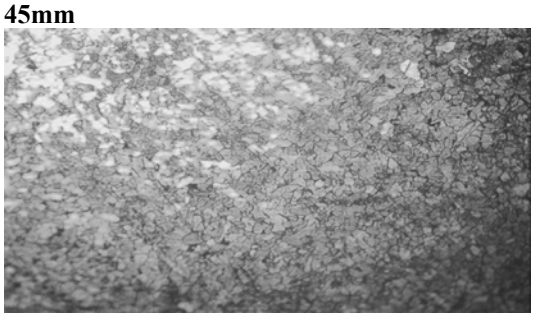

Plate 3: Heat Affected Zone(Water Cooled) at some distances from the fusion zone

From the micrographs presented in plate 3, at 45mm from the weld, ferrite structure is seen to be more and generally dispersed in the microstructure. The ferrite structures are the light-coloured regions of the structure. The amount of pearlite was observed to increase as the cooling distance from the weld reduces (that is, as the material is cooled at a distance nearer to the weld zone).

3.3.2 Heat Affected Zone (salty water)

Plate 4 shows the heat affected zone (HAZ) of the salty water cooled samples. The dark areas are the martensite regions and they appear to be more especially for 15mm plates. The other plates, such as 45mm have lighter appearance. These are pearlite structures (a mixture of iron ferrite and cementite).

15mm

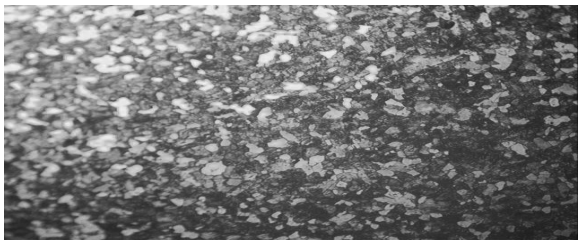

45mm

Plate 4: Heat Affected Zone (Salty Water Cooled)

The micrographs presented in this section show the samples cooled in 3.5percent salty in water. The cooling rate of the salty water cooled samples was faster than the water cooled samples. The grains were also coarse but it was observed that there was an increase, though minimal, in the amount of pearlite layers. At 10mm and 15mm from the weld zone, martensitic structures were observed.

3.3.3 Weld (water cooled)

Weld zone microstructures for water cooled are presented in plate 5. The grain structures were fine and finger-like. This is because of the rapid cooling rate at the weld zone. The micrographs farther away from the weld show more ferrite structures and some few pearlite layers.

3.3.4 Weld (salty cooled)

The micrographs above (plate 6), are also fine grained. The microstructure of the 10mm and 15mm samples show some martensitic layers with some pearlite regions. It was observed that the martensite in the water cooled weld micrographs were more evenly dispersed than that of the salty water cooled weld zone

micrographs. The microstructures of samples cooled far from the weld zone were also more ferritic.

The increase in pearlite and martensite in the salty water cooled samples resulted in an increase of their hardness and strength.

15mm

45mm

Plate 5: Weld Zone Microstructures (Water Cooled)

15mm

45mm

Plate 6: Weld Zone Microstructures (Salty Water Cooled)

4. CONCLUSION

The following conclusions were drawn:

i. The samples cooled with salty water had higher hardness values possibly due to the formation of martensitic structure after quenching, while, air cooled samples were mostly ferrite.

ii. It was observed that the variations in the microstructures were minimal; this was possibly due to the rapid heat input, very short soaking time during welding and the low carbon content of the material.

iii. The closer the cooling position, the more the cooling effect and the more the hardness and metallurgical properties were influenced.

iv. As the cooling rate in the weld zone and heat affected zone varied with cooling distance from the fusion zone of the weld, the phases formed from the transformation was observed to also vary with cooling distance.

v. From the hardness test results, the coarse grained heat affected zone (CGHAZ) had high hardness values compared with the rest of the heat affected zone (HAZ) and unaffected areas of the steel because of the large grain size and high cooling rate in the region.

5. REFERENCES

[1] Ibhadode, A.O.A., Introduction to Manufacturing Technology, Ambik Press, Benin-City, Nigeria, 2001

[2] Pang,W., Ahmed,N. and Dunne, D. Hardness and microstructural Gradient in the heat Affected Zone of Welded Low- Carbon quenched and Tempered Steels, Austral Asian Welding Journal,Volume 56, Second Quarter, pp36-48, 2011

[3] Shome , M., Gupta, O. P and Mohanty, O. N. A Modified Analytical Approach for Modelling Grain Growth in the Coarse Grain HAZ of HSLA Steels. Scripta Materialla 50: Pp 1007- 1010, 2004

[4] (Parmar, R.S., Welding Engineering and Technology, Khanna Publishers, India, 2007.

[5] Fukuoka T. and Fukui S., Analysis for Cooling Process of Underwater Welding -Comparison with Welding in Air, Bulletin of the M.E.S.J., Vo1. 22, No.2. PP 88-92,1994.

[6] Calik, A., Effect of cooling rates on the hardness and microstructure of AISI 1020, AISI 1040, and AISI 1060 steels, International Journal of Physical Sciences Vol.4(9),pp 514-518, 2009. Available online at hhtp://www.academicjournals.org/IJPS

[7] Adedayo, S.M. and Oyatokun, V.O., Effect of saline water cooling on service quality of a welded AISI 1013 Carbon steel plate. Annals of faculty of engineering Hunedoara-International Journal of Engineering, Tome XI, Fascicule 2 pp 25-28, 2013.

[8] Ibarra S., Liu S. and Olson D.L., "Underwater Wet Welding of Steels", Welding Research Council Bulletin, no. 401, PP 1-39,1995.

Authors: **Aweda, E. O.[1], Dr. Dagwa, I.M.[2], Dr. Dauda, M[3]., and Dr. Dauda, E.T.[4]**

[1,3]Department of Mechanical Engineering [4]Department of Materials and Metallurgy Engineering, Faculty of Engineering, ABU Zaria. [2]Department of Mechanical Engineering University of Abuja, Abuja, Nigeria

Email address:

oluwarotimi.aweda@yahoo.com, dagwaim@gmail.com, muhammaddauda@yahoo.com, emmayustoi@yahoo.com

Journal of Production Engineering
Vol.16 No.2

Original Scientific Paper

Savković, B., Kovač, P., Gerić, K., Sekulić, M., Rokosz, K.

APPLICATION OF NEURAL NETWORK FOR DETERMINATION OF CUTTING FORCE CHANGES VERSUS INSTANTANEOUS ANGLE IN FACE MILLING

Received: 29 October 2013 / Accepted: 25 November 2013

Abstract: *Artificial neural networks have been recognized as an inevitable tool whose application can be achieved for improving product quality, increase productivity, decrease response time of the system, increase reliability etc. In this paper, artificial neural network based on the face milling machining processes where is aimed to produce the relationship of cutting force versus instantaneous angle φ. The research conducted in the paper allows solving the problem that is difficult to define and mathematically modeled.*

Key words: *artificial neural networks, face milling, cutting forces, instantaneous angle*

Primena neuronske mreže za određivanje promena sila rezanja u funkciji od trenutnog ugla zahvata pri čeonom glodanju. *Veštačke neuronske mreže su prepoznate kao neizbežan alat čijom se primenom može postići: poboljšanje kvaliteta proizvoda, povećanje proizvodnosti, smanjenje vremena odziva sistema, povećanje pouzdanosti itd. U ovom radu veštačkih neuronkih mreža je zasnovana na procesima obrade rezanjem pri čeonom glodanju gde se želi dati zavisnost promene otpora rezanja u funkciju ugla zahvata. Sprovedena istraživanja u ovom radu omogućuju rešavanje problema koje je otežano matematički definisati i modelirati.*

Ključne reči: *veštačke neuronske mreže, čeono glodanje, sile rezanja, trenutni ugao zahvata*

1. INTRODUCTION

Artificial neural networks in the wider sense of the word represent an artificial replica of the human brain, with which it aims to simulate the process of learning. Such networks are collections of mathematical models that simulate some of the observed properties of biological nervous systems and retreat similarities with biological adaptive learning. They are made up of many interconnected neurons (processing elements) which are similar to biological neurons, connected to its ties containing permeable odds that are similar to his role as synapses.

Artificial neural networks have been recognized as an inevitable tool whose application can be achieved by improving product quality, increase productivity, decrease response time of the system, increase reliability etc. In many of the applications of artificial neural networks have replaced its recent methods and techniques, often are used in combination with other methods, but very often the only way to solve tasks and seeking solutions. Artificial neural networks with its structure, ability to learn and the way of functioning in general, are very applicable systems in specific industrial problems [1, 2].

Specifically in this paper, the application of artificial intelligence and artificial neural network is based on the machining processes in face milling. Since the processing of face, milling is one of the most used and most effective in the field of machining with relatively high productivity, it is logical that the largest number of works and studies are related just to this process. The cutting force in face milling has been extensively studied both analytically and experimentally [3].

The specificity of face milling machining process, such as increased number of teeth that are in cut at the same time, and the variability of the chip cross section of the cutting that cuts a tooth, caused the development of a large number of models for the calculation of cutting force components. The variability of the chip cross section leads to a change in intensity of cutting force and thermal loads during cutting of a tooth [4].

2. ELEMENTS OF CHIP CROSS SECTION

Simplified scheme of face milling with elements of the chip cross section, which cuts one tooth, is shown in Figure 1.

In face milling instantaneous chip cross sectional area, which cuts one tooth of cutter, varies depending on the instantaneous angle φ and is defined as:

$$A = a \cdot s_1 \cdot \cos\varphi \qquad (1)$$

Where is:

s_1 - feed per tooth,

φ - the angle that determines the position of a tooth in cut, measured from the cutter axes,

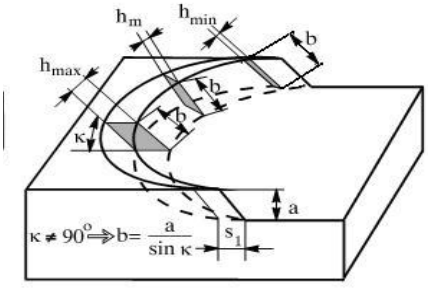

Fig. 1. The elements of the chip cross section in face milling

2.1 Analysis of cutting force in face milling

In face milling the cutting force, of the tooth cutter that acts on workpiece, are variable in time and space as well as the size and direction. The resulting force F_R can be project into axial force F_A parallel to the machined surface the force F_a normal to the machined surface.

Force F_A is called the active force because during the processing load cutter spindle bending, while the force F_a called axial force and its direction does not any movement during machining. In order to easy explanation of the force model studied was one-tooth cutter case, with a width equal to the diameter of milling cutter D. The tool during one rotation removes chips cross section shaded in Figure 2.

The force F_A is changed by the direction and intensity during one tooth cutting, so are its components F_x and F_y different in intensity according the angle from 0° ÷ 180°.

The relationship between time and instantaneous angle φ is given by following equation:

$$\varphi = \omega \cdot t \qquad (2)$$

Where is:

ω - angular cutting speed,

The other two components that can be project force F_A in tangential and radial direction. These are the main cutting force F_g and the passive force F_r.

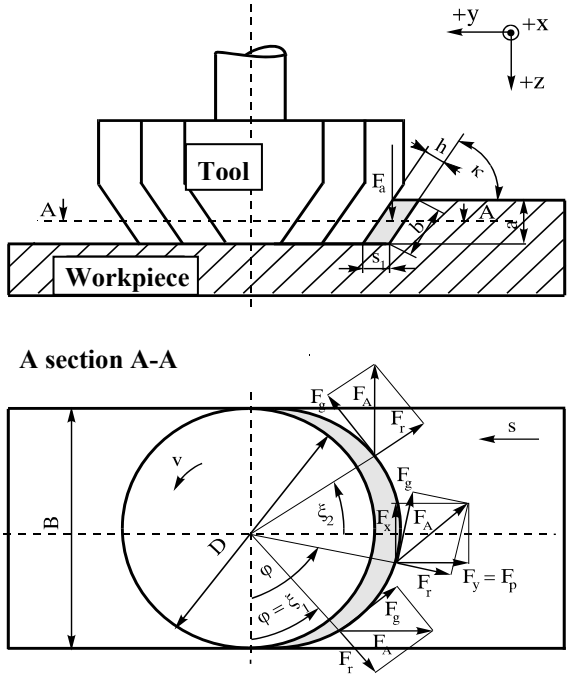

Fig. 2. Pattern of cutting forces in face milling [4]

Solving of the system of equations for cutting force shown in Figure 2 gives the following equation for calculation of the next forces:

$$F_g = F_x \cdot \cos\varphi - F_y \cdot \sin\varphi \qquad (3)$$

$$F_r = F_x \cdot \sin\varphi + F_y \cdot \cos\varphi \qquad (4)$$

$$F_a = F_z \qquad (5)$$

$$F_p = F_x \qquad (6)$$

3. EXPERIMENTAL PROCEDURE

Material processing

In an experimental measurement of the cutting force machined was Č4732 steel, with the chemical composition given in Table 1, and with the mechanical properties given in Table 2.

Alloying element	The chemical composition of in %									
	C	**Si**	**Mn**	**S**	**P**	**Cr**	**Mo**	**Ni**	**Cu**	**V**
Tested composition	0,40	0,427	0,497	0,042	0,039	0,914	0,183	0,35	0,17	0,01
By JUS	0,38-0,45	0,15-0,40	0,5-0,8	0,032	0,035	0,9-1,2	0,15-0,30	-	-	-

Table 1 Chemical composition of the test material

Dimensions of tubes (mm)	Yield stress Rp (Mpa)	Tensile Strength Rm (Mpa)	Ductility A (%)	Contraction z (%)	Hardness HB
15,0 x 6,0	790	975	16,4	43	265

Table 2 Mechanical properties of steel Č4732

Regime of processing

Cutting speed: V=89,17 m/min,
Cutting depth: a=1mm,
Speed table: S=100/min,
Shift per tooth: s_1=0, 281mm/t,
Number of teeth: z=1

Measurement of the cutting force components

The measurement was done in three orthogonal directions using a Kistler dynamometer, using the measuring of acquisition system for measuring forces during milling by use of virtual instrumentation. Machine tools was milling machine - "Prvomajska" FSS GVK-3.

Cutting Tool

During testing was used milling head with positive cutting angle "JUGOALAT" ϕ 80 mm, with mechanically fastened cutting carbide P25 inserts, the following:

Tool cutting edge angle κ = 75 °, rake angle γ = 0 °.

4. IMPLEMENTATION OF NEURAL NETWORKS

For training of the neural network during modeling was used "MatLab" software, which is the most powerful software for technical calculations [5].

Training and testing are the most important characteristics of neural networks because just training and testing determine its characteristics. To create and train a neural network in the MATLAB is used Neural Network Toolbox, Neural Network Toolbox includes

all methods of neural network and makes available a number of different algorithms for learning as well as the other software packages MATLAB. Neural Network Toolbox takes much of the routine work so the user can concentrate on the essential issues of study.

Before starting creation of the neural networks was done entering data in the Command Window in a matrix form. For input was used the instantaneous angle φ (rad), and the output was the main cutting force F_g (N), penetration force F_r (N), feed force F_p (N) and axial cutting force F_A (N) .

Elected as feed-forward, back propagation networks. This network is very suitable for the application because of its structure and the training is very effective in the short time gives the desired results, used was the following functions and sets methods for training:

1. Training Function – TRAINLM
2. Adaption Learning function - is applied LEARNGDM learning function for backpropagation / bias
3. Performance - (applied to the mean square error Mean Square Error - MSE)
4. Transfer Function - selected network has a hidden layer has ten neurons and activation function is TANSIG, the output layer has four neurons and PURELIN activation function, the sigmoid tensing and purelin a linear function.

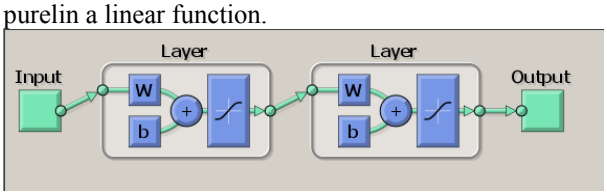

Fig. 3. The window created by a neural network

The data used to train the network are used to test the simulation.

Table 3 shows the values of the angle φ (rad), and the experimental values of measured, or obtained (F_g, F_r, F_p, F_a) cutting forces in face milling by equations 3, 4, 5 and 6. The same Table shows the values obtained by force formed by use of artificial neural networks (F_g nn, F_r nn, F_p nn, F_a nn). In Figure 4 is shown diagram of the cutting force for the operation angle φ.

φ (rad)	Fg (N)	Fr (N)	Fp (N)	Fa (N)	Fg nn (N)	Fr nn (N)	Fp nn (N)	Fa nn (N)
0	-6,48	9,44	6,48	-3,48	57,8166	9,455	6,48	-13,8815
0,096664	2,223742	-3,03957	-1,92	4,92	2,696	107,026	-93,1172	29,5293
0,193329	224,0282	107,7695	-240,56	94,56	52,0282	212,0668	-240,56	69,8774
0,289993	312,3712	181,1239	-351,12	123,32	210,9545	261,1679	-351,12	95,8341
0,386658	390,5127	236,2193	-450,76	96,32	387,8159	273,1436	-450,76	108,8947
0,483322	440,4505	229,9014	-496,84	122,28	470,2797	275,835	-503,0525	114,8924
0,579986	508,1243	288,1854	-582,96	110	509,8242	277,8838	-534,5699	118,1861
0,676651	553,4687	268,0272	-599,36	116,8	544,4545	284,1017	-578,4964	121,6475
0,773315	579,1878	306,3856	-628,48	122,32	604,3688	300,0602	-628,48	127,4711
0,86998	644,7682	319,9022	-660,28	136,32	662,4427	318,9651	-660,28	135,4033
0,966644	692,3485	338,8903	-672,2	142	694,0225	328,2665	-672,2	140,2783
1,063308	708,3748	330,3343	-632,96	140,28	720,9946	331,8722	-669,2928	140,2754
1,159973	760,776	366,4658	-639,8	147,48	746,8648	366,3945	-639,8	144,3782
1,256637	801,6378	369,5682	-599,2	149,64	771,3823	369,5558	-573,3414	154,6755
1,353301	776,4841	341,4103	-500,92	178,16	791,7339	349,8771	-500,92	160,8945
1,449966	794,3614	336,9067	-430,2	165,64	792,8696	349,7997	-430,2	162,4045
1,54663	810,4643	360,3614	-379,84	186,16	752,5806	349,799	-379,84	162,5521
1,643295	727,8642	377,2737	-323,56	148,64	751,1348	349,7936	-319,127	162,582
1,739959	805,351	366,9848	-226,16	138,12	742,8056	349,7794	-226,16	163,9863
1,836623	771,2589	343,3141	-128,64	151,64	732,9486	349,7433	-121,3155	171,4032
1,933288	750,3911	381,8676	-90,96	146,32	746,3346	347,7607	-41,3309	182,4604
2,029952	736,0162	351,0338	11,52	187,56	758,5481	335,8716	11,52	179,7909
2,126617	678,0057	341,3232	67,8	159,6	752,3262	335,3134	67,8	171,9662
2,223281	654,3173	346,092	122,28	177,6	677,517	333,9716	122,28	162,4416
2,319945	609,2676	336,9267	168,2	144,6	572,3079	330,6743	168,2	152,9514
2,41661	549,9591	293,4756	217,04	154,12	540,7647	322,6834	217,04	151,2966
2,513274	509,8723	293,6707	239,88	137,16	524,9152	303,9507	239,88	156,5188
2,609939	450,9108	268,091	252,76	136,76	440,2693	263,2804	237,952	142,2486
2,706603	373,9729	239,6444	238,16	113,68	212,3703	188,3027	199,7788	103,8187
2,803267	121,8544	59,61503	95,16	76,04	36,7504	86,8192	95,16	60,0023
2,899932	6,560278	5,221757	5,12	-11,28	-8,3541	9,8941	5,12	23,3763
2,996596	-6,26995	6,615358	-7,16	-2,88	-14,8292	10,549	-20,5743	-2,724
3,09326	-15,525	-2,21252	-15,4	-6,16	-21,6884	0,2335	-15,4	-19,6448

Table 3 Expected values and the values obtained

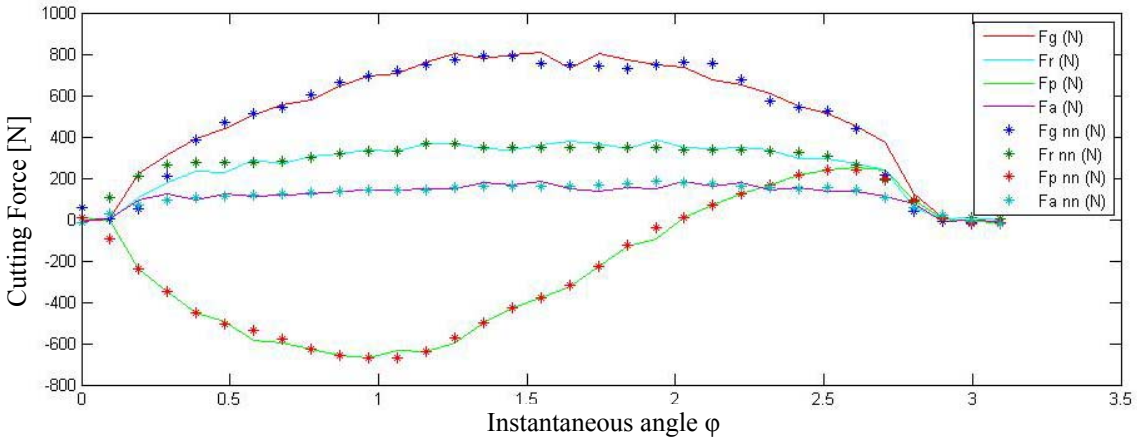

Fig. 4 Diagram of cutting force in function of the instantaneous angle φ

4.1 Analysis of the results

The results obtained using the neural network given in the table indicate good agreement with the experimental values. Noticeable deviation of the results showed only on the tooth entry where tooth hit the material and where are inherently unstable force and not continuous. Hence, this deviation can be neglected while in other cases; obtained results are more than excellent. This shows that the chosen algorithm is good, but that the number of inputs could be higher.

5. CONCLUSION

Based on the developed system, conducted theoretical and experimental studies, performed analysis of the present and previous, can be made the following conclusions:

- Analysis of the cutting force during face milling is very complex because of the influence of a number of different phenomena, and because of the chip cross-sectional thickness, and the corresponding cutting force cyclic change during cutting. Accurate knowledge of the characteristics and values of cutting forces in face milling is necessary to study the dynamics of the cutting process in interaction with the dynamic behavior of the machine tool structure.

- Artificial neural networks have become an indispensable tool for solving problems related to the production processes. Knowledge modeling and machining process parameters can help the optimal process control, which has a positive impact on reducing costs and improving profitability of production.

- The neural network is successfully used to solve problems that are difficult to define and mathematically modeled. During training of the neural network are continuously presented to the input data sets (in this case, the input size of the procedure was the instantaneous angle) and of the corresponding desired output values (in this case the corresponding components of the cutting force in face milling). After training the network, it is ready for use and is able to, for data that is not met by then, the very good references for required parameters. Thus, the well-trained neural network plays the role of an expert in a particular area.

6. REFERENCES

[1] Meireles R.G. Magali, Almeida E. Paulo, „A comprehensive review for industrial applicability of artificial neural networks“, IEEE Trans. Ind., Vol. 50, 2003, pp. 585-601.

[2] Chow M. Y., Sharpe R. N., Hung J. C.: On the application and design of artificial neural networks for monitor fault detection-Part 2, IEEE Trans. Ind. Electron., Vol. 40, 1993, pp. 189-196.

[3] Zuperl Uroš, Čuš Franci: Optimization of cutting conditions during machining by using neural networks, Production Engineering, Maribor, 2000, Slovenia.

[4] Kovac, P., Savkovic, B., Mijic, A., Sekulic, M.: Analytical and experimental study of cutting force components in face milling, Journal of Production Engineering, Novi Sad 2011, UDK 621, Vol.14, No.1, pp. 15- 18, ISSN 1821-4932.

[5] P. Kovac, D. Rodic, V. Pucovsky, B. Savkovic, M. Gostimirovic: Application of fuzzy logic and regression analysis for modeling surface roughness in face milling, Journal of Intelligent Manufacturing, Volume 24, No.4, pp 755-762

Authors: **Assist. Borislav Savkovic, M.Sc.[1], Prof. Pavel Kovac PhD[1], Prof. Katarina Geric PhD[1], Assoc. Prof. Milenko Sekulic PhD[1], Prof. Krzysztof Rokosz PhD[2]**

[1]University of Novi Sad, Faculty of Technical Sciences, Institute for Production Engineering, Trg Dositeja Obradovica 6, 21000 Novi Sad, Serbia, Phone.: +381 21 450-366, Fax: +381 21 454-495.

[2]Wydział Mechaniczny, Politechnika Koszalińska, ul. Racławicka 15-17, 75-620 Koszalin, Poland.

E-mail: savkovic@uns.ac.rs
pkovac@uns.ac.rs
gerick@uns.ac.rs
milenkos@uns.ac.rs
rokosz@tu.koszalin.pl

Note: This paper presents a part of researching at the CEEPUS project and Project number TR 35015.

Journal of Production Engineering
Vol.16 No.2

Original Scientific Paper

Tratar, J., Kopač, J.

ROBOT MILLING OF WELDED STRUCTURES

Received: 11 September 2013 / Accepted: 27 October 2013

Abstract: *Under the influence of sustainability and in search of new low-cost solutions for mechanical processing technologies robots present new intriguing way of modern machining applications. Evolving robot programming equipment offers new applications that can be implemented with existing robot hardware technology. Milling with robots is one of them and represents a relatively new and promising direction of multi-axis machining. In this article we present robot multi-axis milling of robot spatial welded pyramid out of VAC 60 material and machining of the weld stud. We used KUKA anthropomorphic robot, in all machining applications, that is available to us at the Faculty of Mechanical Engineering in Ljubljana, with an attached motor spindle unit. Robot milling of welded structural steel has been successfully completed. That indicates the possibility of using robotic manipulator for machining harder materials with a proper selection of the processing parameters and sufficiently loose tolerances of the finished product.*

Key words: *robot, milling, steel*

Glodanje zavarenih struktura pomoću robota. *Pod uticajem održivosti i u potrazi za novim jeftinim rešenjima za obradne tehnologije, roboti predstavljaju novi intrigantni način upotrebe moderno obradnih tehnologija. Razvoj opreme za programiranje robota nudi nam nove primene koje se mogu implementirati u već postojeći hardver robota. Glodanje pomoću robota je jedna od njih i predstavlja relativno novi i obećavajući pravac višeosne obrade. U ovom radu je predstavljeno višeosno glodanje pomoću robota, robotom navarene piramide od VAC 60 materijala i obrada zavarenog spoja. Korišćen je KUKA antropomorfički robot u svim aplikacijama, koji je dostupan na Fakultetu za mehaničko inženjerstvo u Ljubljani, sa odgovarajućom pogonskom jedinicom. Glodanje robotom zavarenih strukturnih čelika je uspešno savladano. Ovo ukazuje na mogućnost korišćenja robotskog manipulatora za obradu tvrđih materijala sa odgovarajućim izborom parametara procesa i dovoljno labavih tolerancija gotovog proizvoda.*

Ključne reči: *robot, glodanje, čelik*

1. INTRODUCTION

In a time of constant progress, well spread automatisation and findings of a new and more economically feasible technologies, there arises a question, how to find at least a partial replacement for large, unwieldy and very expensive CNC machining centers.

As IFR (International Federation of Robotics) stated in 2011 there has been more than a million industrial robots operating in the world. Annual sales are despite the situation in the global markets since 2010, when there were 78,000 robots sold worldwide, estimated at about 10 % growth. That indicates growing trend of the robotics in industrial automation and the fact that the use of robots also spread to areas where they previously could not be noticed.

One of the possible partial modern replacements of expensive large CNC machining centers seems to be industrial six axis anthropomorphic robots (Figure 1). The development of software in the past few years enabled the robots to be no longer used only in conventional purposes of manipulative ("pick and place") operations and montage applications. Development also opened a new horizon of possibilities including the use of a robot as a multiaxis CNC machine centre.

However this new sustainable way of machining might be intriguing, it is important to know that milling with robot is less accurate than with conventional CNC machine centres and not suitable for all materials. It is because of the segmental robot structure that robots have lower stiffness than conventional CNC machines [1, 2, 3]. In most cases the robot is only suitable of processing softer materials, such as various foam, wood (wood composites), and some metals.

Despite all shortcomings, robots prove to be outstanding when machining very large workpieces and because of high flexibility even appropriate of rapid prototyping large workpieces. Robots can have quite large workspace (depending on the type of the robot). In our work we use KUKA KR 150L110 robot which has a reach up to 3500 mm.

Robots are intriguing by economic aspect because of low initial investment and very low maintenance and running costs [4, 5, 6].

For the purpose of this article we decided to use the robot manipulator for processing (milling) steel workpieces and welded structures. We tried to proof the assumption that it is possible to robot weld optional spatial forms and raw workpieces and rough machine them with two different robots or even with the same robot manipulator with attached weld gun and motor spindle.

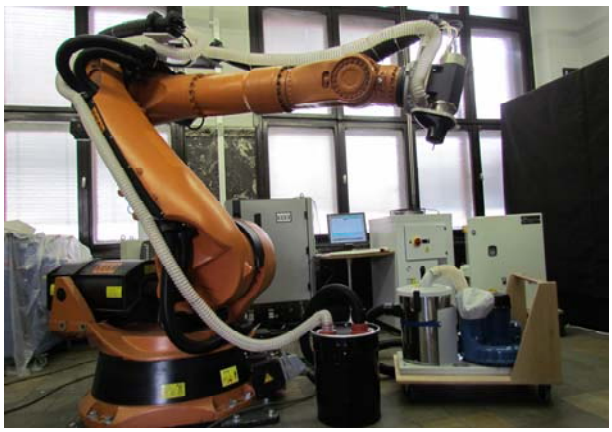

Fig. 1. Robot machining cell.

2. MATERIALS AND PARAMETERS

We used the KUKA robot manipulator to rough mill welded pyramid and weld around the cap to make it suitable for bottoming.
Material used for welding was VAC 60 1mm thick wire. Weld material properties were similar to the structural steel. The pyramid welding programme was programmed in a virtual environment (Robot studio) and implemented on a small ABB robot with attached welding gun. We used CMT (Cold Metal Transfer) welding equipment to create hollow steel pyramid. ABB welding robot was not used in following milling applications.

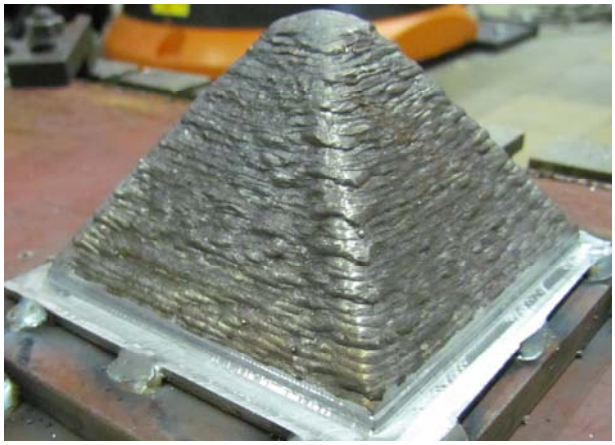

Fig. 2. Robot welded pyramid.

Wall of the pyramid has been welded by two layers (two parallel welds). The thickness of each weld was approximately 9 mm ± 0.5 mm. The dimensions of welded sides were 93 mm and a height of the pyramid was 65 mm (Figure 2).
The cap with a diameter of 32 mm was welded by hand with the same material as a pyramid (60 VAC). The outer diameter of the weld was 45 mm and the height of the weld 6 mm (Figure 3).
Processing parameters and cutting forces were determined by milling tests on a pre-established welded block out of the 60 VAC material. To measure cutting forces Kistler dynamometer has been used. We also measured surface roughness with roughness meter Mitutoyo.

We used six blade carbide cutters with a blue coating (AlTiN and corner phase of 0.5 mm at an angle of 45 °) for all milling purposes. The diameter of the tool was 12 mm.

Fig. 3. Hand welded cap before robot milling

Climb milling strategy has been used with two stepover values (A_p); 60% (7.2 mm) of the diameter of the cutting tool and 40% (4.8 mm) of the diameter of the cutting tool. Depth of cut was variable because we wanted to maximize productivity of the cutting process (P) and maintain satisfactory properties of the newly formed surface.
In all cases feed of the robot manipulator remain the same, 1200 mm / min and the spindle speed 5000 min^{-1}.
There are depth of removal (A_p), measured value of the surface roughness (R_a), the corrugation (R_y) and calculated productivity of the cutting process (P) shown in following table 1 and table2.
In the case of 4.8 mm lateral removal (A_p) we chose to use the 0.4 mm depth in the rough milling and 0.1 mm for the final treatment (Table 1). The same depths were used for 7.2 mm lateral cutting (Table 2).
Selected parameters were used for the production of two sides of the pyramid, and the other two parameters in Table 2 for the other two sides. All the toolpaths were programmed with Robotmaster program.

A_p (mm)	R_a (μm)	R_y (μm)	P (mm^3/min)
0,4	2,4	34,3	2304
0,1	2,1	31,9	576

Table 1. Cutting, lateral withdrawal (A_e) 4,8 mm

A_p (mm)	R_a (μm)	R_y (μm)	P (mm^3/min)
0,35	2,1	43,8	3024
0,1	1,9	41,3	864

Table 2. Cutting, lateral withdrawal (A_e) 7,2 mm

3. IMPLEMENTATION

Programming of the robot tool path is almost the same as classic three and/or more axis CAM programming of conventional CNC machines. Differences occur only in the final stages of programming, where additional simulations and calculations to check singularities, availability and collisions are carried out. For the production of the final product (Figure 4), we used a model of the equilateral pyramid with 90 mm long sides and a height of 58 mm.

We chose simultaneous 5 axis one-way strategy with parameters as described earlier. Milling was performed using one-way strategy because we longed to avoid vibrations that occur when changing the milling direction in material in milling with robot. Excessive wear occurs in the sharp edges of the tool path when machining in the workpiece because of vibrations which are caused by poor rigidity of the robot.

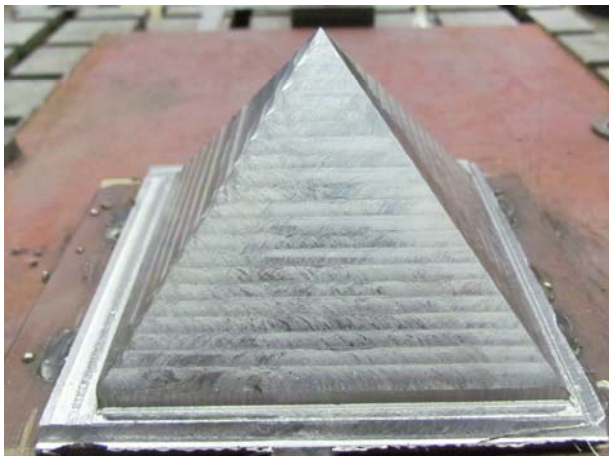

Fig. 4. Robot 5- axis machined pyramid.

Pyramid workpiece was positioned on the working table at the distance of x = 1470 mm and y = 1205 mm from the robot base to achieve best results. Than workpiece has been clamped and processed (Figure 4). Workpiece was machined in about 80 minutes.

Fig. 5. Multiaxis robot machining.

The same procedure has been used to machine the plug. We used four flute ball cutter with diameter of 6 mm coated with TiAlCN coating to carry out all milling operations. Due to the circular shape of tool path cutting speed was limited to 850 mm/min. Machining was completed within 10 minutes. We used co-spiral a strategy of milling without intermediate lifting of the cutting tool (Figure 5 and Figure 6).

Fig. 6. Multiaxis machined plug.

4. RESULTS AND DISCUSSION

Robotic manipulator allows very wide range of mechanical processes which can be carried out. Anthropomorphic robot has six degrees of freedom, so it can be used in any multiple (five) axis machining, as well as in the conventional three-axis machining operations.

After performed machining processes, we made measurements of the pyramid by the coordinate measuring machine DEA Diamond Model 2.1. Repeatability of the measuring machine is 0.35 mm, the linearity error ± 2.5 +4 L/1000 (L [mm]). Aligning of the measured piece was done by rule 3-2-1 (plane, line, point). Performed measurements showed that the pyramid workpiece has been machined in ± 0.5 mm overall accuracy.

The tool wear has also been observed during milling process. Due to the lower stiffness of the robot (in comparison with conventional CNC machines) vibration occur during the milling process, especially in the sharp edges of the tool paths, which greatly affected tool life. Therefore, it is necessary to properly program tool paths with properly chosen parameters in order to avoid excessive wear or even tool breakage.

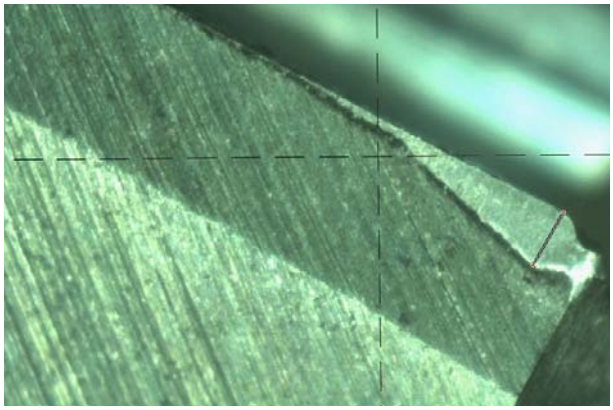

Fig. 7. Cutter flank wear.

Figure 7 presents a microscope Mitutoyo image of the cutting edge of milling cutter with a diameter of 12 mm, which has been used to machine the pyramids and in the previous milling tests to define parameters.
Visible abrasive flank wear can be noticed (length of the line is 24 μm) with fracture of the tool edge in corner stage.
Tool has been than used for the processing of another pyramid and examined on the microscope (Figure 8).

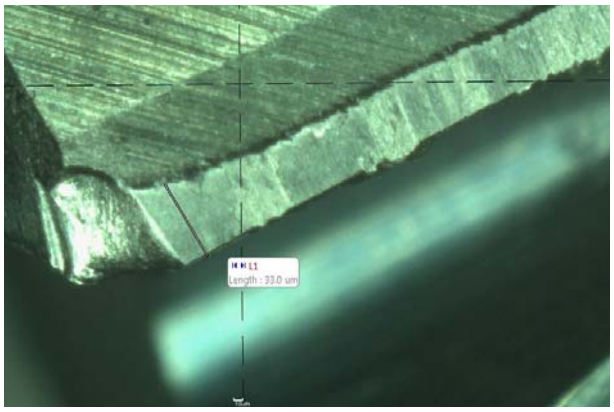

Fig. 8. Cutter flank wear after all operations

Visible progressive abrasive wear (33 μm), and fracture edge of the stage tool can be noticed. Build up edge has appeared, tears on the cutting edge of the tool can be clearly seen. Fracture increased at the edge of the tool stage.

5. CONCLUSION

The robot manipulator in general can be used to mill softer materials such as; various prototype foam, plastics and wood. It is also possible to machine welded structures and welds in almost all shapes and sizes, for which the requirements for tolerances are a bit loose.
Anthropomorphic robot manipulator can be well adapted to machine complex workpiece shapes due to high flexibility and the six degrees of freedom. As such, it can effectively machine workpieces that other machines are not able to process because of limited reach or too complex shapes of the workpiece. Mostly robots can be successful and cost-effective replacement of hand finishing labour such as; grinding, milling or welding, even at an angle, or the inside of welded pipes and other complex structures where more demanding adaptive multi axis machining is needed. In our work we have been using two robots, smaller for welding and large for milling. With appropriate designed machining head attached to the top of the robot manipulator we could combine both operations in a single robot. Such preparation would save both costs as well as processing time and could be implemented for robotic cells which could replace manual labour of welding and milling, potentially grinding.
Robotic manipulators are attractive alternative to conventional and special machines for applications in multiple axis processing and will in future present significant part of modern production.

6. REFERENCES

[1] International Federation of Robotics (www.ifr.org)
[2] J. Tratar, P. Kržič, J. Kopač: Uporaba robota v tehnologiji z odrezavanjem. Ventil, Vol. 17, No. 6, pp. 522-526, 2011.
[3] P. Kržič, D. Eržen, J. Duhovnik, J. Kopač: Offline programiranje industrijskih robotov s programom Mastercam. Orodjarstvo 2008- zbornik posvetovanja, Portorož, Slovenija, pp. 53-57, 2008.
[4] E. Abele, M. Weigold, S. Rotherbucher: Modeling and identification of an industrial robot for machining applications. CIRP Annals-Manufacturing Technology, 56, pp. 387-390, 2007.
[5] KUKA, Datasheet and manuals.
[6] C. Bates: Move over machine tools here come robots. American Machinist, 2006.

Authors: **J. Tratar, J. Kopač**, Laboratory for Cutting, University of Ljubljana, Slovenia
E-mail: janez.kopac@fs.uni-lj.si

Journal of Production Engineering
Vol.16 No.2

Original Scientific Paper

Murčinková, Z., Vasilko, K.

THE REAL SHAPE OF THE WORKPIECE AFTER TURNING AND MILLING

Received: 09 October 2013 / Accepted: 15 November 2013

Abstract: *The paper presents analyses of real shape of workpiece surfaces machined by turning and milling. Each construction of cutting machine activates dimensional and geometric inaccuracies of the workpieces as a result of different stiffness of its joints. The acting of cutting force and the moving of its position leads to the deformation of the elastic joints of cutting machine and the elastic deformation of the workpiece appears. The aim is to maintain dimensional and geometric modifications of the workpiece in required tolerances. The paper identifies these inaccuracies for case of a centre lathe and vertical mill.*
Key words: *elasticity, deformation, accuracy, centre lathe, vertical mill, measurement*

Stvarani oblik obradka nakon obrade struganjem i glodanjem. *U radu su prikazane analize stvarnog oblika površine obradka pri obradi straganjem i glodanjem. Svaka konstrukcija mašine inicira dimenzionalne i geometrijske greške obradka kao rezultat različitih krutosti njenih spojeva. Delovanjem sila rezanja i kretanja mašine dovodi do deformacije elastičnih spojeva mašine i dolazi do pojave elastičnih deformacija obradka. Cilj je da se održi geometrijska tačnost obradka u zadatim tolerancijama. Rad identifikuje ove greške za slučaj centričnosti struga i vertikalnosti glodala.*
Ključne reči: *elastičnost, deformacija, tačnost, centričnost struga, vertikalnost glodala, merenje*

1. INTRODUCTION

The many present works [1, 2, 3] consider workpiece clamping as rigid. In some works [4] the clamping and fixture stiffness is assumed to be known or only contact stiffness is taken into account. The presented work shows real surfaces after turning and milling. The detailed experimental works are developing in case of turning.

The workpiece is loaded by the machining force F during cutting. In case of turning, machining force F can be divided into three components according to Fig. 1. [5, 6, 7]. The workpiece is loaded by the machining force F according to Fig. 1. The machining force F is decomposed in three components: cutting force F_c, feed force F_f and passive force F_p. [5, 8, 9, 10]. Force F_p causes the displacements and deflection of the workpiece.

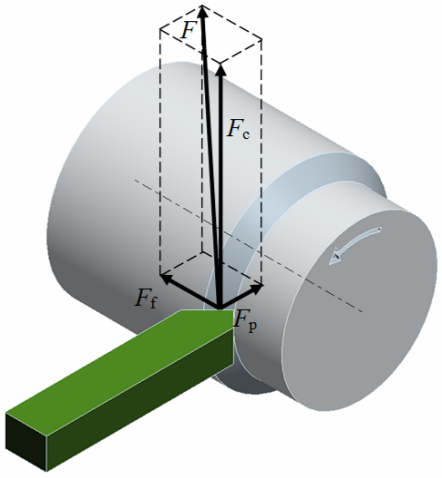

Fig. 1 Division of cutting force during turning

Tangentially situated cutting (main) force F_c lies in the direction of cutting force. The value of force F_c is necessary for the calculation of the power of the main movement, tool stiffness and machine mechanism parts. It determines torsion moment on the spindle. If the centre of the force effect point is considered to be in the centre of the cutting edge, the following equation is valid:

$$M_k = F_c \cdot \left(\frac{D}{2} - \frac{a_p}{2} \right) \quad (1)$$

because D is usually much larger than a_p, therefore a_p can be neglected in practical conditions.

Radially situated passive force F_p influences the movement of parts and the stiffness of turning machine and tool. Its values are necessary for the calculation of the accuracy of turned parts and the stiffness of technological system [11].

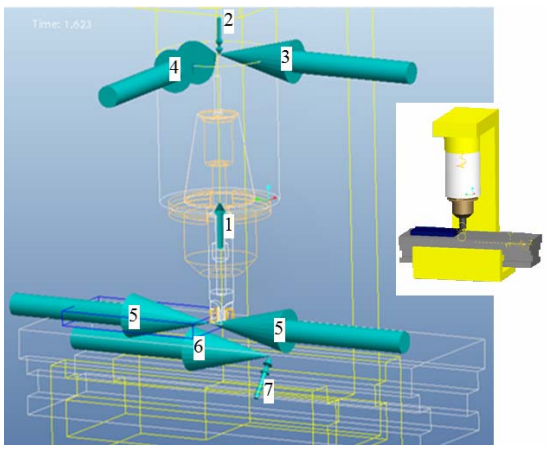

Fig. 2 Forces and moments during milling

Fig. 2 shows magnitudes and directions of forces and moments directly in assembly model graphically in moment of contact between tool tip and workpiece. 1 is axial force, 2 is axial moment, 3 is radial force, 4 is radial moment, 5 is normal forces, 6 is force in worktable, 7 is moment in worktable. The final of simulation is illustration of forces and moments by arrows (vectors). The magnitudes of forces and moments are described by their thickness (except axial force and moment in Fig. 2 that are 600-times lower according to simulation).

2. EXPERIMENTAL MEASURING

Experimental measuring was made for turning in centre machine. The machining force was moving from tailstock to headstock. The cutting conditions were arranged to evoke minimal vibrations during turning. The length of steel cylindrical workpiece is 300 mm with uniform cross-section of original diameter 20 mm. The diameter of the workpiece was measured after turning by dial indicator (Fig. 3).

Fig. 3 Measurement of the workpiece shape

The stiffness of the chuck is larger than the one of the tailstock, but different jaws have different stiffness. The situation is more complicated. During measurement of the roundness of the workpiece in fixing by minimal fixing force $F_{u\ min}$, a shift of the workpiece axis (e), which corresponds with spindle run-out, is identified. Deformed triangle workpiece profile (Fig. 4) shifted by run-out is measured applying the fixing forces. The different stiffness of individual jaws is visible.

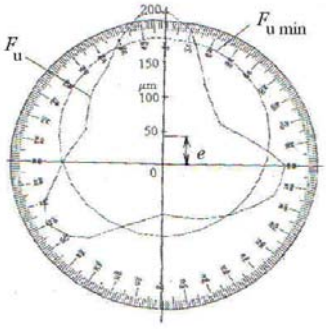

Fig. 4 Workpiece profile in the vicinity of chuck with elastic three-jaw

3. NUMERICAL APPROACH BY FEM

The values of the displacements cause shape (geometric and dimensional) inaccuracy of turned cylindrical surface and milled plain surface. The aim of numerical experiments was the comparing of measured data and computed data in case of turning. The milling was analysed regarding the displacements causing concavity of plain surface.

Computational model used p-version of the Finite Element Method (FEM). The oscillation of the system machine-tool-workpiece is not considered.

3.1 Turning

During real experiment the workpiece was clamped into a chuck and centre, the stiffness of which was unknown [12]. During numerical experiment, their stiffness and the type of workpiece clamping was determine, i.e. fix-fix (Fig. 5), fix-pin constraint. If clamping into the centre is considered as a elastic pin, than the numerically and experimentally obtained values show considerable difference. The different mechanical behaviour is for the tailstock side modelled as elastic pin even in case of different ratios of stiffness of the tailstock and headstock. Therefore this type of constraint is not considered in further solution.

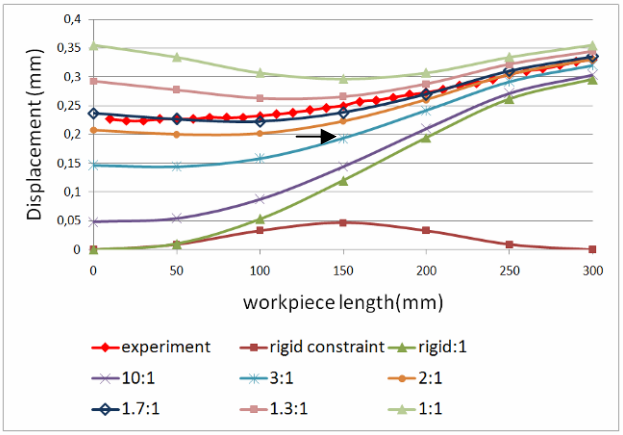

Fig. 5 Constaint: elastic fix – elastic fix

The best fitting with the experimentally measured curve ♦ in Fig. 5 is shown by ◊ with the ratio of stiffness of the headstock c_h and the tailstock c_t 1.7:1 (c_h =1700 N/mm, c_t =1000 N/mm). Maximum difference in values is 0.012 mm what is 4.8%.

Fig. 6 shows deflection curves of the workpiece with changing position of working force F_p. The deflection curves (shape of workpiece axis) are being changed in individual phases of turning and they are considerably different. The ratios of stiffness of headstock and tailstock as well as their values contribute to the differences of deflection curves. The resulting curve presenting the shape of workpiece final profile is obtained from the deflections (shape differencies) in the places where force F_p acts. The effect point of the force is presented by a circle. In Fig. 6 the ratio of the stiffness of the headstock c_h and the tailstock c_t is 3:1 (c_h=3000N/mm, c_t=1000N/mm).

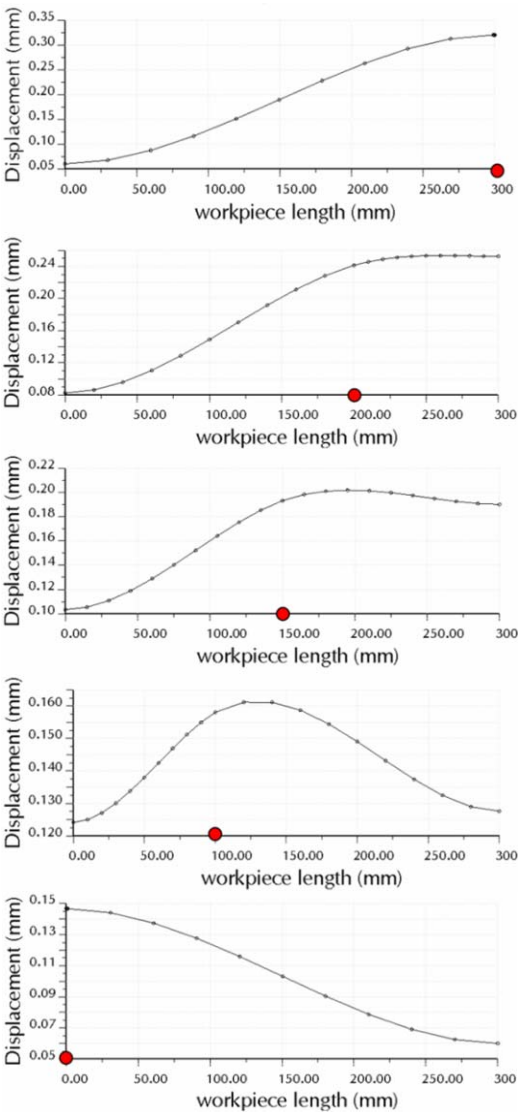

Fig. 6 Deflection curves during turning with elastic fixes

Fig. 7 presents comparison of final surface shape for rigid and elastic workpiece clamping. (a, b) and final shape of workpiece clamped in rigid chuck with elastic jaws. The difference is obvious. The deformations are shown 100-times larger as calculated ones (a, b). The workpiece in Fig. 7a represents final surface shape for rigid fixes, Fig. 7b for elastic fixes (c_h: c_t is 1.7:1). The real clamps are elastic as the each component joint of machine structure.

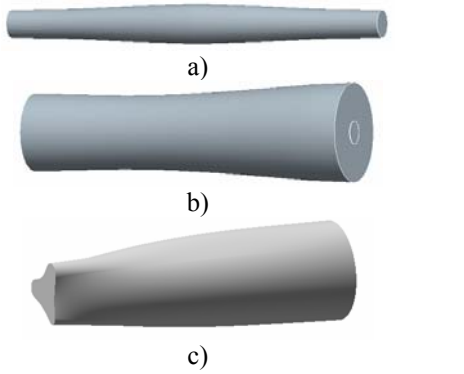

Fig. 7 Final surface shape: rigid (a) and elastic clamping (b) rigidchuck with elastic three-jaw (c)

3.2 Milling

Spindle tilt produces a concave machined surface and results flatness error. The depth of concavity d_f (Fig. 8) can be calculated from the Kirchner-Schutz formula [10]:

$$d_f = tg\theta\left[\frac{D_e}{2} - \left(\frac{D_e^2}{4} - \frac{e^2}{4}\right)^{\frac{1}{2}}\right] \quad (2)$$

where D_e is effective diameter of cutter, mm, e is the width of workpiece (Fig. 8), mm, θ is the spindle tilt angle, °.

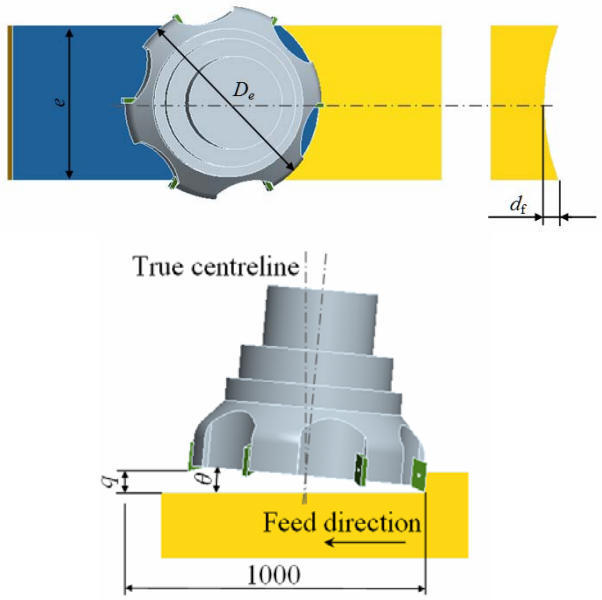

Fig. 8 Concavity d_f (upper) and spindle tilt angle θ

According to [13], mill spindle tilt q is about 0.1mm for length 1000mm, Fig. 8. Deformed and un-deformed numerical model and displacement of point A that caused concavity of milled surface is shown in Fig. 9.

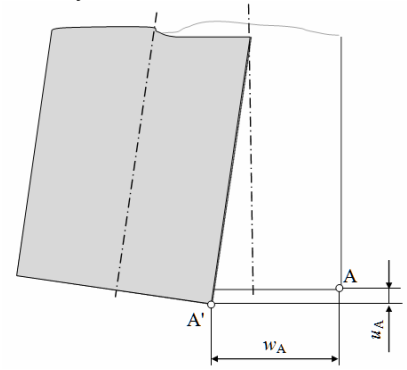

Fig. 9 Numerical model with displacement of A

4. ANALYTICAL CALCULATION

4.1 Turning

By the consideration of elastic fixes it is necessary to solve three times statically indeterminate beam with elastic fixes according to Fig. 10 with given stiffness. By the use of the method of canonic equations the values of reactions, distribution of shear forces and bending moments of this statically indeterminate task been obtained [14].

The displacement of the headstock y_h and tailstock y_t can be calculated as follows:

$$y_h = H\, w_h$$
$$y_t = T\, w_t \tag{3}$$

where H and T are reactions in headstock and tailstock.

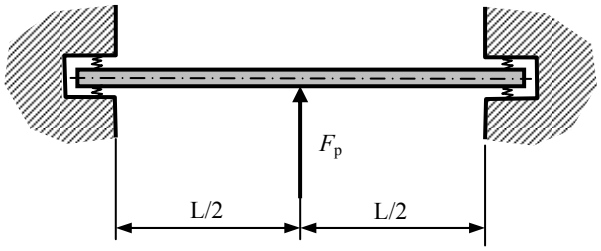

Fig. 10 Calculation model - turning

The displacement y that corresponds with final accuracy is:

$$y = y_{work} + y_{ax} \tag{4}$$

where y_{work} for F_p in the middle of workpiece length (Fig.10) is calculated as follows:

$$y_{work} = \frac{F.L^3}{192.E.J_y} \tag{5}$$

where E is Young's modulus of elasticity and J_y is moment of inertia of y axis: $J_y=\pi.r^4/4$.

The displacement of the workpiece axis y_{ax} in the middle of the workpiece considering different elasticity of the headstock and the tailstock can be determined:

$$y_{ax} = \frac{1}{2}\left(H\, w_h + T\, w_t\right) \tag{6}$$

4.2 Milling

We can recognize the spindle with tool as the cantilever beam loaded by feed force F_f (denoted as normal force – 5 in Fig. 2) causes the displacements and deflection of spindle and consequently the inaccuracy of milled workpiece.

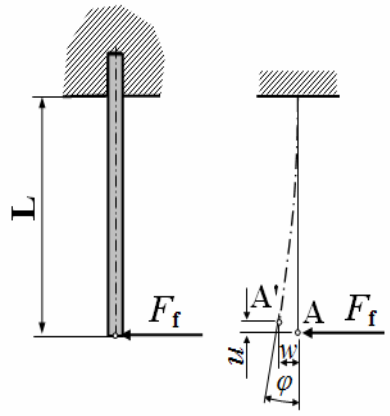

Fig. 10 Calculation model - milling

The known formulas for analytical calculation the cantilever beam deflection w due to bending and slope φ in the end point A:

$$w_A = \frac{F_f\, L^3}{3\, E\, J}\ ;\quad \varphi_A = \frac{F_f\, L^2}{2\, E\, J} \tag{7}$$

5. CONCLUSION

It can be seen that the stiffness of technological system considerably influences workpiece accuracy. It can be said that the productivity of maching depends on the stiffness of technological system. When the stiffness is not sufficient, it is necessary to adjust cutting conditions, increase the number of finishing transfers or apply minimal displacement. Similarly, the geometric deflections for miller can be identified.

6. REFERENCES

[1] DEMEČ, P., SVETLÍK, J., SEMJON, J.: *Vitrtuálne prototypovanie obrábacách strojov z hľadiska dynamiky procesov obrábania*, Košice: SF TUKE, 2011, 182 s.

[2] QIANG, L. Z. Finite difference calculations of the deformations of multi-diameter workpieces during turning. In: *Journal of Materials Processing Technology*, Vol. 98, pp. 310-316, Elsevier, 2000.

[3] SLATINEANU, L. et al: Static Deformation of a Workpiece Fixed in Universal Chuck and Life Centre. In: *Tehnomus – New Technologies and Products in Machine Manufacturing Technologies*, pp. 233-238, No. 18, Stefan Cel Mare University of Suceava, 2011.

[4] ZENG, Y.: *Finite Element Analysis of Fixture Stiffness*. Ph.D. Dissertation. Worchester Polytechnic Institute, Worchester, 2005.

[5] BUDA, J., BÉKÉS,J.: *Teoretické základy obrábania kovov.* Bratislava: ALFA, 1967.

[6] GRZESIK, W.: *Podstawy skawania materialow metalowych.* Warszawa: Wydawnictwa Naukowo-Techniczne, 2010, 526 s.

[7] PŘIKRYL, Z., MUSÍLKOVÁ, R.: *Teorie obrábění.* Praha: SNTL, 1982, 235 s.

[8] WEBER, H., LOLADZE, T.N.: *Grundlagen des Spanens.* Berlin: VEB Verlag Technik, 1986.

[9] DUGIN, A., POPOV, A.. Effect of the processing materials on the ploughing force values. *Manufacturing Technology,* Vol. 12, No. 13, 2012, pp.102-105.

[10] SMITH, G. T.: *Advanced machining*. pp. 198-233, Springer-Verlag, New York, 1989.

[11] MÁDL, J., KVASNIČKA, J.: *Optimalizace obráběcího procesu.* Praha: Vydavatelství ČVUT, 1998, 168 s.

[12] KUNDRÁK, J., GYÁNI,K., DESZPOTH, I.: The effect of the borehole diameter on the machining times in hard machining. *Manufacturing Technologies*, Vol. 12, No. 13, pp. 144-150.

[13] Sandvik Coromat, *Příručka obrábění (Handbook of manufacturing)*. Scientia, 1997.

[14] MURČINKOVÁ, Z.: *Pružnosť a pevnosť 1 Mechanika poddajných telies*, pp. 121. Technical University in Košice, Prešov, 2011.

Authors: **Assoc. Prof. M.Sc. Zuzana Murčinková, PhD., Dr.h.c. prof. M.Sc. Karol Vasilko, DrSc.,** Faculty of Manufacturing Technologies, Technical University in Košice, Bayerova 1, 080 01 Prešov,
E-mail: zuzana.murcinkova@tuke.sk
karol.vasilko@tuke.sk

Journal of Production Engineering
Vol.16 No.2

Original Scientific Paper

Pucovsky, V., Kramar, D., Sekulić, M.

HIGH-PRESSURE JET ASSISTED TURNING PROCESS MODELLED WITH EVOLUTIONARY ALGORITHM

Received: 09 September 2013 / Accepted: 30 October 2013

Abstract: *Genetic algorithms present an efficient way of machining processes modelling. They have proven this on numerous occasions so it was assumed that they can be used in this advanced machining system. Inconel 718 was machined with high-pressure jet assisted turning process and the main cutting force F_v was measured. Model for calculating the cutting force F_v depending on the process parameters was used to, with genetic algorithms adapt constants figuring in this function so that modelled results were as much as possible closer to experimental values.*
Key words: *high-pressure jet assisted turning process, main cutting force, genetic algorithm, modelling.*

Proces struganja hlađen mlazom visokog pritiska modelovan sa evolutivnim algoritmima. *Genetski algoritmi predstavljaju efikasan način modelovanja procesa obrade. Ovo je dokazano u brojnim prilikama pa se stoga opravdano pretpostavljalo da će se moći iskoristiti i kod ovog naprednog sistema obrade. Inconel 718 je pri struganju hlađen mlazom visokog pritiska i merena je glavna sila rezanja F_v. Model za izračunavanje sile rezanja, u zavisnosti od parametara procesa, je bio namenjen da sa genetskim algoritmima prilagodi konstante figurišuće u ovoj funkciji tako da modelovani rezultati budu što je moguće bliže eksperimentalnim vrednosti.*
Ključne reči: *struganje potpomognuto hlađenjem visokom pritiskom, glavna sila rezanja, genetski algoritmi, modelovanje*

1. INTRODUCTION

With everyday increasing demand of the market, each branch of the industry is trying to meet those demands in order to gain profit. Meeting this goal is not always easy. Sometimes it's not all about working hard but rather working smart. Machining industry, as one of the main driving forces in modern world, has to keep up with contemporary technical and technological trends. Many times, just to be in line with market demands, it has to set up new trends. This radical type of influence has to be supported with adequate knowledge base and scientific guidance. Content of this paper has, although in small dose, injected that much needed scientific contribution to the practical realization of machining industry. Combining two highly potential tools from engineering branch, authors managed to improve existing machining process and thus hopefully save both financial funds and resources.

On the one side there is a machining technology that already showed its ability and had secured its place in modern machining shops. Turning process with assisted high-pressure jet coolant is a modern way to improve classical machining technology. With added feature of high pressure coolant it expanded the use of classical machining range and now can be also used on hard to machine materials.

On the other side lies a powerful artificial brain with its algorithms being improved almost on a daily basis. Genetic algorithms, as a subgroup of evolutionary algorithms, had already shown their potential in machining industry and new usage is still being discovered.

This paper presents a modelling of the main cutting force values during high-pressure jet assisted turning process. Modelling is done with genetic algorithms, as a type of artificial intelligence. Comparison is than made between experimentally obtained data and modelled results [1, 2].

2. EXPERIMENT AND MODELING

The experimental work was carried out at the Laboratory for Machining, the Faculty of Mechanical Engineering in Ljubljana. The experiments were conducted in longitudinal turning process on conventional lathe, fitted with a Hammelmann high-pressure plunger pump of 150 MPa pressure and 8 l/min capacity. The fluid used was the Vasco 5000 cooling lubricant from Blaser Swisslube Inc., a 5,5% emulsion without chlorine on the basis of vegetable oil mixed with water (pH 8,5-9,2). The jet was directed normal to the cutting edge at a low angle (about 5-6°) with tool rake face. As an input data five process parameters were varied: diameter of the nozzle D_n (mm), desistance between the impact point of the jet and the cutting edge d (mm), pressure of the jet P (MPa), cutting speed v_c (m/mm) and feed rate f (mm/rev) [3, 4].

All experiments were carried out using the nickel-based alloy Inconel 718 supplied as bars (145 mm diameter x 300 mm long) with hardness between 36 and 38 HRC by orthogonal arrays with three levels (coded by: 1, 2 and 3), Table 1. A PVD TiAlN-coated carbide tool (grade P25) SNMG 12 04 08-23 has been chosen. The cutting tool was mounted on the static dynamometer (Kistler® 9259A). The measurement chain also included a charge amplifier (Kistler® 5001), a data

acquisition hardware (NI® USB-6218 BNC) and a graphical programming environment (NI® LabVIEW) for data analysis and visualization. Subject of this study is to modeling dependence of the main cutting force F_v on the input data five process parameters by genetic algorithms.

Symbol	Parameters	Levels		
		1	2	3
A	Diameter of the nozzle, D_n (mm)	0,25	0,3	0,4
B	Dist. between the impact point of the jet and the cutting edge, d (mm)	0	1,5	3,0
C	Pressure of the jet, P (MPa)	50	90	130
D	Cutting speed, V_c (m/min)	46	57	74
E	Feed rate, f (mm/rev)	0,2	0,224	0,25

Table 1. Machining parameters and their levels

For modelling purposes only 20 instances were used (Table 2) and remaining 7 (Table 2) were used for evaluation of model. As a modelled function, linear regression model (Eq 1) will be used.

$$F_v = C_1 + C_2 \cdot D_n + C_3 \cdot P + C_4 \cdot v + C_5 \cdot f + C_6 \cdot P \cdot v \quad (1)$$

Within this paper, genetic algorithms will be employed to search for optimal values of constants C_1, C_2, ... C_6 for which modelled equation will give the smallest deviation from experimentally obtained data. Genetic algorithms are, as mentioned above, a part of evolutionary algorithms which means that their main principle is based on theory of evolution resp. survival of the fittest. On the beginning of the process 1000 individuals are randomly created. These individuals are actually possible solution for the problem and contain constants C_1, C_2, ... C_6. Next step is to incorporate all those constants to Equation 1 and send every result to the fitness function for evaluation. Fitness function is a measure of success for each individual and is directly involved in direction of further population development. Fitness function is actually an average of percent errors (Eq 2) for all instances with one solution of constants:

$$\Delta = \sum_{i=1}^{20} \left| \frac{E_i - M_i}{E_i} \right| \cdot 100[\%] \quad (2)$$

where E_i is an experimentally obtained value of the main cutting force and M_i is its modeled value. After an evaluation, 40 of the top ranked are automatically transferred to the next generation. This step is called elitism and is necessary in order to preserve the best genetic material. Next, potential parents for the next generation of individuals are created. This is done by putting into effect so called tournament selection. 80 individuals are randomly selected from current generation and the best one is placed into the mating pool. This step is repeated until enough parents are selected to form 80% of the next generation which are created by crossover of individuals from mating pool. Remaining individuals are created with direct mutation of their predecessors. Mutation is employed in order to insert fresh genetic material in population and prevent an algorithm to get stuck in local minimum. After 1000 generations the best solution contained constants, which implemented into Equation 1 creates an Equation 3.

3. RESULTS

Values of process parameters, used to model the resulting function, implemented into Equation 3 will make the following results (Table 2).
Mentioned resulting equation will be:

$$F_v = 37{,}758 + 8{,}015 \cdot D_n + 11{,}757 \cdot P + 19{,}936 \cdot v + 41{,}232 \cdot f - 0{,}185 \cdot P \cdot v \quad (3)$$

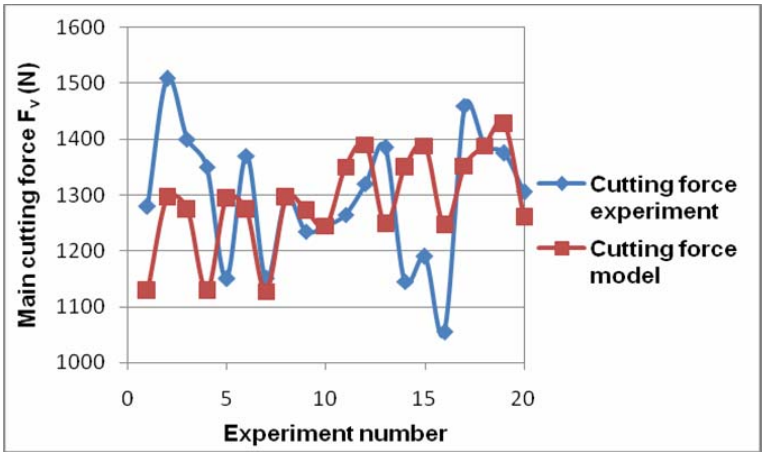

Fig. 1. Graphical comparison between modelled and experimental data, used for modelling of the main cutting force F_v

No	D_n (mm)	d (mm)	P (MPa)	v (m/min)	s (mm/o)	F_v, exper. (N)	F_v, model (N)	Error (%)
1	0,25	0	50	46	0,2	1280	1128	11,9
2	0,25	0	90	57	0,224	1508	1295	14,1
3	0,25	0	130	74	0,25	1400	1274	9
4	0,25	1,5	50	46	0,25	1350	1128	16,4
5	0,25	1,5	90	57	0,2	1150	1293	12,4
6	0,25	1,5	130	74	0,224	1370	1273	7,1
7	0,25	3	50	46	0,224	1150	1127	2
8	0,25	3	90	57	0,25	1295	1295	0
9	0,25	3	130	74	0,2	1235	1272	3
10	0,3	0	50	57	0,2	1245	1245	0
11	0,3	0	90	74	0,224	1265	1350	6,3
12	0,3	0	130	46	0,25	1320	1390	5,3
13	0,3	1,5	50	57	0,25	1385	1248	9,9
14	0,3	1,5	90	74	0,2	1145	1349	17,8
15	0,3	1,5	130	46	0,224	1190	1388	16,6
16	0,3	3	50	57	0,224	1055	1246	18,1
17	0,3	3	90	74	0,25	1460	1352	7,4
18	0,3	3	130	46	0,2	1390	1388	0,1
19	0,4	0	50	74	0,2	1375	1427	3,8
20	0,4	0	90	46	0,224	1305	1260	3,4
							Δ→	**8,23**

Table 2. Data used for experiments and results of the main cutting force obtained both experimentally and modelled by Equation 3 (modelling data).

No	D_n (mm)	d (mm)	P (MPa)	v (m/min)	s (mm/o)	F_v, exper. (N)	F_v, model (N)	Error (%)
1	0,4	0	130	57	0,25	1320	1345	1,9
2	0,4	1,5	50	74	0,25	1250	1429	14,3
3	0,4	1,5	90	46	0,2	1275	1221	4,2
4	0,4	1,5	130	57	0,224	1465	1345	8,2
5	0,4	3	50	74	0,224	1187	1428	20,3
6	0,4	3	90	46	0,25	1160	1260	8,6
7	0,4	3	130	57	0,2	1450	1344	7,3
							Δ→	**8,87**

Table 3. Data used for experiments and results of the main cutting force obtained both experimentally and modelled by Equation 3 (only verification data).

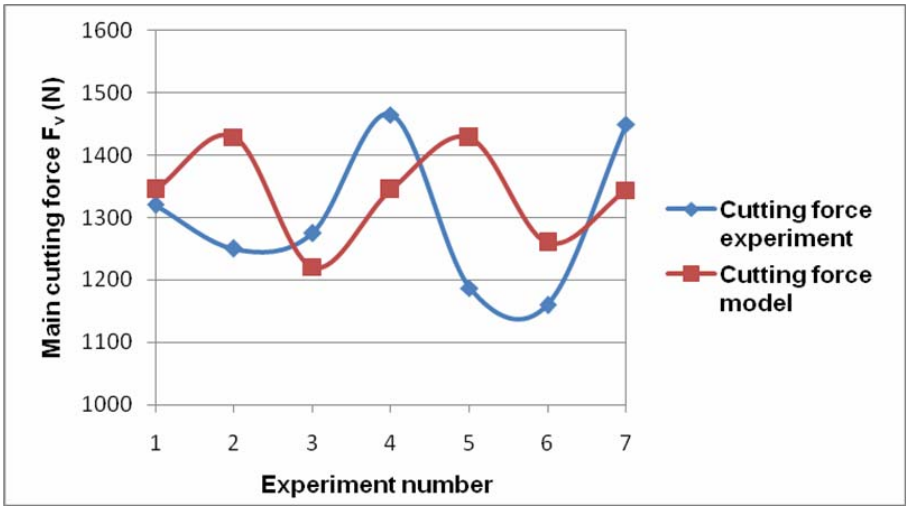

Fig. 2. Graphical comparison between modelled and experimental data, used only for verification of the model, of the main cutting force F_v

As can be seen the average percent error is 8,23% which is, taking in consideration an amount of data used for modelling, acceptable value. Graphical representation of these values, and direct comparison between experimental and modelled data, is shown in Fig 1.

Remaining 7 instances, which were not used for modelling purposes, are now employed to judge the quality of yielded model. As presented in Table 3 the average percent error in this case was 8,87% which is near to that in Table 2. This indicates that the model is adequate and valid. Figure 2 presents a graphical representation of results from Table 3.

4. DISCUSSION

Yielded results generated average percent error of 8,23 resp 8,87%. These results, by authors opinion, are acceptable because of couple of factors; data used for modelling is scarce and the model of the function (Eq 1) is simple linear type which offers very little flexibility. Despite of these limiting factors obtained results are independent and can be used without the use of computer.

5. CONCLUSIONS

Generated results, as mentioned in previous chapter, are in acceptable range. Further improvement can be done by increasing the quantity of experimental instances. Also various types of equations for modelling of cutting force can be tried and hopefully find some model which will suite this purpose better.

6. ACKNOWLEDGEMENT

This work was supported by CEEPUS – Central European Exchange Program for University Studies network: CIII-RS-0507-03-1314 with title 'Research develpement and education in Precision machining'.

7. REFERENCES

[1] V. Pucovsky, P. Kovac, M. Tolnay, B. Savkovic, D. Rodic: The Adequate Type of Function for Modeling Tool Life Selction by the Use of Genetic Algorithms. Journal of Production Engineering, pp. 25-28, Vol. 15, (1), 2012.

[2] D. Kramar, M. Sekulic, P. Kovac, M. Gostimirovic, J. Kopac: The Implementation of Taguchi Method for Quality Improvement in High-pressure Jet Assisted Turning Process. Journal of Production Engineering, pp. 23-26, Vol. 15 (2), 2012.

[3] D. Kramar, M. Sekulic, Z. Jurkovic, J. Kopac: The Machinability of Nickel-based Alloys in High-pressure Jet Assisted (HPJA) Turning. Metalurgija, pp. 512-514, Vol 52 (4), 2013.

[4] D. Kramar, J. Kopac: High Pressure Cooling in the Machining of Hard-to-Machine Materials. Strojniski vestnik – Journal of Mechanical Engineering, Vol. 55 (11), 2009.

Authors: **Vladimir Pucovsky, Milenko Sekulić,** University of Novi Sad, Faculty of Technical Sciences, Institute for Production Engineering, Trg Dositeja Obradovica 6, 21000 Novi Sad, Serbia, e-mail: pucovski@uns.ac.rs, milenkos@uns.ac.rs

Davorin Kramar, University of Ljubljana, Slovenia

Journal of Production Engineering
Vol.16 No.2

Original Scientific Paper

Duspara, M., Kosec, B., Stoić, M., Kramar, D., Stoić, A.

APPLICATION OF VORTEX TUBE FOR TOOL COOLING

Received: 18 September 2013 / Accepted: 29 October 2013

Abstract: *The environmental pollution and health hazards of traditional tool cooling technique applied for machining processes will be evaluated and compared with new acceptable alternatives, based on six main sustainability aspects: cost, environment impact, energy consumption, waste management, safety and personal health. The innovative technique with the analytical predictive models has to be developed for industrial applications. This technologies show high potential of productivity increasing while assuring sustainability principles. The introduction of dry machining is one of sollution of today's metal cutting industry that tirelessly endeavours to reduce machining costs and impact from chemicals in the environment. Modern tool tips are already capable of maintaining their cutting edge at higher temperatures, but even with these improvements in tool materials, the cutting edge will eventually break down. Applying cold air to the tool interface of these modern tool tips will also extend their tool life reducing the cost of metal cutting.*
Key words: *Dry machining, air-cooling, principle of work of vortex tube*

Primena vrtložne cevi za hlađenje alata. *Zagađivanje okoline i zdravstveni rizik koji predstavljaju tradicionalne tehnike hlađenja alata u procesima obrade će biti ocenjene i upoređene sa novim prihvatljivim alternativama, baziranih na šest glavnih aspekata održivosti: troškovi, uticaj na životnu sredinu, potrošnja energije, upravljane otpadom, bezbednost i lično zdravlje. Inovativne tehnike sa analitički predvidljivim modelima se moraju razvijati za industrijske primene. Ove tehnologije su pokazale veliki potencijal povećanja proizvodnosti a ujedno i obezbeđivanje principa održivosti. Uvođenje suve obrade je jedno od rešenja današnje industrije koja neumorno pokušava da smanji troškove obrade ali i uticaj hemikalija na okolinu. Rezne ivice modernih alata su sposobne da zadrže oštrost i pri povišenim temperaturama ali i sa ovim poboljšanjima, vremenom će doći do njihovog habanja. Korišćenje hladnog vazduha za hlađenje alata će takođe poboljšati postojanost a ujedno smanjiti troškove obrade.*
Ključne reči: *suva obrada, hlađenje vazduhom, princip rada vrtložne cevi*

1. INTRODUCTION

The vortex tube was discovered by Ranque [1] and first described in detail by Hilsch [2]. Vortex tubes are now commercially used [3] for low-temperature applications, e.g. to cool parts of machines, to set solders, to cool electronic control cabinets, to chill environmental chambers, to cool food, to test temperature sensors, and they are also applied to dehumidify gas samples [4].
Recently it has been proposed that vortex tubes could be used as components in refrigeration systems replacing the conventional expansion nozzle in order to increase the efficiency [5].
The coolants in refrigeration systems pass through a thermal cycle in which the pressure may well drop below atmospheric.

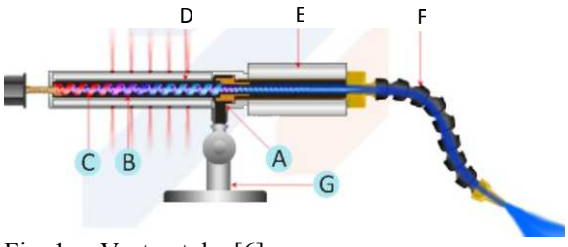

Fig. 1. Vortex tube [6]

ADJUSTABLE SPOT COOLER ADVANTAGES

- No moving parts.
- Quiet
- Driven by air and not electricity.
- Small and light weight-portable.
- Low in cost compared to most others
- Superior design and performance
- Maintenance free operation
- Made of durable stainless steel and metal parts, no cheap plastic parts
- Adjustable temperature range
- Generators are interchangeable
- System uses strong magnetic base

Figure 1 shows adjustable Spot Cooler-Compressed air enters at point (A) into the vortex tube component of the spot cooler. The vortex tube splits the compressed air into a hot (B) and cold (C) stream of air. The hot air from the vortex tube is vented to the atmosphere at point (D) after being muffled to reduce noise. Cold air enters into the muffler (E) and then distributed through the hose distribution kit (F) and onto the item being cooled. A strong magnet (G) holds the spot cooler in place. The temperature of the cold air is controlled by an adjustable knob.

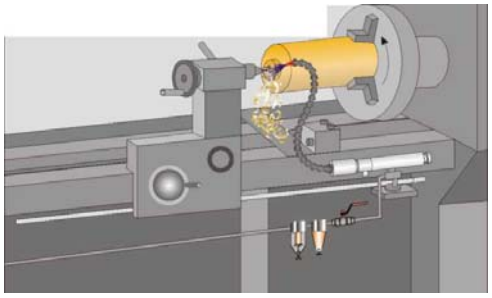

Fig. 2. Using vortex tube for cooling turning process [6]

2. PRINCIPLE OF WORK OF VORTEX TUBE

The flow rate and temperature in a Vortex Tube are interdependent. When you open the adjusting valve at the hot end, the cold air flow decreases and the temperature drops. As you close the valve the cold air end flow increases and temperature rises. The percentage of the total input air that exits the cold end is termed the "cold fraction". Depending on inlet air temperature a cold fraction of between 60% and 80% produces the optimum combination of flow and temperature drop for maximum cooling effect, when using an H generator. Lower cold fractions produce colder air but do not cool as well because of reduced flow. Most industrial applications require the 60% to 80% setting and the H generator for optimal cooling. In some instances such as cooling laboratory samples, testing circuit boards and other "cryogenic" applications, a 'C generator is used which limits the cold end flow rate to lower levels and produces very cold temperatures. To set the Vortex Tube to the desired temperature simply insert a thermometer at the cold end and adjust the hot end valve.

The inlet nozzle is tangential to the vortex generator and therefore can provide a high speed rotating airflow inside the vortex generator. Subsequently, there is a radial temperature gradient increasing from the inner core of the tube to the outside wall of the tube. This is primarily because of the potential energy of compressed air converting to kinetic energy due to the forced vortex caused by the external torque near the tangential air inlet. Therefore the high-speed swirling flow inside the tube and away from the walls is created. The existing air inside the vortex hot tube is normally at the atmospheric temperature and so, when the rotating flow enters the vortex tube it expands and its temperature drops to a temperature lower than the ambient temperature. The difference between these two temperatures will lead to a temperature gradient along the tube producing colder peripheral air than the core air. As a result, the central air molecules will lose heat to those in the outer region as shown in Fig. 3.

It is notable that this system is a dynamic system due to the nature of the airflow in the tube and so will not reach equilibrium. Hence the peripheral air has a higher kinetic energy (hotter) than the inner air (colder). The existence of a major pressure gradient due to the forced vortex in the radial direction will provide a centripetal force for circular swirling and therefore it will lead to a high pressure at the tube wall and low pressure at the centre. When the air enters to peripheral region (A), as it expands, the outer air will be cooled due to its expansion. Consequently, the inner core air (B) will get warm because it is compressed by the expansion of the peripheral air.

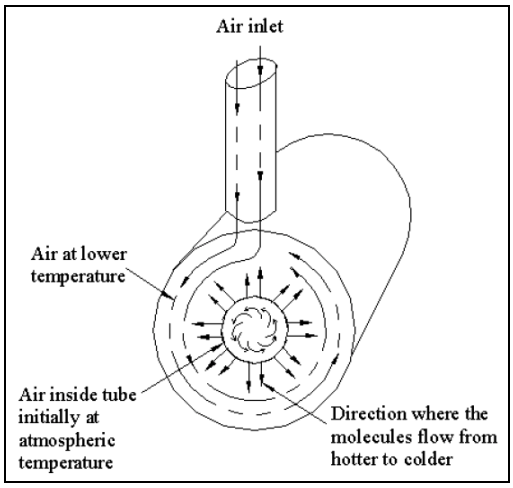

Fig. 3. Radial heat convection in vortex tube due to the expansion of the compressed air [7]

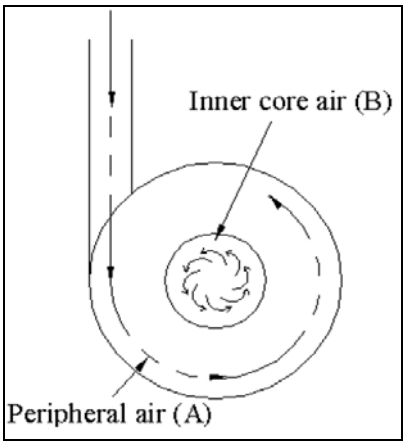

Fig. 4. Schematic positions of the peripheral and inner core air [7]

Heat is then transferred from the inner core (B) to the outer core (A).

As the inner air is being compressed, it naturally tries to push against the periphery by expanding. Work is therefore done on the outer core air, which then gets heated and the difference in pressures results in the expansion and contraction of the air, which causes work to be done on the peripheral air. Work is therefore done on the outer core air, which then gets heated and the difference in pressures results in the expansion and contraction of the air, which causes work to be done on the peripheral air. Therefore, heat is transferred radially outward as shown in Fig. 4.

2.1 Temperature of hot/cold side on vortex tube

The vortex tube with atmospheric inlet pressure was operated for a variety of cold gas fractions $Y = j_c/j_0$. The temperature measurements are shown in Fig. 5.

Clearly the temperature splitting effect is obtained. The cooling is well developed, but it appears as if the heating is not quite as pronounced. We have lately

become aware that varying the moisture content of the ambient air will change the thermal capacity of this working fluid significantly and hence contribute to variations of the temperature change. This effect could easily amount to several degrees and it should be more pronounced in the hot flow component than in the cold stream.

To put the temperature measurements into perspective several high-pressure curves for the same vortex tube are given in Fig. 6.

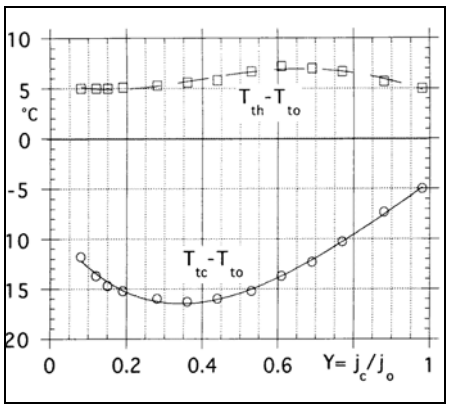

Fig. 5. Exit temperatures for vortex tube with atmosperic inlet pressure [8]

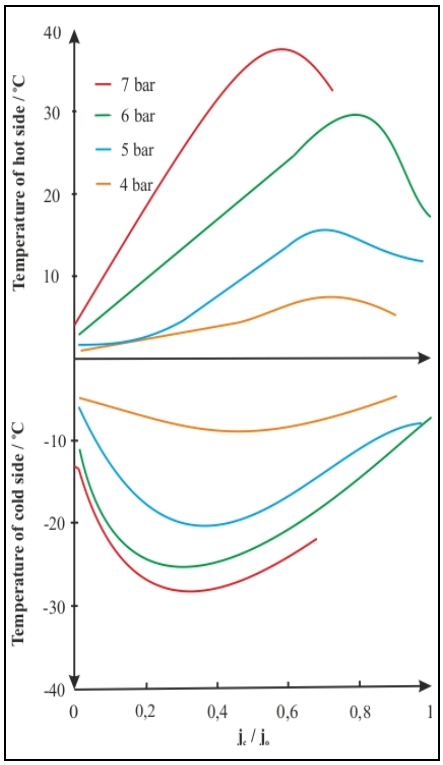

Fig. 6. Total temperature separation for vortex tube operated with compressed air [8]

3. EFFECT OF AIR-COOLING ON TOOL LIFE

It is known that all the wear mechanisms increased at elevated temperatures reducing the tool life [9]. The application of cold air to the tool tip is shown to reduce the temperature at the tool tip enabling the tool tip to have a longer tool life [10]. The effectiveness of the air-cooled system can be shown when a comparison is made between the wear for a dry cut and an air-cooled cut for one minute and seven minutes of machining. Fig. 7a-d show the flank wear as seen under a microscope.

The development of the flank wear was shown to take longer to develop when the cooled air was applied to the cutting zone as shown in Fig. 7d.

After seven minutes of dry machining the top rake face is starting to develop crater wear, at 0.5 mm from the flank face as shown in Fig. 8. Further dry machining will accelerate this rate of wear. At this stage the tool radius shows no sign of wear and the top flank edge has no observable notches.

The air-cooled tool tip shows no visible sign of tool wear on the top rake face and the flank wear is also substantially reduced. Observation of the chips produced during dry and air-cooling indicated that much of the heat was being dissipated from the cutting zone.

Figure 9 shows the chips produced during the dry and air-cooled tool tip test. The left hand chips produced during dry cutting and the right hand produced during air-cooling.

4. CONCLUSION

The results obtained from using compressed air combined with the vortex tube have shown that this method of cooling the tool interface is effective and compares exceedingly well with traditional cooling methods. The temperature recoded during air-cooling was found to be 60°C which is 40 °C cooler than that obtained during traditional wet machining and 210 °C cooler than dry machining as shown by Fig. 10. These temperatures were measured 1 mm from the tool interface and for that reason the temperatures recorded at this position are considerably reduced from that of the tool interface.

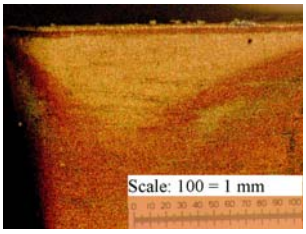

Fig. 7a. Picture showing flank wear for a dry cut after 1 minute of machining at a cutting speed of 190 m min-1 and feed rate of 0.23 mm/rev with a 2 mm depth of cut [7]

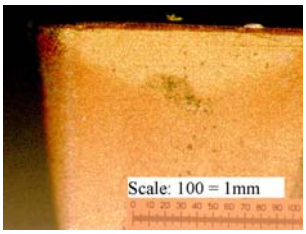

Fig. 7b. Picture showing flank wear for an air-cooled cut after 1 minute of machining at a cutting speed of 190 m min-1 and feed rate of 0.23 mm/rev with a 2 mm depth of cut [7]

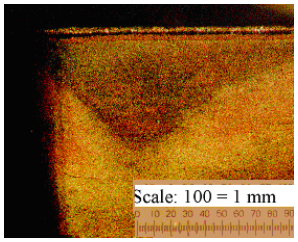

Fig. 7c. Picture showing flank wear for a dry cut after 7 minute of machining at a cutting speed of 190 m min-1 and feed rate of 0.23 mm/rev with a 2 mm depth of cut

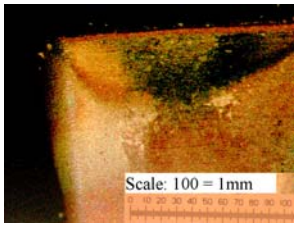

Fig. 7d. Picture showing flank wear for a air-cooled cut after 7 minutes of machining at a cutting speed of 190 m min-1, and feed rate of 0.23 mm/rev with a 2 mm depth of cut

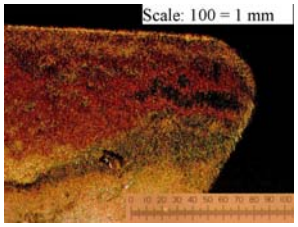

Fig. 8a. Picture showing top rake face wear for a dry cut after 7 minutes of machining at a cutting speed of 190 m min1, and feed rate of 0.23 mm/rev with a 2 mm depth of cut [7]

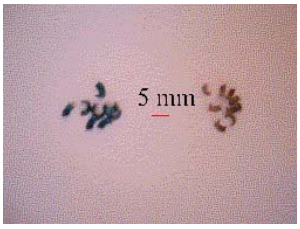

Fig. 9. Picture showing chips produced by a 2 mm depth of cut at 0.23 feed rate, and cutting speed of 190 m min-1 [7]

The most convenient method of determining the effectiveness of the air-cooling is by determining the tool life, as it is known that there is a relationship between tool life and the wear mechanisms that are shown to increase at elevated cutting temperatures. Inspection of the tool tip using a microscope confirmed that the tool wear is reduced when being air-cooled, resulting in longer tool life. The vortex tube air-cooling systems proved to be effective at dissipating the heat from the tool tip, proving that air-cooling is an effective method of cooling tool tips. Therefore, whenever dry machining is the preferred method of metal cutting, aircooling should be incorporated as there are no associated environmental issues and will extend the life of the tool.

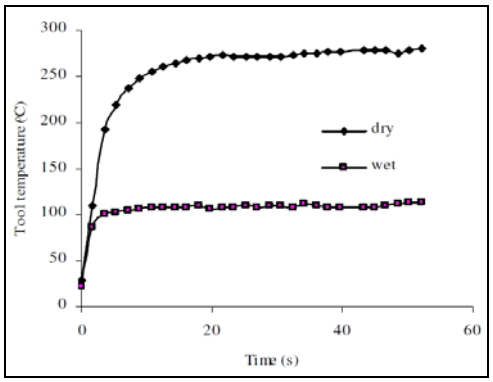

Fig. 10. Temperatures recoded at the tool tip for dry and air-cooling [7]

5. REFERENCES

[1] Ranque G J 1933 Exp´erienesd sur la detente giratoire avecproductions simultanes d'un echappement d'air chand etd'un echappement d'air froid J. Phys. Radium IV (7) 112–14.

[2] Hilsch R 1946 Die expansion von gasen im zentrifugalfeldals k¨alte prozess Z. Naturforsch. 1 208–14.

[3] Swirl Tubes Norgren 5400 South Delaware, Littletown, Colorado; Vortex Tubes Exair products, 1250 Century Circle North, Cincinnati, OH, 45246, USA; Vortex Tubes Vortec Corp, Cincinnati OH, USA.

[4] von Linde R 1950 Einrichtung zum abk¨uhlen einesverdichteten gases German Patent 926729 (24 October 1950).

[5] Keller J U 1993 J. Kl Klima Luft K¨alte Heizung 21 300–4.

[6] http://www.nex-flow.com/vortex_tube.htm (15.07.2013)

[7] Brian Boswell and Tilak T Chandratilleke; Air-Cooling Used For Metal Cutting, American Journal of Applied Sciences 6 (2): 251-262, 2009.

[8] B Ahlborny, J Camirey and J. U. Keller; Low-pressure vortex tubes, J. Phys. D: Appl. Phys. 29 (1996) 1469–1472.

[9] Young, H.T., 1996. Cutting temperatures to flank wear. Wear, 201: 117-120.

[10] Cook, N., 1973. Tool wear and tool life. ASME Tran. J. Energy. Ind., 95: 931-938.

Authors: **Miroslav Duspara, Antun Stoić**, Mechanical Engineering faculty in Slavonski Brod, e-mail: antun.stoic@gmail.com
Borut Kosec, Faculty of Natural Sciences and Engineering, Ljubljana
Marija Stoić, College of Slavonski Brod
Davorin Kramar, Faculty of Mechanical Engineerig, Ljubljana

Journal of Production Engineering
Vol.16 No.2

Original Scientific Paper

Zabkar, B., Kopač, J.

AN INVESTIGATION INTO ROLLER BURNISHING PROCESS

Received: 11 September 2013 / Accepted: 17 October 2013

Abstract: *Plastic deformation processes have been used to modify the surface roughness and integrity properties by generating fine grain size gradients in the surface region of many materials. These fine grained materials often exhibit enhanced surface integrity properties and improved functional performance (wear resistance, fatigue life, etc.) compared with their conventional coarse grained counterparts. Burnishing is a superficial plastic deformation process used as a surface smoothing and surface enhancement finishing treatment after some machining processes that eliminate secondary operations. In roller burnishing, a hard roller is pressed against a rotating cylindrical workpiece and parallel to the axis of the workpiece. Burnishing is a cold forming process, in which the material near a machined surface is displaced from peaks to fill the valleys of the surface profile. Roller burnishing is an economical process, which can be effectively used in many industrial fields. In the present work, various experiments are conducted to investigate the effect of burnishing force, burnishing feed and pre-machined surface roughness on surface roughness of roller burnished bearing steel.*

Key words: *Roller burnishing, surface roughness, process parameters*

Istraživanje procesa valjanja kotrljanjem. *Proces plastične deformacije se koristi za promenu površinske hrapavosti i integriteta osobina stvaranjem sitnozrne strukture na površinskom sloju mnogih materijala. Ovi sitnozrni materijali često pokazuju poboljšanje površinskog integriteta i poboljšanje funkcionalnih performansi (otpornost na habanje, zamor, itd) u poređenju sa njihovim konvencionalno grubljim kolegama. Valjanje kotrljanjem je proces površinske plastične deformacije, koji se koristi za ravnanje površina i poboljšavanje površinskih osobina posle nekih od procesa obrade, koji eliminiše skundarne obrade. Pri valjanju kotrljanjem tvrdi valjak je pritisnut uz rotirajući cilindrični pripremak i paralelan je sa osom obradka. Valjanje je proces hladne obrade u kome se materijal sa vrhova površine premešta u doline i na taj način popunjava površinski profil. Valjanje kotrljanjem je ekonomski proces koji može biti iskorišćen u mnogim poljima privrede. U ovom radu razni eksperimenti su sprovedeni radi istraživanja efekta sile valjanja, pomaka valjanja i hrapavosti površine pre obrade na hrapavost čelika za ležajeve valjanog kotrljanjem.*

Ključne reči: *valjanje kotrljanjem, površinska hrapavost, parametri procesa*

1. INTRODUCTION

The properties of machined components such as surface integrity, fatigue strength and load bearing capacity are becoming increasingly important. The burnishing process is considered as cold forming finishing process which has positive influence on surface integrity. Most significant impacts of roller burnishing are increased surface hardness and decreased surface roughness. The process also transforms tensile residual stresses, present in the surface zone after turning, into compressive residual stresses [1]. The burnishing process is applied to cylindrical workpieces of both, external and internal surfaces and does not involve material removal. Under certain conditions, this process provides a manufacturing alternative to grinding, precision turning and honing operations. In most cases, burnishing process is performed on the same lathes where workpieces were machined [1].

Figure 1 show how the surface's peaks are pressed down, almost vertically, into the surface and the material then flows into the valleys between the peaks. The resulting smooth surface occurs not because the peaks are bent into the surface, but because the material at the workpiece surface is plastically deformed and the material flows, eliminating surface roughness [2].

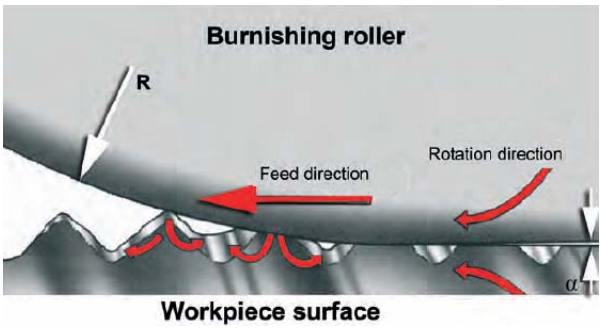

Fig. 1. Roller burnishing process [2]

The curved arrows pictured at the material's surface demonstrate how the material is displaced into the valleys between the peaks. Plastic deformation increases the roller's contact with the surface in that the applied rolling pressure (or burnishing force) affects the peaks that lie ahead of the roller's current position while causing the peaks at the point of contact to flow. The region found between the arrows labeled "rotation direction" demonstrates how the material's surface is

shaped during the burnishing process. The roller suppresses the plasticized material, preventing it from flowing backwards against the feed direction, while clearance angle α ensures that the surface is not over-burnished [2].

Advantages of roller burnishing:

- Produces mirror-finish surfaces.
- Increases surface hardness, decreases friction and wear.
- Provide compressive residual stresses.
- Consistent dimensional tolerance and repeatability.
- Single pass operation which requires short cycle time.

The principle of roller burnishing is transferring the force applied on a roller to the surface in a certain path. During the rotation action the contact area is so small that hertz type pressure occurs on material surface. This provides low energy and rolling force requirement. Roller burnishing process is done below the recrystallization temperature therefore the residual stresses are not released. The real crystal structure contains various irregularities that should come first to the slip formation, because the maximum stress occurs on these locations. If the load on the crystal is big enough, it will start to move and dislocation can be moved.

Figure 2 presents a diagram of roller burnishing process for a spherical roller. The first contact to the machined surface occurs in Section (A). In section (B) the yield strength of the surface is exceeded and plastic deformation takes place. Pressurized depth can be seen here as (D). After the material has been subjected to the maximum compressive strain, in section (C) it begins to elastically relieve (E) through the finishing zone finally leaving with a smooth surface and a compressive residual stress of significant peak value. The stresses formed on the material during the compression decrease towards the center. [3]

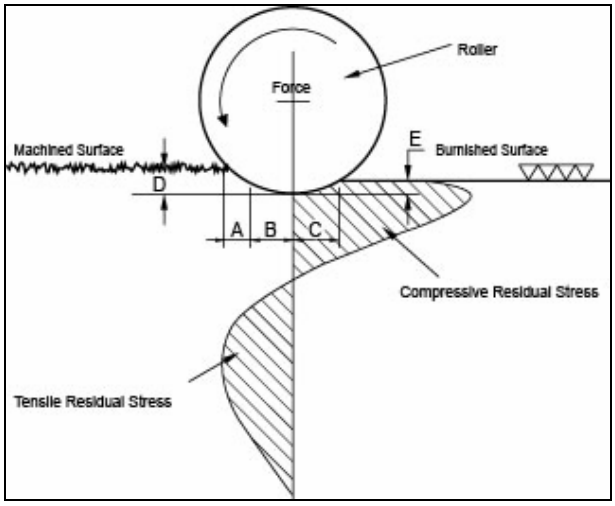

Fig. 2. Roller burnishing process [3]

2. ROLLER BURNISHING TOOLS

There are several types of tools depends on the application of use. Some of them are single roller tools that consist of a tool body equipped with a tool shank, a spring assembly that allows the roller head to move with no play and very low friction, and a gauge that indicates the burnishing force as measured by spring deflection. Single roller tools are designed to machine a wide variety of irregular surfaces, including specific contours, fillets, and grooves. These tools can be used for burnishing internal and external cylindrical surfaces of different diameter dimensions. Burnishing force is variable, and accurately measured [2].

Fig. 3. Single roller tool [2]

Multiple roller tools are designed to machine external pins and internal cylindrical bores. Tool automatically collapses when retracted to prevent surface damage [2].

Fig. 4. Multiple roller tool [2]

3. INFLUENTIAL PARAMETERS

Surface roughness after the roller burnishing is dependent on the contact pressure of roller and feed rate. These are the variable process parameters. Contact pressure is defined as the quotient of the burnishing force and the contact area between the roller and the workpiece. The contact area is affected by the clearance angle α between the roller and workpiece, roller diameter and fillet of roller.

3.1 Input parameters

Roller burnishing is a cold forming process where a compression stress is applied to the workpiece surface. Therefore material mechanical properties have big influence on output results of the process. Especially yield strength of material.

Input surface roughness Ra_i also affects the achieved surface quality. The values of R_Z may vary from 5 and 50 micrometers. Typically, the value of R_Z is 5 to 15

micrometers [4]. The best pre-treatment of the surface is achieved through the choice of turning feed rate that is less than half the radius of the cutting insert.

3.2 Geometry conditions

Roller must be placed in relation to the workpiece in that way, there is a clearance angle α between the roller surface and the surface of the workpiece. The size of the clearance angle is usually between 0,5 and 1,5°. It also depends on the workpiece material, harder than the material of the workpiece is, greater than the clearance angle. If the angle is too small the surface quality decreases, because it could be over-burnished.
We can achieve the same finish result with bigger or smaller roller diameter *d*. For a large roller we need to increase burnishing force. This can cause bending if we are dealing with longer workpieces. Therefore, we use smaller diameter rollers for machining thin walled workpieces that can not be clamped enough firmly. In other cases, we rather use large diameter rollers.
Depending on the material of the workpiece, the roller fillet *r* is 1 to 5mm. For most of the steels the situable fillets are from 1 to 2mm.

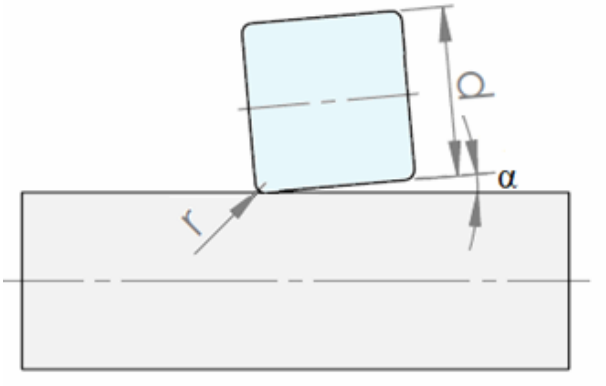

Fig. 5. Geometry of burnishing process

3.3 Process parameters

The burnishing force *F* is an important factor in the burnishing process. If the force is too small, the required surface quality is not achieved. Higher burnishing forces can lead to cracking and peeling of the workpiece surface, as in the surface layer the tensile strength of the material is exceeded and microstructure fracture is achieved.
Feed rate *f* has big impact on the quality of the surface after burnishing process. It is also linked to the changes in the clearance angle of the roller α. When working with larger clearance angle means that feed rate value should be reduced if we want to achieve required surface quality.
Burnishing speed *v* does not have significant influence on the surface roughness, because roller burnishing is a cold forming process that is running below recrystallization temperatures and under this conditions velocity of transformation does not affect material's yield strength [5]. Moreover, there are guide values which depend on the design tools and the size of the workpiece.
In some experimental studies, the number of passes *n* is presented as an influential parameter on the final surface roughness. In principle, the roller burnishing increases surface hardness, so the question appears if it is reasonable to roll surface with multiple passes because after first tool passage, the surface is already hardened. Too many passes can also result peeling of the workpiece surface.

4. EXPERIMENTAL WORK

Specimens were turned and burnished on a lathe model Mori Seiki SL-153. The workpiece material was AISI 52100 (100Cr6) bearing steel in normalized condition of hardness 220 HV. We used two workpieces with nine sample lengths, which were turned to different input roughness values. Diameter of specimens after fine turning was 43,6 mm. Roller burnishing tool consists of radial roller bearing INA NUTR 1542X and thrust roller bearings INA 81104-TV, by which the backlash in the feed direction of the tool is compensated. Hardness of the bearing outer tread surface is 60 HRC. The tool was clamped into the lathe revolver using a Kistler 9129AA dynamometer.

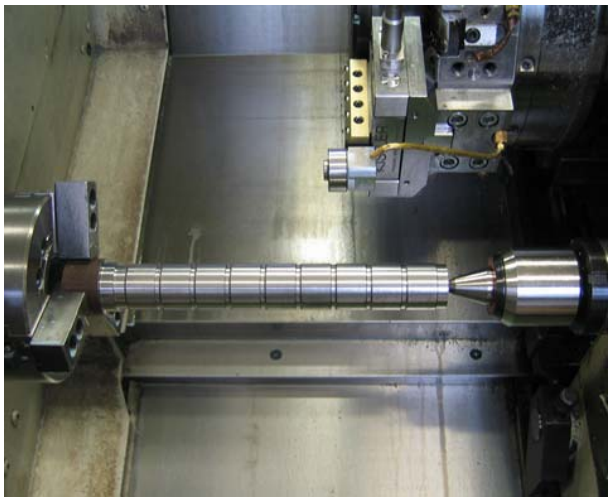

Fig. 6. Experimental setup

4.1 Design of experiments

Using the Taguchi orthogonal matrix, we defined constant and variable factors (parameters) and their levels.
Constant parameters of roller burnishing:

- Clearance angle: α = 1.3°
- Roller diameter: d = 42 mm
- Roller fillet: r = 1 mm
- Burnishing speed: v = 150 m / min
- Number of passes: n = 1

Variable parameters of roller burnishing:

- Burnishing force: F = 600, 1200, 1800 N
- Feed rate: f = 0.1, 0.2, 0.3 mm / rev
- Input surface roughness: Ra_i = 0.39, 0.96, 3.44

4.2 Results and discussion

Table 1 shows the results of experiments carried out in this research. Analysis of the results was performed in the program Minitab 16.

Analysis of the results gives us the values of signal to noise ratio for each parameter, and the influence of

parameters on the output measured value Ra. Figure 7 shows the influence of each parameter on surface roughness. From the graphs can be seen that the most significant factor is feed rate (f), followed by the burnishing force (F) and the input surface roughness of the workpiece (Ra_i). Larger slope of the line connecting the levels of the parameter means that factor is more influential.

No.	F [N]	f [mm/rev]	Ra_i	Ra
1	600	0,1	0,39	0,15
2	600	0,2	0,96	0,31
3	600	0,3	3,44	0,50
4	1200	0,1	0,39	0,12
5	1200	0,2	0,96	0,20
6	1200	0,3	3,44	0,43
7	1800	0,1	0,96	0,10
8	1800	0,2	3,44	0,18
9	1800	0,3	0,39	0,22
10	600	0,1	3,44	0,20
11	600	0,2	0,39	0,26
12	600	0,3	0,96	0,46
13	1200	0,1	0,96	0,12
14	1200	0,2	3,44	0,22
15	1200	0,3	0,39	0,31
16	1800	0,1	3,44	0,11
17	1800	0,2	0,39	0,14
18	1800	0,3	0,96	0,23

Table 1. Experimental conditions and results

5. CONCLUSION

Many factors affect the result of roller burnishing process. It is important to find optional burnishing conditions. The purpose of this study was to examine the influence of three input parameters: burnishing force, feed rate and input surface roughness on the response surface roughness. The best response results were obtained at the lowest value of burnishing feed. Feed rate is also the most significant factor in the roller burnishing process.

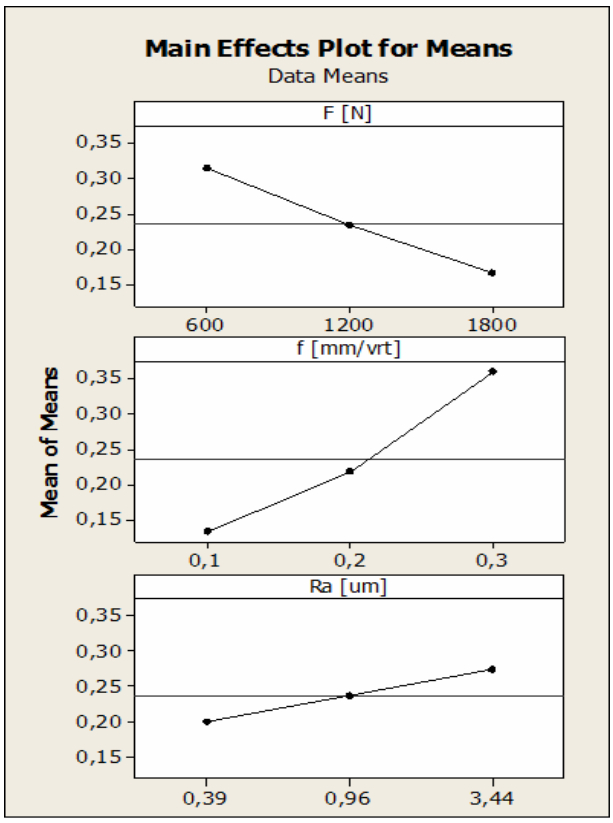

Fig. 7. Influence of parameters on output surface roughness Ra

6. REFERENCES

[1] S. Swirad: The surface texture analysis after sliding burnishing with cylindrical elements. Wear, 2010.

[2] Ecoroll catalogue, http://www.ecoroll.de

[3] http://www.yamato.com.tr/roller_burnishing3.html

[4] Yamasa roller burnishing catalogue, http://yamasa.com.tr

[5] J. Puhar: Mehanska tehnologija: Preoblikovanje - postopki. I/1. Fakulteta za strojništvo, Univerze Edvarda Kardelja, 1990

Authors: **B. Zabkar, J. Kopac,** Laboratory for Cutting, University of Ljubljana, Slovenia
E-mail: janez.kopac@fs.uni-lj.si

Journal of Production Engineering
Vol.16 No.2

Original Scientific Paper

Matin, I., Potran, M., Hadžistevic, M., Hodolič, J., Vukelić, Đ., Puškar, T., Drstvenšek, I., Vrba, I.

DEVELOPMENT OF THE SIMULATION MODEL FOR CASTING OF METAL SUBSTRUCTURE OF METAL-CERAMIC CROWN

Received: 19 September 2013 / Accepted: 17 October 2013

***Abstract**: This paper presents the aplication of a feature-based design features within simulation model development procedure. Based on a review of the feature technology and previous research work, paper focuses on the modeling of intricate relations among features of different design aspects. The authors propose a set of CAD-CAE features that are oriented to both the design and analysis processes. This paper describes flow chart of the simulation model modelling. The secondary objective of the research is to prepare correct solid model for numerical simulation in software package MAGMASOFT. The dental faced model which is imported from My VGL software has some unclear geometry and uncorrected facets. This model requires analysis, and subsequently corrections and reconstruction using advanced modelling Pro/E tools. Integrated CAD-CAE model is parametric, object-oriented, and feature-based.*

***Key words:** IC; analyze; solid; numerical simulation, DB*

Razvoj simulacionog modela metalne substrukture za metalokeramičku krunicu. *U radu se predstavlja razvoj simulacionog modela metalne substrukture za metalokeramičku krunicu sa stanovišta modeliranja zasnovanog na obeležjima. Na osnovu prethodnog istraživanja, predlaže se skup CAD/CAE obeležja, potrebnih za razvoj geometrijskih i tehnoloških karakteristika modela. Jedan od ciljeva istraživanja je priprema čvrstog modela metalne substrukture za simulaciju livenja u programskom sistemu MAGMASOFT. Poligonalna struktura geometrijski zahtevnog modela nakon korekcije u programskom sistemu My VGL sadrži nečistu (ne jasnu) geometriju i netačno pozicionirane poligone. Takav model je neophodno analizirati i rekonstruisati korišćenjem programskog sistem Pro/E. Integrisani CAD/CAE model je parametarski, objektno orijentisan, zasnovan na tipskim oblicima, i tehnološkim informacijama.*

***Ključne reči**:precizno livenje, analiza, čvrst model, simulacija, BP*

1. INTRODUCTION

Investment casting (IC), or "lost-wax" casting, is a precision casting process where wax patterns are converted into solid metal parts following a multi-step process. IC enables economical production of near net shaped metal parts containing complex free-form geometries and features from a variety of metals, including difficult-to-machine or non-machinable alloys. To produce precise components, the near net shape of castings can reduce machining time and cost to bring components into specifications. Despite its popularity, traditional IC suffers from high tooling investments for producing wax patterns. As such, IC is prohibitively expensive for low-volume production typical in prototyping, pre-series, customized or specialized components productions. IC has benefited numerous industries as an economical mean for mass-producing quality near net shape metal parts with high geometric complexity and acceptable tolerances. The economic benefits of IC are limited to mass production. The high costs and long lead-time associated with the development of hard tooling for wax pattern molding renders IC uneconomical for low-volume production. [1, 2, 3, 4].

Traditional IC using casting machine by „BEGO" consists of the block mold and the more common ceramic shell processes. The process chain for the ceramic shell process (Fig. 1) consists of the tooling, shell fabrication and casting stages [2, 5].

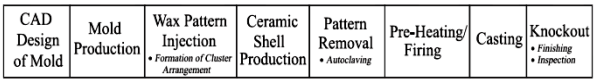

Fig. 1. Convental investment casting

Upon cooling, the mold is stripped to extract the patterns. Individual patterns are attached onto a wax sprue system to form a cluster in the shell fabrication stage. The cluster is repeatedly dip coated in investment slurry containing graded suspensions of refractory particles and followed by stucco application to build shell thickness and strength. When dried, the wax pattern is melted out via autoclaving to reveal the cavities (impressions) of the ceramic shell. The shell is fired to build strength and remove residual volatiles. In the casting stage, molten metal is poured into the heated shells to form the castings, which are extracted after cooling by cracking the shell during the knockout process. Individual castings are separated, cleansed and subjected to finishing processes. [2, 6, 7, 8].

Besides human factors, the CAD system used can sometimes be limiting factor in the production of accurate digital representations of the required design and the conversion of native CAD data from My VGL to data fully acceptable by RP or MAGMASOFT. [7, 11].

The aim of this study is to create a simulation model with correct solid features and the gate subsystem, for casting of metal substructure of a metal-ceramic crown.

2. SPECIFICATION OF SCANNING MODEL

A complete surface model of a typical 3D object is constructed from the integration of its multiple partial views. Since the method is effective in the registration of range images, it is attractive for applications where surface models of 3D objects must be constructed. My VGL is concerned with the problem of range image registration for building 3D facet model [7]. Facet model exported from My VGL to into Pro/E for further unclear feature reconstruction. VGL is used in a variety of application areas such as industrial CT, medical research, life sciences, and many others. Project files (and folders) i.e., VGL files contain basic information on the project including references to the object files and supplementary files belonging to the project. The data range mapping determines the range of gray values used for scanning object, i.e. it specifies the maximum number of different gray values available for dental cast. The size of the data range is always smaller or equal to the numbers of gray values in the data type. The window shows the result image of the rendering process (Fig. 2.). The coordinate system tripod in the lower left corner of the window indicates the orientation of the currently chosen coordinate system as is presented in Fig. 2. Software provides basic features of the scanned object as well as for saving images or image stacks. Thus, the software allows user to handle the two basic file types: object files, and project files. Object files contain voxel data representing dental real object, basically the output of the CT-scanner „Zeiss Metrotom 1500“ (after scanning and low reconstruction) or contain other data for representing object, such as polygons. Scanner settings and additional information might be included in the data files or in separate files. Few X-sections and shaded representation view of the scanning simulation model generated in My VGL software are presented in Fig. 2.

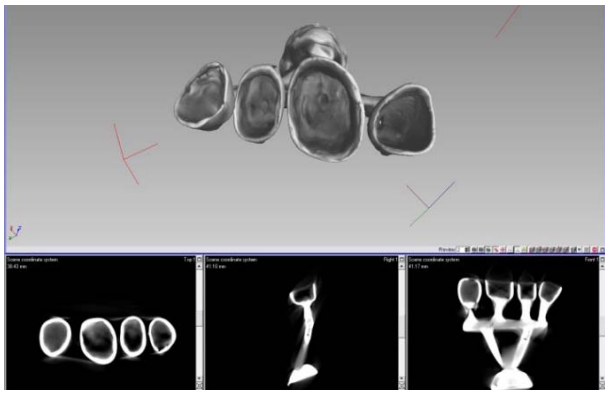

Fig. 2. Few sections of the scanned model

Simulation model consists of the model of metal substructure of metal-ceramic crown, together with adequate gate subsystem. [7]. A complete flow chart of simulation model design is shown in Fig. 3. The flow chart of the modelling of simulation model, can be divided into two operation boxes. The first one presents 3D scanning and facet model creation into My VGL software package. Second operation box presents revise facet/solid model and assembly creation into Pro/E software package as total solution (Fig. 3.).

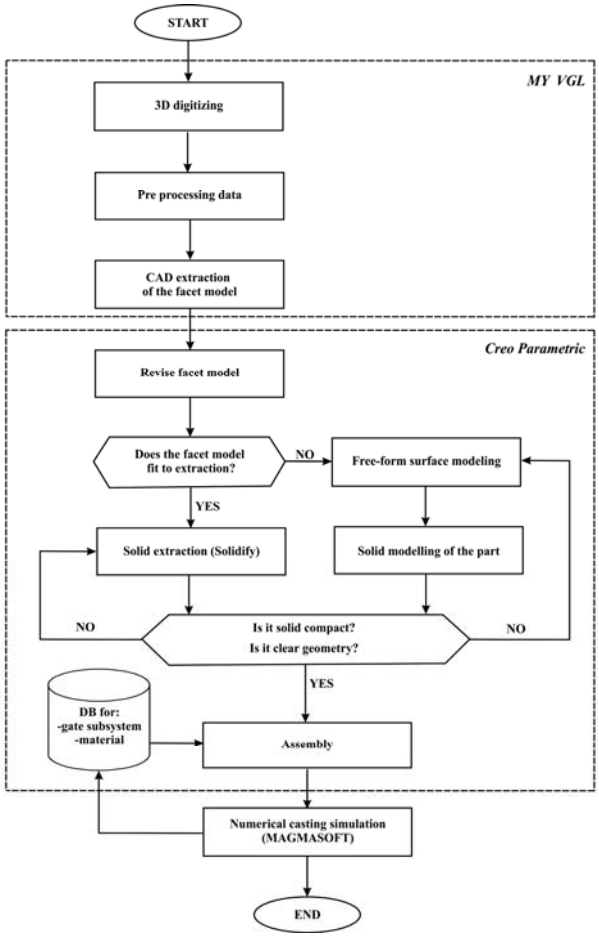

Fig. 3. Flow chart of the modeling of simulation model

3. REVISE OF THE MODEL USING PRO/E

3.1 Super-feature design

Free-form surfacing features are called super-features, because they can contains limitless number of curves and surfaces. Freeform surfacing features are flexible; they have their own internal parent/child relationships, and can also have relationships with other advanced UDF. Free-form surfacing (ISDX) is a design environment within Pro/E that allows user to create free-form curves and surfaces quickly and easily, and to combine multiple elements into super-features. Our researchers' team used free-form surfacing advanced tools such as: [7, 10, 12, 13]

- Create curves and surfaces at the facet part level.
- Create simple features or multiple-element super-features.
- Create a curve on surface (COS), a special curve type that lies on a surface.
- Create surfaces from boundaries that do not have to be trimmed to corners.
- Reconstruction individual geometric entities or a combination of entities in the feature.

- Create internal parent/child relationships for Free-form surfacing features.
- Create an integration of CAD-CAE UDF.

We used inner and outer quilts for creating and manipulating of non-solid surfaces. Quilts represent a “patchwork” of connected nonsolid surfaces. A quilt consists of a single surface or a collection surfaces. A quilt contains information describing the geometry of all surfaces that compose a quilt and information on how quilt surfaces are “stitched” (joined or intersected). Quilts are generated as set of blend boundary surfaces. All quilts were joined to one surface (OQ). After that our research team generated inner join quilt using same operation (IQ) and used (OQ) for thin solid design (TS). After creation joined surface using merge join option we analyzed Pro/E functions in free-form surfacing such as curvature, radius, tangent options, draft check, dihedral angle and shaded curvature. If analyses pass, then surface have G1 characteristics.

3.2 Cleaning the facet geometry and shrink wrap model extraction

A facet model of a metal-ceramic crown substructure, without the gate subsystem and after the use of clean command (with the free-form option) is indicated in Fig 4.

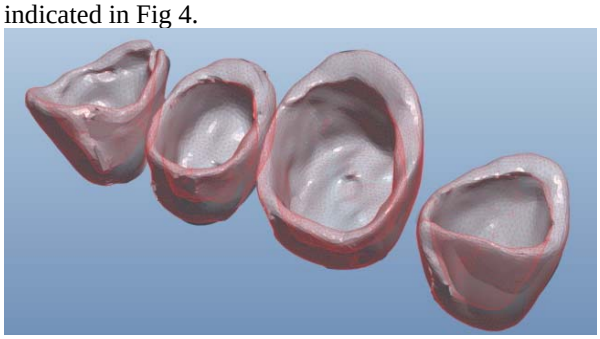

Fig. 4. Facet dental model without gate subsystem

Facet model with gate subsystem after the use clean command with the mechanical option is indicated in Fig. 5.

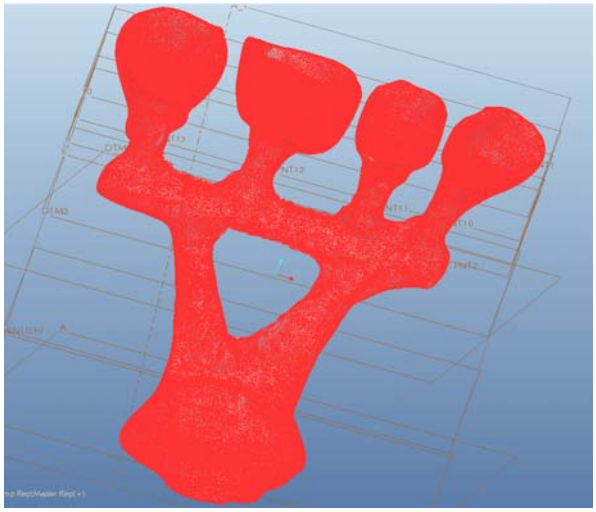

Fig. 5. Facet model of metal substructure with gate subsystem,

After cleaning of irregularities in facet geometry, the model of metal substructure was extracted to shrink-wrap model. The recommended method for creating a shrink-wrap model is to specify a low quality setting, preview the results, and gradually increase the quality level as necessary. All geometry imported and created inside the style feature becomes part of the Style feature. Objects internal to the Style feature, such as individual surfaces, curves, and so on do not have parent-child dependencies outside the Style feature or between each other. This enables that to free manipulate surfaces without being concerned with references and parent-child relationships between Style feature objects and the rest of the model. Quality is inversely proportional to the size of the triangles used for creation of the facet model. At a lower setting, the system creates fewer, larger triangles more quickly, producing a roughly accurate representation of the object's shape. At a higher setting, the system creates smaller triangles, producing a more detailed and accurate representation of the model.

3.3 Checking the geometry and verifying the feature

All imported and exported geometry need to verify into Import Data Doctor (IDD). IDD was used for control import options from VGL file, providing user with immediate access to most commonly used import settings including use template, enable ATB, and accurate import facet model. IDD extends the troubleshooter dialog box with a series of new error and informational geometry checks unique to the environment. Match tool is a repair mode tool that replaces poor quality imported facets with good quality facets, surfaces or patches.

3.4 Data Base of the gate subsystem

Data base (DB) consists of few CAD models of the gate subsystem. Model contains different GPS features such as Average diameter of the runners (Ø4mm, Ø5mm, Ø6mm); Central angle between sprue and vertical runner datum plane (12^0, 15^0, 18^0, 20^0, 22^0); Investment materials (remanium 2000+ (CoCrMoW) acc. to DIN EN ISO 9693 / DIN EN ISO 22674, Trivest, Castorit super C, BEGO`s Wirobond C (CoCrMoW), Heranium Partial Denture Alloys (CoCr) acc. to EN ISO 22674 etc.) and IC parameters for ICM „BEGO“ [7,9].

4. CONCLUSION

The results indicate that the use of decribed tools can enhance performance, which can further improve the quality of a dental restorations. The objective of this research was to develop a correct simulation model of metal substructure of dental crown (facet and solid) with good performance using Pro/E. The described working process modelling are feature-based, parametric, based of solid and facet models, and object-oriented. The resulting models can be directly imported into CAD or CAE systems without loss of the semantics and topological information inherent in feature-based representations. In addition, the feature-

based approach facilitates methods capable of producing highly accurate models, even when the original data has substantial errors. The IDD improves quality redesign, reduces errors, and provides geometric and precision information necessary for numerical simulation. Future research will be directed towards two main goals. The first will be to generate IC parameters using SA method and selection of optimal IC parameters, dental materials with appropriate gate subsystem from DB, using contemporary KBE techniques such as PDT, RBR, IR, MHS, LP, and NP. The second goal will be to design collaborative KBS.

ACKNOWLEDGMENT

Results of the investigation presented in this paper are a part of the research realized in the framework of the project *"Research and Development of Modeling Methods and Approaches in the Manufacturing of Dental Recoveries with the Application of Modern Technologies and Computer Aided Systems"* TR-035020, financed by the Ministry of Education and Science of the Republic of Serbia.

5. REFERENCES

[1] Brusco, N., Andreetto, M., Lucchese, L., Carmignato, S., Cortelazzo, G.M.: *Metrological validation for 3D modeling of dental plaster casts*, Medical Engineering and Physics, Vol. 29, p.p. 954-966, 2007.

[2] Cheah, C.M., Chua, C.K., Lee, C.W., Feng, C., Totong, K.: *Rapid prototyping and tooling techniques: A review of applications for rapid investment casting*, International Journal of Advanced Manufacturing Technology Vol. 25, p.p. 308–320, 2005, DOI 10.1007/s00170-003-1840-6.

[3] Heike R., Luthardt, R.G., Walter, M.H.: *Computer-aided analysis of the influence of digitizing and surfacing on the accuracy in dental CAD/CAM technology*, Computers in Biology and Medicine, Vol. 37, p.p. 579-587, 2007.

[4] Jevremovic, D., Puskar, T., Budak, I., Vukelic, DJ., Kojic, V., Eggbeer, D., Williams, R.J.: *An RE/RM approach to the design and Manufacture of removable partial dentures with a biocompatibility analysis of the F75 Co-Cr SLM alloy*, Materiali in Tehnologije, Vol. 46, p.p. 123-129, 2012.

[5] Jokinen, J., Makkonen, P., Saarelainen, T., Coatanea, E.: *A strategy for cast part shape design optimisation*, International Conference on engineering design, ICED'07., Paris, France, 2007.

[6] Matin, I., Hadzistevic, M., Hodolic, J., Vukelic, DJ.: *Practical aspects of integration in the developed mold design system*, International Conference on Accomplishments in Electrical and Mechanical Engineering and Information Technology"- DEMI, p.p 501-506, Faculty of Mechanical Engineering, Banja Luka, Bosnia and Herzegovina, Republic of Srpska, 2013., ISBN 978-99938-39-46-0

[7] Matin, I., Markovic, D., Puskar, T., Hadzistevic, M., Hodolic, J., Vukelic, DJ., Potran, M.: *Reconstruction of the dental CAD model*, International Scientific Conference "Flexibile Technologies"- MMA, Faculty of Technical Sciences, Novi Sad, p.p. 501-504, 2012., ISBN 987-86-7892-429-3.

[8] Miyazaki, T., Hotta, Y.: *CAD/CAM systems available for the fabrication of crown and bridge restorations*, Australian Dental Journal, Vol. 56, p.p. 97–106, 2011.

[9] Puskar, T., Jevremovic, D., Eggbeer, D., Lapcevic, A., Trifkovic, B., Vukelic, D., Williams, R.J.: *Determination of corrosion characteristics of dental alloy by inductively coupled plasma mass spectrometry*, Journal of Production Engineering, Vol.16, p.p. 77-80, 2012.

[10] Williams, R.J., Eggbeer, D., Lapcevic, A., Trifkovic, B., Puskar, T., Budak, I., Jevremovic, D.: *RE-CAD/CAM approach in design and manufacturing of dental ceramic crowns in combination with manual individualization*, Journal of Production Engineering, Vol.15, p.p. 91-94, 2012.

[11] Wu, M., Tinschert, J., Augthun, M., Wagner, I., Schaedlich-Stubenrauch, J., Sahm, P.R, Spiekermann, H.: *Application of laser measuring, numerical simulation and rapid prototyping to titanium dental castings*, Dental Materials, Vol.17, p.p. 102-108, 2001.

[12] Yue, Sh., Wang, G., Yin, F., Wang, Y.: *Application of an integrated CAD/CAE/CAM system for die casting dies*, Journal of Materials Processing Technology, Vol. 139, p.p. 465-468., 2003.

[13] Zhang, L., Wang, H., Xu, H.: *Application of the reverse engineering to 3D reconstruction on a denture*, 2nd International Conference on Mechatronics and Intelligent Materials, Advanced Material Research, Vol. 490-495, p.p. 2032-2036, 2012.

Authors: **Mr. Ivan Matin, Prof. Dr Miodrag Hadžistević, Prof. Dr Janko Hodolič, Assist. Prof. Dr Đorđe Vukelić, Dr Igor Vrba,** University of Novi Sad, Faculty of Technical Sciences, Department for Production Engineering, Trg Dositeja Obradovica 6, 21000 Novi Sad, Serbia, Phone.: +381 21 450-366, Fax: +381 21 454-495.
E-mail: matini@uns.ac.rs
miodrags@uns.ac.rs
hodolic@uns.ac.rs
vukelic@uns.ac.rs
ivvrba@uns.ac.rs

Assist. Prof. dr Tatjana Puškar, Dr Michal Potran, Medical faculty Novi Sad, Clinic for Prosthodontics, Department of dentistry, Hajduk Veljkova 12, 21000 Novi Sad, Serbia, Phone.: +381 21 661-33-62, Fax: +381 21 526-120.
E-mail: michalpotran@gmail.com
tpuskar@uns.ac.rs

Prof. Dr Igor Drstvenšek, University of Maribor, Faculty of mechanical engineering, Smetanova 17, SI-2000 Maribor, Slovenia, Phone.: +386 2 220-75-93.
E-mail: drsti@uni-mb.si

Journal of Production Engineering
Vol.16 No.2

Original Scientific Paper

Vrba, I., Palenčar, R., Hadžistević, M., Štrbac, B., Hodolič, J.

THE INFLUENCE OF THE SAMPLING STRATEGY AND THE EVALUATION METHOD ON THE CYLINDRICITY ERROR ON A COORDINATE MEASUREMENT MACHINE

Received: 29 September 2013 / Accepted: 31 October 2013

Abstract: *Coordinate measuring machines, due to their flexibility and high accuracy, have gained a wide application in the geometric specification inspections. However, there are numerous factors influencing the accuracy of geometric tolerance assessment. This paper investigates the manner in which the sampling strategy and the evaluation method influence the cylindricity deviation error on a coordinate measuring machine. Proper conclusions follow from experimental researches and the application of statistical methods.*
Key words: *cylindricity error, CMM, sampling strategy, evaluation method, DOE.*

Uticaj strategije merenja i metode procene na grešku cilindričnosti pri merenju na koordinatnoj mernoj mašini *Koordinatne merne mašine su zbog svoje fleksibilnosti i visoke tačnosti merenja našle široku primenu u inspekciji geometrijskih specifikacija. Međutim, postoje brojni faktori koji utiču na tačnost procene geometrijskih tolerancija. U ovom radu je ispitivano kako strategija merenja i metoda procene utiču na grešku procene odstupanja od cilindričnosti na koordinatnoj mernoj mašini. Na osnovu eksperimentalnih istraživanja i primenom statističkih metoda doneseni su odgovarajući zaključci*
Ključne reči: *cilindričnost, KMM, strategija merenja, metoda procene, DOE.*

1. INTRODUCTION

In the last few years, numerous research results have been published in relation to the form tolerance inspection on a coordinate measuring machine [1-4]. These papers mainly deal with the measurement uncertainty estimation in measuring diverse form deviations. The reason for this is in the fact that the measuring result of a form deviation is dependent on the factors related to the measurement uncertainty [5]. Measurement uncertainty contributors for CMMs can be classified in four categories: workpiece, hardware, sampling strategy and evaluation strategy [6].Weckenmann and Knauer presented the manner in which the selection of a measuring strategy by an operator can have a clear impact on the result value and uncertainty in coordinate measurement of dimensional and geometric characteristics [5]. According to the new generation of product specification, the accordance with the specification can be granted only if measurement uncertainty is included. Measurement uncertainty in the form error evaluation should not be directly related to the values of the maximum permissible error.

Diversely from the above mentioned papers where the focus has been on determining the values of measurement uncertainty, a number of authors investigated the manner in which the alteration of a factor related to the measuring uncertainty influences the measuring values on CMMs. Raghunandan and Venkateswara investigated how the quality of the cut surface influences the flatness error [7]. Hadzistevic et al. investigated the manner in which the accidental error by an operator influences the value of standard deviation in styli calibration [8].

In this paper, the authors compared results from measuring the cylindricity error on CMMs by applying diverse measuring strategies and evaluation methods of substitutive geometry. Measurement uncertainty values are not explicitly expressed in this paper.

2. CYLINDRICITY TOLERANCE

The cylindrical feature is one of the main geometric primitives, whose accuracy in form has a fundamental significance for the machine products, such as turning elements, assembly parts, transition systems and accurate measurement devices, to accomplish the set functionality. Measuring and estimating the cylindricity error is of fundamental significance for providing regularity in assembly and for satisfactory performances. In order to obtain a reliable assessment of the deviation from cylindricity, it is necessary to apply adequate strategy for achieving extracted geometry.

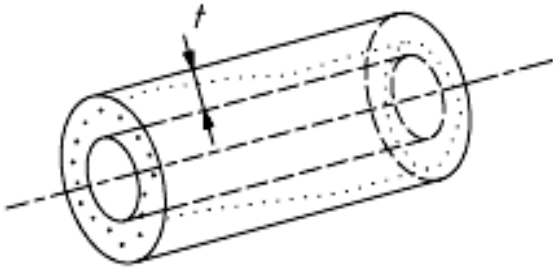

Fig. 1. Cylindricity tolerance

According to the definition of ISO 1101 [9], cylindricity tolerance is a tolerance zone defined with two coaxial cylinders (Figure 1). The cylindricity tolerance limits the deviations of straightness deviations of cylinder generatrices (axis), roundness deviations of cylinder cross-sections, and parallelism deviations of opposite generatrices [10].

Cylindrical feature can only sensibly be tested on a coordinate measuring machine or a form tester. ISO 12180-2 states conditions for performing the measuring operation of estimating the cylindricity deviation. Conditions include filter characteristics, filter conditions, probe feature, stylus tip radius, and probing force. Furthermore, the standard states that the selected sampling strategy in estimating the cylindricity deviation has a significant impact on the measurement error. However, the current standard does not provide clear directions for CMM inspection and cylindricity tolerance evaluation. CMM users intuitively determine which sampling method to use, what number of measuring points to have and which filtering criteria to utilize.

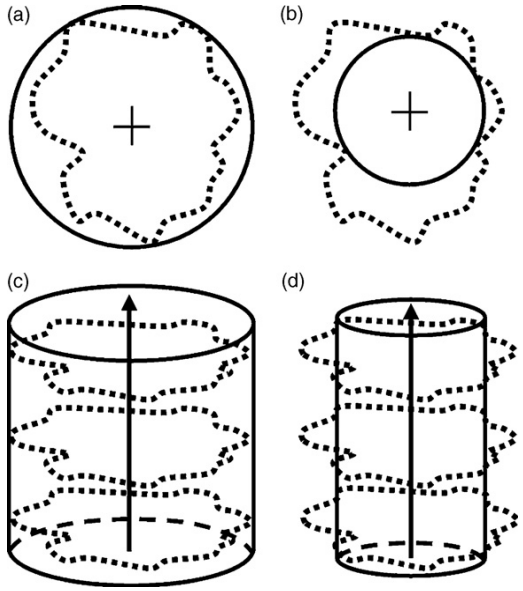

Fig. 2. Minimum circumscribed (a) circle and (c) cylinder and maximum inner (b) circle and (d) cylinder [11]

CMMs perform the cylindricity inspection on the basis of measured point coordinates, and generate an ideal – associated cylinder, which is further compared to nominal geometry. For the evaluation of the form error, the least square method (LSQ) is often utilized. It is based on a well-known mathematical principle; however, in the general case, the errors determined by this method are larger, which can lead to rejecting the "good" workpieces [11]. To overcome the problem, numerous numerical methods have been developed, so today, apart from the LSQ method, minimum circumscribed (MC) cylinder and maximum inscribed (MI) cylinder [12, 13] are utilized as well. MC cylinder is the smallest cylinder encompassing all measured points and passing through at least five extreme outer points. Since MC cylinder cannot be smaller than the largest MC circle determined in every cross section, it is necessary to construct MC circles in all cross sections. The centre of the largest circle determines the axis of the MC cylinder. The largest MC circle is also known as a control circle, and the appropriate vertices are also called control vertices. MI cylinder is determined by five extreme inner points. The procedure for determining the MI cylinder is similar to the one for MC cylinder, with a difference that MI circles define the MI cylinder. The smallest MI circle of all cross sections is the control circle, and its centre defines the axis of the MI cylinder. To determine other points on the axis, the control circle is set in relation to the control vertices for MI circles in other cross sections [12, 14]. The procedure for determining MC and MI cylinders is illustrated in Figure 2.

3. EXPERIMENT

To investigate the influence of individual parameters in the measuring process on the cylindricity measurement error, the calibrated cylinder was measured with, according to the calibration certificate, the diameter of 2 μm. The measurement was performed in a highly controlled laboratory conditions on the CMM Carl Zeiss Contura G2 RDS, with the measurement uncertainty $MPE_E = \pm (1{,}9 + L/K)$, stylus whose ball diameter was d_k = 3 mm in the scanning regime with the velocity v = 5 mm/s, and with the approximately same number of points (about 150). Measuring cylinder and measuring stylus are presented in Figure 3. The factor plan of the experiment DOE [15, 16] is applied, which contains 2 factors on 3 levels each, meaning that the structure of the factor plan of the experiment is 3^2. Planning the experiment is utilized in many applications to aid in understanding the behaviour of a certain process or a variable.

Experiments were conducted in a random order and each one was repeated 3 times, so 27 measurements were performed in total.

Parameters that were varied were the following:

1. *Sampling strategy*. The cylinder was measured with three different strategies (Fig. 4):
   a) circumferential section method,
   b) generatrix method,
   c) helix path method.
2. *Cylindricity evaluation method*. The measured results were evaluated using three above listed methods.

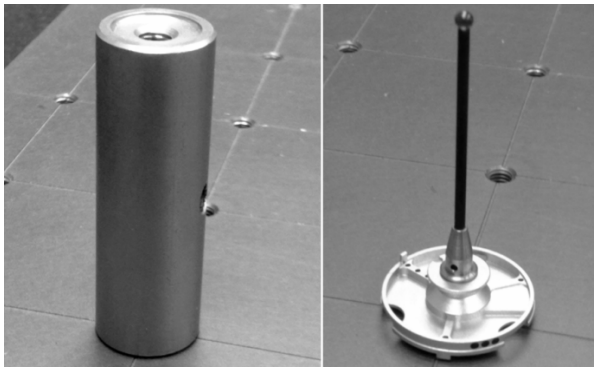

Fig. 3. Calibrated cylinder and measuring stylus

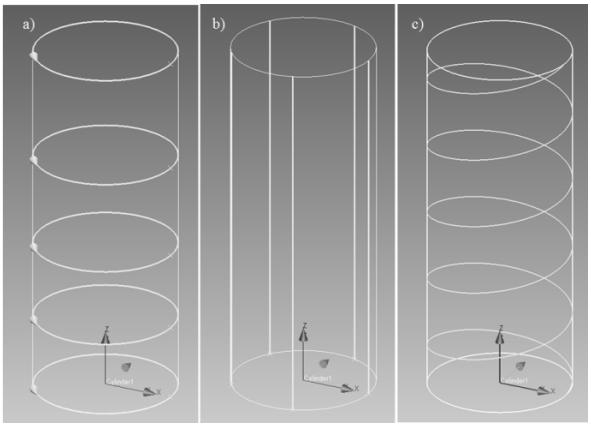

Fig. 4. Cylinder sampling strategies: a) circumferential section method; b) generatrix method; c) helix path method

All sampling strategies applied in this experiment operate on the principle of scanning or continuum measurement. In this case, the point method strategy is left out; this method is also described in the standard and it is well known as having less measurement uncertainty in relation to the applied methods.

The experiment plan, as well as the results, is presented in Table 1.

Table 1. Experiment plan and results

No.	Sampling strategy	Evaluation method	Cylindricity [µm]
1	circumferential section meth.	LSQ	3.8
			3.7
			3.9
2	circumferential section method	MCC	3.7
			3.6
			3.9
3	circumferential section method	MIC	3.8
			3.6
			3.8
4	generatrix method	LSQ	4.9
			5.2
			4.9
5	generatrix method	MCC	4.3
			4.6
			4.4
6	generatrix method	MIC	5.1
			4.7
			4.9
7	helix path method	LSQ	7.2
			7.5
			6.9
8	helix path method	MCC	6.6
			6.2
			6.7
9	helix path method	MIC	6.6
			6.5
			7

4. RESULT ANALYSIS

For statistical analysis of the result, i.e. of DOE experiment, the software package MiniTab 15 was used. First, there were values of the ANOVA analysis obtained as an output of DOE. The results of the ANOVA analysis are presented in Table 2.

Table 2. ANOVA analysis

Source	DF	SS	MS	F	p
Sampling strategy	2	43.209	21.604	525.5	0.000
Evaluation method	2	0.889	0.444	10.81	0.001
Interaction	4	0.449	0.112	2.73	0.062
Error	18	0.74	0.041		
Total	26	45.287			

Based on the results of the ANOVA analysis, i.e. based on p-value from Table 2, it can be concluded that on the level of significance α=0.05, the sampling strategy and the evaluation method have an influence on the cylindricity measurement error. It can also be concluded on the basis of p-value that the mutual influence of these two factors is not statistically relevant. Figure 5 presents the main effects plot for the cylindricity error.

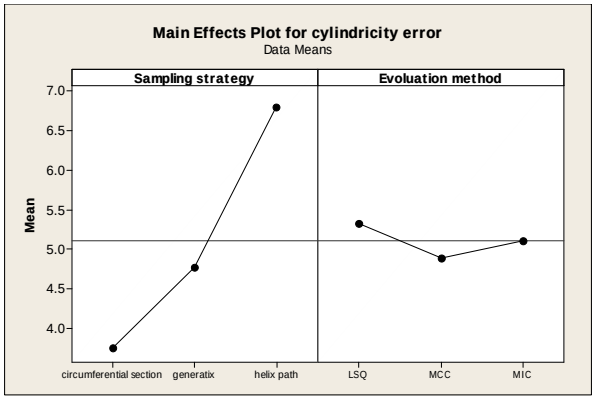

Fig. 5. Main effects plot for the cylindricity error

On observing Figure 5, it can be concluded that the applied sampling strategy has a much greater influence on the cylindricity error than the evaluation method.

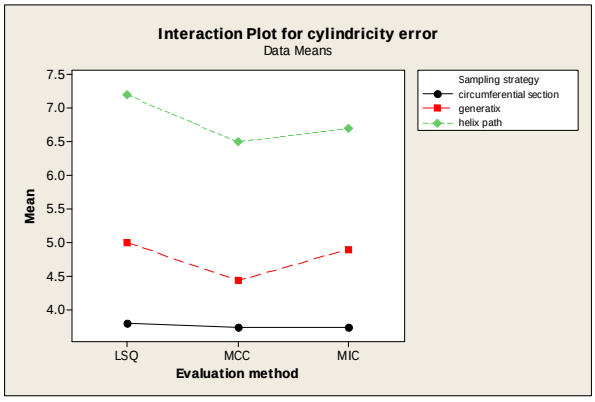

Fig. 6. Interaction plot for the cylindricity error

Figure 6 describes the diagram of interaction

between two factors. Observing the diagram, it can be concluded that, if the circumferential section method is applied as a sampling method, it is not relevant which evaluation method will be used. In the case when generatrix method and helix path method are used as sampling strategies, the least cylindricity error is obtained when MCC is applied as an evaluation method.

5. CONCLUSION

The influence of two parameters in the measuring process on the cylindricity error has been analysed. The results point that both parameters present an influence, though the sampling strategy is significantly more influential than the evaluation method.

In Table 1, it can be observed that the highest error values are present with helix path sampling method and LSQ evaluation method. This is probably due to the fact that the influences of positioning errors and stylus position in the direction of all three axes are combined on such a path. In this research, the point filtration has not been performed. The influence of the filter on the measurement error can be an interesting topic for a future research.

6. REFERENCES

[1] Wen, X.L., Zhao, Y. B., Wang, D.X, Pan, J.: *Adaptive Monte Carlo and GUM methods for the evaluation of measurement uncertainty of cylindricity error*, Precision Engineering, 37, pp. 856-864, 2013.

[2] Dhanish, P.B., Mathew, J.: *Effect of CMM point coordinate uncertainty on uncertainties in determination of circular features*, Measurement, 39, pp. 522-531, 2006.

[3] Wen, X., Xu, Y., Li, H., Wang, F, Sheng, D.: *Monte Carlo Method for the Uncertainty Evaluation of Spatial Straightness Error Based on New Generation Geometrical Product Specification*, Chinese Journal of Mechanical Engineering, 25, pp. 875-881, 2012.

[4] Wen, X.L., Zhu, X.C., Zhao, Y.B., Wang, D.X., Wang, F.L.: *Flatness error evaluation and verification based on new generation geometrical product specification (GPS)*, Precision Engineering, 36, pp. 70-76, 2012.

[5] Weckenmann, A., Knauer, M.: *The influence of Measurement Strategy on the Uncertainty of CMM-Measurements*, Annals of the CIRP, 47, pp. 541-545, 1998.

[6] Kruth, J.P., Gestel, N.V., Bleys, P., Welkenhuyzen, F.: *Uncertainty determination for CMMs by Monte Carlo simulation integrating feature form deviations*, CIRP Annals – Manufacturing Technology, 58, pp. 463-466, 2009.

[7] Raghunandan, R., Venkateswara Rao, P.: *Selection of sampling points for accuracy evaluation of flatness error using coordinate measuring machine*, Journal of Materials Processing technology, 202, pp.240-245, 2008.

[8] Hadžistević, M.; Štrbac, B.; Budak, I.; Vukelić, Đ., Hodolič, J.: *Analysis of the operator influence on the accuracy of the calibration styli results in CMM*, Journal of Production Engineering, 15, pp. 41-44, 2012.

[9] ISO1101:2004, *Geometrical Product Specifications (GPS) – Geometrical tolerancing – Tolerances of form, orientation, location and run-out*, International Standard Organization. Geneve, 2004.

[10] Hamienny, Z., Bialas, S., Osanna, P.H., Tamre, M., Weckenmann, A., Blunt, L., Jakubiec, W: *Geometrical Product Specifications – Course for Technical Universities,* Warsaw, Warsaw University of Technology, 2001, ISBN 83-912190-8-9.

[11] Shunmugam M.S.: *On assessment of geometric errors*. The International Journal Production Research, 24, pp. 413–425, 1986.

[12] Venkaiah N., Shunmugam M.S.: *Evaluation of form data using computational geometric techniques, part II: cylindricity error*, The International Journal Machine Tools Manufacture, 47, pp.1237–1245, 2007.

[13] Shunmugam M. S., Venkaiah N.: *Establishing circle and circular-cylinder references using computational geometric techniques*. The International Journal of Advanced Manufacturing Technology, 51:261–275, 2010.

[14] Goch G., Lübke K.: *Tschebyscheff approximation for the calculation of maximum inscribed/ minimum circumscribed geometry elements and form deviations*. CIRP Annals - Manufacturing Technology, 57, pp.517–520, 2008.

[15] Montgomery DC. *Design and analysis of experiments*. New York: Wiley & Sons; ISBN 978-0471316497, 2006.

[16] Hodolič, J., Hadžistević, M., Tkač, M, Hajduova, Z.: *Alati za statističko upravljanje kvalitetom*. FTN izdavaštvo ISBN 978-86-7892-362-3, Novi Sad, 2011.

Authors: **PhD. Igor Vrba, prof. Ing. Rudolf Palnčar**, Slovak Technical University in Bratislava, Faculty of Mechanical Engineering, Institute of Automation, Measurement and Applied Informatics, Namestie Slobody 17, 81231 Bratislava 1, Slovakia, Phone: +421252497193, Fax: +42125245315
E-mail: igor.vrba@stuba.sk
rudolf.palencar@stuba.sk

Associate Prof. Dr Miodrag Hadzistevic, MS.c Branko Strbac, Prof. dr Janko Hodolic, University of Novi Sad, Faculty of Technical Sciences, Institute for Production Engineering, Trg Dositeja Obradovica 6, 21000 Novi Sad, Serbia, Phone: +381 21 485-2344, Fax: +381 21 454-495.
E-mail: miodrags@uns.ac.rs
strbacb@uns.ac.rs
hodolic@uns.ac.rs

Journal of Production Engineering
Vol.16 No.2

Original Scientific Paper

Blanuša, V., Štrbac, B., Živković, A., Hadžistević, M.

MODELING DIAGNOSIS THERMAL SOURCE ON CNC MACHINE TOOLS USING INFRARED THERMOGRAPHY

Received: 28 October 2013 / Accepted: 30 November 2013

Abstract: *This paper presents the values of the temperature of metal, ceramic and plastic materials in which there is a causation of burns in contact with hot surfaces. Experiments were performed on heat sources and thermal dangers on the machine tool Index GU 600 in the stationary state of the machine and they show values of temperature on the characteristic points of the machine. The temperature source diagnostics and their quantitative values were measured using the infrared (IR) thermography.*
Key words: *machine tool, source thermal, infrared (IR) thermography.*

Modelovanje dijagnoze termalnog izvora CNC mašine alatke korišćenjem infracrvene termografije. *Ovaj rad predstavlja vrednosti temperature metalnih, keramičkih i plastičnih materijala u kojima postoji opasnost od sagorevanja u dodiru sa vrućim površinama. Eksperimenti su sprovedeni na termalnim izvorima toplote i termičkim opasnostima na mašini alatki Indeks GU 600 u stacionarnom stanju mašine i oni pokazuju vrednosti temperature na karakterističnim tačkama mašine. Dijagnostika temperaturnih izvora i njihove kvantitativne vrednosti su merene pomoću infracrvene (IC) termografije.*
Ključne reči: *mašina alatka, termalni izvori, infracrvena (IR) termografija*

1. INTRODUCTION

Temperature is probably the most measured industrial variable since virtually every process, in nature and industry, is temperature dependent. Temperature has a significant role as the indicator of the product or the machine part condition, both in production and in quality control. The occurrence of high temperatures on machine tools during the processing operations can cause danger from the aspect of the occupational safety of the operator. In the contact between the operator and hot surfaces, burns can occur. Temperature areas where burns can occur are determined on the basis of scientific results of diverse groups. Moritz and Henriques have performed experiments on the pigs' skin which is similar to the human one. They were researching skin temperatures when burns occur [1].

In concrete, the temperature influence on machine tools is manifold. The increase in temperature and heat deformation of the main spindle (machine element) directly influences the accuracy of the workpiece and the working ability of the bearing. Therefore, the permitted increase in the temperature of the main spindle bearing is defined by the demanded accuracy of the machine tool. Temperature in the cutting zone has a great impact to the machine itself, the workpiece and the tool as well, and the researches related to this phenomenon deserve greater attention. Apart from the previously mentioned heat sources on machine tools, there are also heat sources in the motors as well (for the main motion, supplementary motion, chip transport, etc.), their gears for the main and supplementary motion, electrical cabinets, operational units, etc.

As a diagnostic tool for revealing temperature sources, the infrared thermovision camera is applied. This technique is employed for the measurement of surface characteristics for a variety of researches involving all possible heat transfer phenomena. The method is especially important and useful because it gives spatially resolved surface temperature distributions non-intrusively, even when large gradients of surface temperature are present [2].

2. METHODOLOGY

Each body with the temperature above the absolute zero has infrared radiation in the function of one's own temperature. In physics, it is well-known that the temperature is a measure of average atomic kinetic energy, and based on this definition, a machine tools temperature can be determined by measuring the intensity of the emitted electromagnetic radiation in the infrared spectrum respecting the Stefan-Bolzmann's law. Electromagnetic waves originating from the mechanical particle motion can be characterized with their intensity and wavelength. Both these characteristics refer to temperature, i.e. a warmer object has shorter wavelength and vice versa. Infrared radiation emitted from the black body is described using the Plank's radiation law [3]. The energy which reaches the thermal sensor consists not only of the energy emitted by the surroundings and intercepted by the object's surface. The radiation reaching the thermovision camera consists of the radiation emitted by the analyzed object and the radiation reflected by other sources in the object vicinity, as well as from the transmitted radiation [4].

The atmosphere between the scanner and the object partly absorbs and therefore weakens the radiation, but then, at the same time, the emissivity of the atmospheric

gases helps strengthening it. All the above are major sources of the method-related errors and should be considered when calculating the object temperature. For obtaining accurate measuring results, it is necessary to recognize the reflected radiation sources and prevent their influence on the overall measuring result. Apart from these factors, the accuracy of measuring results is also influenced by the following: ambient temperature, observation angle, air humidity, and the distance between the thermovision camera sensor and the analyzed object.

3. EXPERIMENTAL RESEARCH OF TEMPERATURE ON THE CONTACT SURFACES OF THE CNC MACHINE - INDEX GU 600

For the demands of the present study, a ThermoPro TP8S thermal camera (Wuhan Guide Infrared Technology) is employed. The field of this camera is 16° × 12°/35 (mm) and the IR resolution is 384 × 288 pixels. The camera performs measurements in the long-wavelength infrared range of the electromagnetic spectrum, with the measuring insecurity of ±0.5°C [5]. For the emissivity value calibration, a contact thermocouple PCE-T396 with the accuracy ±0.2% is used. Researchers are performed in the stationary temperature condition. Generally, on all tool machines, the heat generation locations are motors for motion on determined axes, a motor for the hydro aggregate, main spindle bedding (contact between rolling elements with bearing rings), processing zone, electrical cabinets, managing area electronics, etc. Heat sources in beddings and processing zone have been described in details in a large number of papers dealing with the issue. When considering the joints of the main spindles, whether bedded by cylindrical bearings or ball bearings in the former or the later bedding, there will not be any surface heating which can cause the burns. [6].

In the case of heat generation in the processing zone, the contact surface temperature can reach the value that can cause burns if the cooling and lubricant agent is off or it is simply missing from the process zone. The machine tool Index GU 600, on which the heat sources and the heat dangers were researched.

The analysis of the infrared thermal images of the software package of the IR camera presents the temperature values that can prove the fact that the burns will not occur during the contact of the employees with the machine surfaces. Ambient temperature during the experiment was TP=21.5 °C. The appearance of the infrared thermal image of the transfer for the main motion is presented in Fig. 1a, and for the front of the machine is shown in Fig. 1b.

Temperature value on the characteristic points of the transfer for the main motions was TS1=33.8 °C and TS2=31.6 °C. Temperature of the warmest surface from the Figure 1b was TR1tp=33.8 °C with the thermal vapour, and TR1 tv.k=34.1 °C with the thermovision camera. The image also shows temperature on the managing board keys, and that temperature is TS1t=27.5 °C, while the temperature on the protection door handle is TS2r =27.0°C.

a)

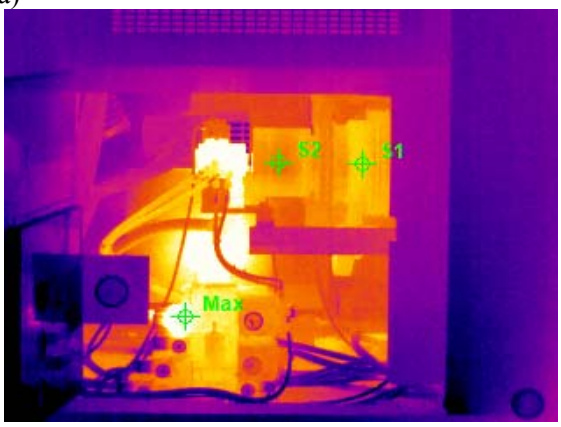

b)

Fig. 1 Transfer for the main motion (a) and for the front of the machine (b)

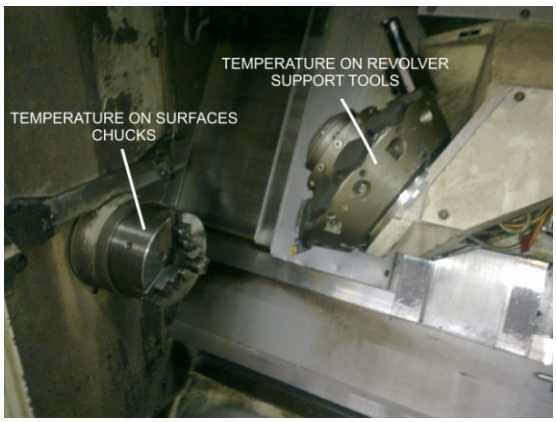

Fig. 2 Workplace of the machine tool

Figure 2 presents the appearance of the machine workplace with the surfaces on the revolver support tools and on surface chunks, on which the temperature was also measured. Temperature on the revolver support tool was TRN=31.0 °C, and on the surface chunk was TSG=32.5 °C (surface temperatures were measured using the four-channel measuring instrument with thermocouples).

Temperature value on the motor for (supplementary) transversal motion (y axis) using the temperature measuring instrument with the thermocouple in a stationary temperature condition was TMP=32.0 °C, and on the protective motor box for longitudinal motion (z axis) was TMU=28.0 °C.

Measuring the temperature from the side of the machine defines heat sources on the surfaces, and temperature was measured with the thermocouple, and its value on the characteristic point was T2st=33.1 °C (Fig. 3a); on the motor gear for chip transporter was TTS=41.2 °C (Fig. 3b); while on the motor for driven tools was TGA=29.7 °C (temperature value on the motor for driven tools depends on the spin number, processing operations, etc.). It is important to mention that temperature on the surface of the motor gear for the chip transporter can vary depending on the chip type and the type of material, and the temperature value is higher in the transportation of the band chip).

a)

b)

Fig. 3 Side of the machine (a) and motor gear for chip transporter (b)

From the rear side of the machine, heat sources are the motor for hydro-aggregate, motor for the main motion and the system for electrical cabinet cooling. Temperature value on the motor for hydro-aggregate was THA=33.1 °C, and on the hydro-aggregate gear was TPHA=45,9 °C. On the motor for the main motion, using the infrared thermometer, temperature was TMGK=33.0°C. Figure 4 a) shows the motor for the hydro-aggregate, and 4b) shows the motor for the main motion.

Temperature value on the plastic opening for the electrical cabinet ventilation, using the infrared thermometer, was TUS=43.0 °C from the inside, and TBS=37.2 °C from the side of the ventilation element.

Workpiece temperature after processing depends on the type of material being processes, processing operations, processing regimes, cooling and lubricant agents, etc. Workpiece temperature after processing and applying the cooling agent was TIZ=38 °C. In the cases when the cooling and lubricant agent is spent, or it is excluded from the process, the workpiece temperature can go up to TIZ=80-120 °C.

a)

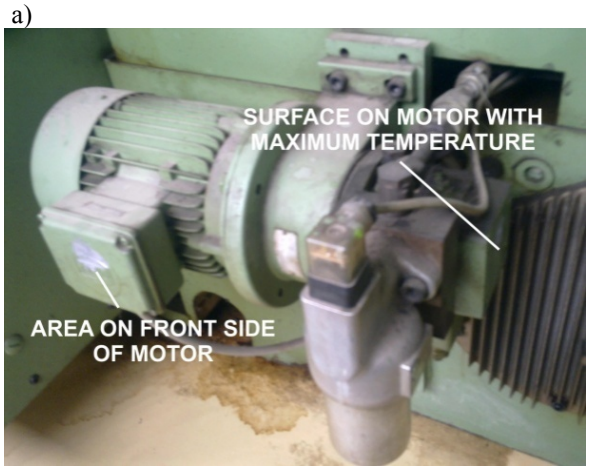

b)

Fig. 4 Motor for hydro-aggregate (a) and motor for the main motion (b)

Table 1 presents the temperature values during the beginning of the chip occurrence for the contact time over one minute, and Table 2 shows the experimentally obtained temperature values on the characteristic points of the machine tool.

Table 1. Beginning of the chip occurrence in the surface contact for the contact length of 1 min and longer

MATERIAL	*Beginning of the chip occurrence for the contact time T_P*		
	1 min °C	*10 min °C*	*8 h and longer °C*
Metal	*51*	*48*	*43*
Ceramics, glass and stone	*56*	*48*	*43*
Plastic masses	*60*	*48*	*43*

Table 2. Temperature values on characteristic points

Action zone	*Characteristic points*	*Temperature values [°C]*
Front of the machine	T_{R1}	*33.8*
	T_{S1t}	*27.5*
	T_{S2r}	*27.0*
Machine workplace	T_{RN}	*31.0*
	T_{SG}	*32.5*
Main motion gear	T_{S1}	*33.8*
	T_{S2}	*31.6*
Motors for longitudinal and transverse motion	T_{MP}	*32.0*
	T_{MU}	*28.0*
Side of t he machine	T_{2st}	*33.1*
	T_{TS}	*41.2*
	T_{GA}	*29.7*
Rear of t he machine	T_{HA}	*33.1*
	T_{PHA}	*45.9*
	T_{MGK}	*33.0*
	T_{US}	*43.0*
	T_{BS}	*37.2*

4. CONCLUCION

The application of contemporary measuring instruments can be used to define heat sources on machine tools. The comparison of theoretical temperature values when burns occur with the experimentally obtained values can be useful for defining the potential burn locations. If these locations exist, the application of the infrared thermography can be a useful and fast manner to diagnose these locations and warn all the employees who can have any contacts with these hot surfaces.

5. REFERENCES

[1] Moritz, A., Henriques, F.: *The Relative Importance of Time and Surfaces Temperature in the Causation of Cutaneous Burns*, Studies of Thermal Injury II, Am J. Path, Vol. 23, Page 695-720, 1947.

[2] Kowalewski, TA., Ligrani, P., Dreizler, A., Schulz, C., Fey, U., Egami,.Y.: *Temperature and heat flux*. Springer handbook of experimental fluid mechanics. Berlin, Heidelberg: Springer-Verlag; 2007.

[3] Ehinger, K., et al.:*125 years temperature*, 03/TEMP-EN Rev. B 06.2008.

[4] Orzechowski, T.: *Determining local values of the heat transfer coefficient on a fin surface*, Experimental Thermal and Fluid Science, 31 (2007), 947-955.

[5] *ThermoPro TP8S thermal infrared camera*, Wuhan Guide Infrared Technology Co., Hongshan District, Wuhan, China, 2007.

[6] Blanuša, V., Zeljković, M., Živković, A., Štrbac, B., Hadžistević, M.: *Savremeni postupci merenja temperature,* Zbornik radova, CD rom, Infoteh-Jahorina, Sesija PRS-Proizvodni sistemi, Ref. Prs 6, ISSN: 99938-624-2-8, 2012.

Authors: M.Sc. Vladimir Blanuša, M.Sc. Branko Štrbac, dr Aleksandar Živković, Prof. dr Miodrag Hadžistević.

Faculty of Technical Science, Trg Dositeja Obradovica 6, 21000 Novi Sad, Phone: +381 21 4852332, Fax: +381 21 458 133.

E-mail: blanusa@uns.ac.rs
strbac@uns.ac.rs
acoz@uns.ac.rs
miodrags@uns.ac.rs

Acknowledgement

Results of investigation presented in this paper are part of the research realized in the framework of the project "Research and Development of Modelling Methods and Approaches in Manufacturing Dental Recoveries with the Application of Modern Technologies and Computer Aided Systems" – TR 035020, financed by the Ministry of Science and Technological Development of the Republic of Serbia**.**

Journal of Production Engineering
Vol.16 No.2

Original Scientific Paper

Kosec, B., Soković, M., Karpe, B., Gojić, M., Nagode, A., Kosec, G.

FAILURE ANALYSIS OF DIES FOR ALUMINIUM ALLOYS DIE-CASTING AS THE KEY TO THE QUALITY

Received: 09 October 2013 / Accepted: 15 November 2013

Abstract: *For economical production of die castings it is of great importance to ensure high quality of die manufacture and long working life. The repair or replacement of a die has a high cost in time and money. Dies for* aluminium alloys die-casting fail because of a great number of a different and simultaneously operating factors. Die *design, material selection, and thermal stress fatigue due to the cyclic working process, as well as to low and inhomogeneous initial die temperature contribute to the failures and cracks formation on/in dies.In the presented work the intensity and homogeneity of the temperature fields on the working surface of the testing die were checked through thermographic measurements, and failures and cracks on the working surface of the die were analysed by the non-destructive metallographic examination methods.*

Key words: *die-casting, die, aluminium alloy, temperature field, thermographic measurements, failure analysis, quality*

Analiza grečke kalupa pri livenju pod pritiskom legura aluminijuma kao ključ kvaliteta. *Da bi livenje pod pritiskom bilo ekonomično od velikog je značaja da se obezbedi visok kvalitet kalupa i dug radni vek. Popravka ili zamena kalupa ima visoku cenu u vremenu i novcu. Greške kod kalupa pri livenju pod pritiskom legura aluminijuma su prisutne zbog velikog broja različitih faktora koji istovremeno deluju. Projektovanje kalupa, izbor materijala, termalni zamor, kao i na niske i nehomogene temperature livenja u ciklusu procesa rada doprinose greškama i pukotinama kalupa. U radu predstavljen intenzitet i homogenost temperaturnog polja na radnoj površini testiranog kalupa koji su provereni kroz termografska merenja, greške i pukotina na površini radnog kalupa su proverene ne-destruktivnim metalografskim metodama ispitivanja.*

Ključne reči: *livenje pod pritiskom, kalup, legura aluminijuma, temperaturno polje, termografska merenja, analiza greške, kvalitet*

1. INTRODUCTION

Die-casting is the most economical and technical easy process of casting very sophisticated and precise aluminium products of big-scale series. Comparison of nine parameters of the die-casting versus stamping, forging, sand casting, permanent mold casting and plastic molding is presented in Table 1.

Aluminium die-castings are made for final installation and need very little machining. They are used in automotive industry, household appliences, electrical industry and instalations, fittings, etc. [2]. Aluminium die-casting dies fail because of a number of different and simultaneously operating stresses. The stresses are of two basic kinds the first which are created during the manufacturing of the die, and the second which are produced during exploatation process. For economical production of aluminium and its alloys die-castings it is important that the dies have a long working life. The replacement of a die is expensive in both: money and production time. The most frequent failures of aluminium die-casting dies are [1]:

- heat checking,
- gross cracking or cleavage cracking,
- cracking in corners, sharp radii, or sharp edges, and
- wear or erosion.

It is generally agreed that one of the principal causes of termination of die life is heat checking, which occurs through a process of crack initiation and propagation from the thermal stress fatigue induced on a die surface [3]. Some of the factors that affect die failures may be controlled to some extent by the die-casting experts (designers, manufacturers and operators). These factors include [4]:

- design,
- materials selection,
- heat treatment,
- finishing operations, and
- handling and use.

When hot aluminium or its alloy strikes the active working surface of the die, the die expands and then contracts during cooling, as the heat in the casting is conduced into the steel bellow the surface of the die. The greater difference between the temperature of the die and that of the hot aluminium shot into the die, the greater will be the expansion and contraction of the die surface, and sooner the die surface will be heat check. Since the stresses produced on the die surface are inversely proportional to the die temperature, it is good practice to run the dies as hot as is practical and/or economical. Aluminium die-casting dies should be

preheated to approximately 240 to 300 °C. Experiences have shown that by increasing the die operating temperature from 205 to 315 °C, die production may be doubled [5].

Table 1. Comparison of nine parameters of the die-casting vs other processes [1]

		Compared with				
Nine points of comparison		Stampings	Forgings	Sand castings	Permanent mold castings	Plastic molding
1	Cost	Lower machining	Lower final	Lower production and machining	Lower labor, production and machining	Generally higher
2	Design flexibility	More complex shapes	More complex shapes	Thinner wall sections possible	Thinner wall sections possible, less draft required	Much greater
3	Functional versatility	Better designs possible	More versatile with less machining	More versatile with less machining	More versatile with less machining	Many more uses
4	Tolerances	Closer	Closer	Closer	Closer	Closer
5	Wall thickness	Greater variations	Thinner sections	Thinner sections	Thinner sections	Thinner sections for the same strength
6	Surface finish	Wider variety	Smoother	Smoother	Smoother	Wider variety
7	Material waste	Less	Less	Less	Less	Less
8	Strength	Depends on design	Lower tensile	Greater with same alloy	Greater with same alloy	Much greater
9	Weight	Depends on design	Lighter	Lighter	Less	Less

2. INVESTIGATION

In the frame of our investigation work a complex analysis of a typical dies for aluminium alloys die-casting has been carried out. The fixed half of the testing die-casting die is shown in Figure 1.

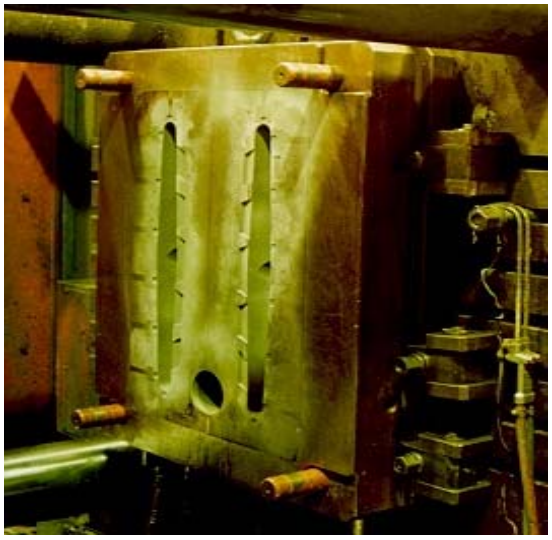

Fig. 1 Fixed half of the investigated die-casting die.

The investigated die was made from the well known BOEHLER W300 ISODISC [6] hot work tool steel. This steel is mostly applied and considered material for all kinds of hot working dies. The chemical composition of the steel is given in the Table 2. It can be seen that the steel corresponds to AISI H11 and DIN X40CrMoV5-1 steel [7].

Table 2. Chemical composition of BOEHLER W300 ISODISC steel [6]

Element	C	Si	Mn	Cr	Mo	V
(mass. %)	0.38	1.10	0.40	5.00	1.30	0.40

Thermal and mechanical properties of BOEHLER W300 ISODISC steel are well known [6,7]. Liquidus temperature of aluminium alloy AlSi9Cu3 is approximately 593 °C, therefore the properties in the temperature interval from 20 up to the 700 °C are important for the analysis of the discussed case. The density of BOEHLER W300 ISODISC steel at 20 °C is approximately equal of 7800 kg/m^3, and it decreases with higher temperature. Up to the temperature of 700 °C it drops for about 200 kg/m^3. It is very interesting that this steel has relatively low and nearly linear increasing heat conductivity (19.2 to 26.3 W/m·K), and proportionally constant thermal diffusivity (the whole time aproximately $5 \cdot 10^{-6}$ m^2/s). Specific heat is increased with higher temperature to its values of 456 or 587 J/kg·K, respectively for the boundary values of the chosen temperature range. Linear coefficient of elongation slowly increases from $10.7 \cdot 10^{-6}$ /K (at 20 °C) to $13.2 \cdot 10^{-6}$ /K (at 700 °C), while modulus of elasticity, with boundary values of 211 and 168 GPa, decreases with the higher temperature.

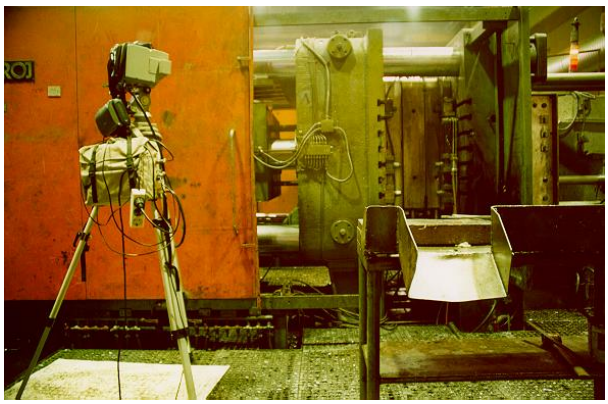

Fig. 2 Position of the thermographic camera.

By thermographic measurements the required intensity and homogeneity of the initial temperature field on the working surface of the fixed die half have been carried out due to the relatively simple geometry of the discussed die, so the simple heat images (thermographs) analysis have been performed.

On the working surface of the fixed die half thermographic measurements have been carried out in the preheating period (Figure 3) of the die heating to its initial operating temperature (expected 240 °C and homogeneous through the whole working surface of the die).

The temperature fields between the working process have been measured, too. And two typical sequences of the die-casting process are presented in Figure 4. Thermographs (temperature images) in Figure 3 are represented in the temperature range between 90 and 161 °C and 90 and 124 °C, and in Figure 4 in the range between 90 and 195 °C, in both cases black (uncoloured) regions are below 90 °C.

The cracks which appeared on the working surface of the fixed die half after less than thousand shots were revealed and identified by the use of penetrants. Some of them were also clearly seen by the use of magnifying glass or even by naked eye]. In the frame of our experimental work also non-destructive metallographic examination by optical microscopy (OM) and by scanning electron microscopy (SEM) of polymeric replicas was applied.

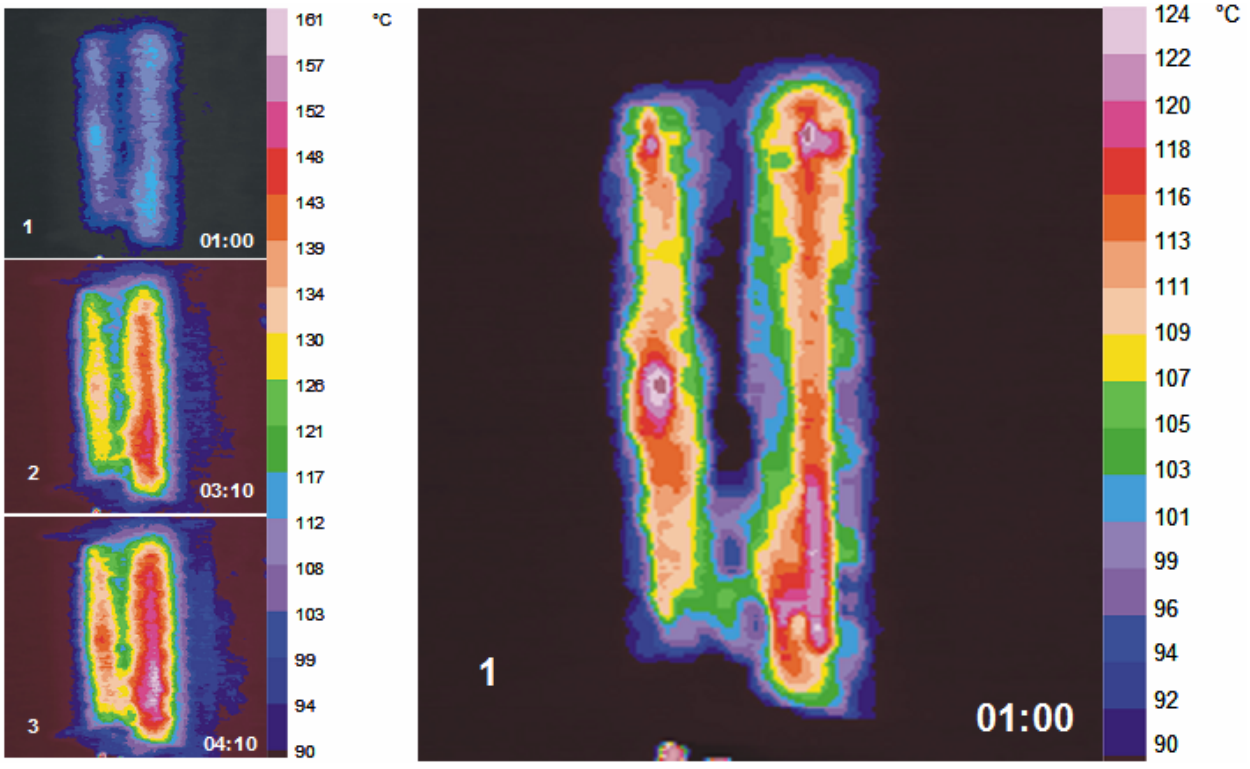

Fig. 3 Thermographs. Working surface of the fixed part of die-casting die: at the beginning (1), after approx. 2 hours (2), and at the end (3 – initial temperature field) of the die preheating process (left). Working surface of the fixed part of die-casting die at the beginning (1) represented in the temperature range between 90 and 124 °C (right).

The failures observed on the working surface (Figure 5) belong to heat checking initiated at identification marks, and cracking in corners, sharp edges and transitions.

At the process of the die-casting of aluminium alloys are the temperature and cyclic temperature loading respectively the main load of the die. The influence of the other loads is practically negligible. For the engineering praxis the stress in the individual points of the die surface can be determinate successful by the following expression:

$$\sigma = \frac{E \cdot \alpha \cdot \Delta \vartheta}{1 - \nu} \qquad (1)$$

where: σ is stress [N/mm^2], E is Young's modulus [GPa], α is coefficient of linear expansion [K^{-1}], Δϑ temperature difference [K], and ν Poisson's ratio [-]. Calculation of the die strain and stress state is logical following step at the solution of the dies for aluminium alloys die-casting complex quality improvement problematic.

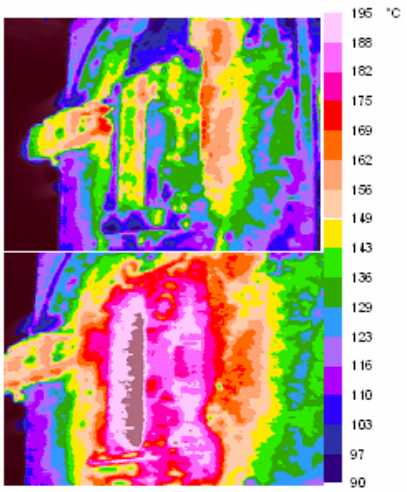

Fig. 4 Working process. Thermographs. The fixed part of the die-casting die: working surface and casting (above), working surface without casting (below).

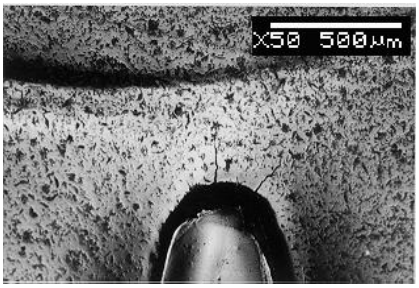

Fig. 5 Working surface of the testing die-casting die. Surface cracks and pits. OM.

3. CONCLUSIONS

Cracking on/in die-casting dies for aluminium alloys is caused by a number of different and simultaneously operating factors. Some of them that affect die failures may be controlled to some extent by the die-casting experts.

In the experimental part of our work the failures on the working surface of the fixed half of the testing die for die-casting of aluminium alloys were observed with the use of non-destructive testing (NDT) methods: such as thermographic analysis, penetrants, and metallographic examination of polymeric replicas.

The failures observed on the working surface of the discussed fixed die half for die-casting of aluminium alloys belong to heat checking initiated at identification marks, and cracking in corners, sharp edges and transitions. Calculation of the die strain and stress state is logical following step at the solution of the dies for aluminium alloys die-casting quality improvement.

4. REFERENCES

[1] S. Kalpakjian: *Tool and Die Failures - Source Book*, ASM International, Metals Park, Ohio, 1982.

[2] B. Kosec: *Failures of Dies for Die-Casting of Aluminium Alloys*, Metallurgy, 47 (2008) 1, 51 – 55.

[3] F. Kosel, L. Kosec: *Heat Checking of Hot Work Tools*, Journal of Mechanical Engineering, 29 (1983) 7-9, 151 - 158.

[4] Handbook of Case Histories in Failure Analysis, Vol. 1, ASM International, Materials Park, Ohio, 1992.

[5] B. Kosec, G. Kosec, M. Soković: *Temperature Field and Failure Analysis of Die-Casting Die*. Archives of Materials Science and Engineering, 28 (2007) 3, 182-187.

[6] Böhler Edelstahlhandbuch auf PC V2.0, Kapfenberg, 1996.

[7] B. Jocić: *Steels and Cast Irons*, BIO-TOP d.o.o., Dobja Vas, 2008.

Authors: **Prof. Dr. Borut Kosec, Dr. Blaž Karpe, Assist. Prof. Dr. Aleš Nagode,** University of Ljubljana, Faculty of Natural Sciences and Engineering, Aškerčeva 12, 1000 Ljubljana, Slovenia, Phone.: +386 1 2000410, Fax: +386 1 4771214.

Prof. Dr. Mirko Soković, University of Ljubljana, Faculty of Mechanical Engineering, Aškerčeva 6, 1000 Ljubljana, Slovenia, Phone.: +386 1 477114, Fax: +386 1 4771218.

Prof. Dr. Mirko Gojić, University of Zagreb, Faculty of Metallurgy, Aleja narodnih heroja 3, 44103 Sisak, Croatia, Phone.: +385 43 533378, Fax: +385 43 533379.

Assist. Prof. Dr. Gorazd Kosec, ACRONI d.o.o., c. Borisa Kidriča 44, 4290 Jesenice, Slovenia, Phone.: +386 4 5841016, Fax: +386 4 5841003.

E-mail: borut.kosec@omm.ntf.uni-lj.si
blaz.karpe@omm.ntf.uni-lj.si
ales.nagode@omm.ntf.uni-lj.si
mirko.sokovic @fs.uni-lj.si
mgojic@simet.hr
gorazd.kosec@acroni.si

Journal of Production Engineering
Vol.16 No.2

Original Scientific Paper

Škorić, B., Schrittwieser, R., Cavaleiro, A.

NANOSCALE DIMENSIONAL METROLOGY AND PHYSICAL CHARACTERIZATION

Received: 19 October 2013 / Accepted: 16 November 2013

Abstract: *The nanometrology is a scientific and technical discipline paying attention to the measurement of different physical quantities on the nanoscale. Its significance grows hand in hand with the grow of nanotechnology which can be observed in many fields of science and technique during last years. The aim of these papers is to introduce this interesting and relatively new domain and to present a summary of various measurement methods used in nanometrology. Recent advances in nanotechnology are expressed by the atom scale insights successes related to development in nanometrology. New approaches in nanometrology will be required in the near future.*
Key words: *nanometrology, nanomaterials, nanoscale*

Metrologija i fizikalne karakteristike na nano skali. *Nanometrologija je naučna i tehnička disciplina koja obraća pažnju na merenje različitih fizičkih kvantiteta na nano skali. Njena važnost raste sa porastom nanotehnologije koja može biti posmatrana na mnogim naučnim poljima i tehnikama tokom prethodnih godina. Cilj ovog rada je da uvede ovaj interesantan i relativno novi domen i da predstavi sažetak raznih mernih metoda korišćenih u nanometrologiji. Skoriji napredak u nanotehnologiji je izražen uspehom uvida na atomskoj skali u okviru nanometrologije. Novi pristupi nanometrologiji će biti neophodni u skorijoj budućnosti.*
Ključne reči: *nanometrologija, nanomaterijali, nanoskala*

1. INTRODUCTION

Nanometrology is a subfield of metrology, concerned with the science of measurement at the nanoscale level. Nanometrology is the science of measurement at the nanoscale level and it has a crucial role in producing nanomaterials and devices with a high degree of accuracy and reliability in nanoscale manufacturing. Metrology of complex structures is a highly demanding application that requires extreme precision, reproduciblilty, and referencing to attributable standards. The first use of the term nanometrology in a peer reviewed publication appears in April 1992, in the journal Metrologia [1].
Metrology instruments should be compliant with good laboratory practices, and produces a comprehensive suite of charged particle microscopy tools to examine and measure materials over a wide range of lengths, from millimeters down to Ångströms in both 2D and 3D, for measuring surfaces and cross-sections to provide quantitative data on critical dimensions.
Nanometrology has a crucial role in order to produce nanomaterials and devices with a high degree of accuracy and reliability in nanomanufacturing. Nanometrology solved the technical issues which are today at the forefront of the industry's most critical problem area: feature edge definition. In order to solve this problem, it is necessary to first calibrate the tool used for measurement, and then with the properly calibrated perform precise and accurate metrology. The needs for measurement and testing that may be derived from the foreseen developments in nanotechnology are substantial and wide range. Prosperous industrial sectors are Precision Engineering, Micro- & optoelectronics, as well as Bio-molecular technology [2]. The measurement techniques used for macro systems cannot be directly used for measurement of parameters in nanosystems.

2. MEASUREMENT TECHNIQUES

Various techniques based on physical phenomena have been developed which can be used for measure or determine the parameters for nanostructures and nanomaterials. Some of the popular ones are X-Ray Diffraction, Transmission Electron Microscopy, High Resolution Transmission Electron Microscopy, Atomic Force Microscopy (Fig.1), Scanning Electron Microscopy, Field Emission Scanning Electron Microscopy.

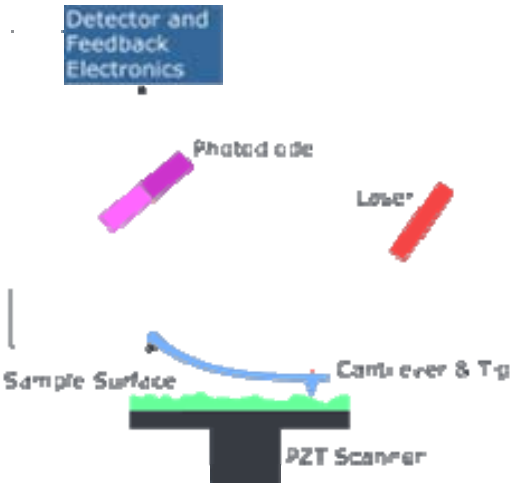

Fig. 1. Diagram of Atomic Force Microscope

Atomic Force Microscopy (AFM) is one of the most common measurement techniques. It can be used to measure Topology, grain size, frictional characteristics and different forces. It consists of a silicon cantilever with a sharp tip with a radius of curvature of a few nanometers. The tip is used as a probe on the specimen to be measured. The forces acting at the atomic level between the tip and the surface of the specimen cause the tip to deflect and this deflection is detected using a laser spot which is reflected to an array of photodiodes.
The analysis of the nano indents of TiN coating was performed by Atomic Force Microscope (Figure 2a).It can be seen a cross section of an indent during indentation.(Figure 2b) [3].

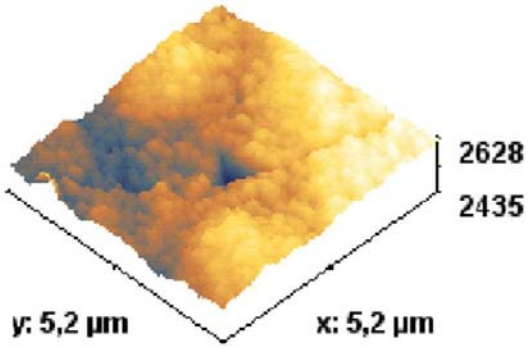

Fig. 2a. AFM image of a nanoindentation

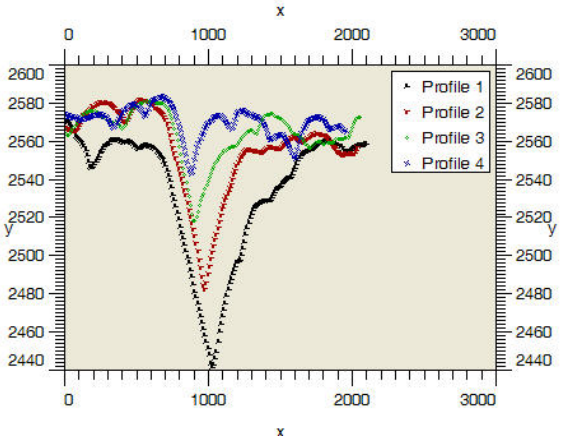

Fig. 2b. Cross-section of the indentation

Scanning Tunneling Microscopy (STM) is another instrument commonly used (Fig.3). It is used to measure 3-D topology of the specimen. The STM is based on the concept of quantum tunneling. When a conducting tip is brought very near to the surface to be examined, a bias (voltage difference) applied between the two can allow electrons to tunnel through the vacuum between them. Measurements are made by monitoring the current as the tip's position scans across the surface, which can then be used to display an image.
Another commonly used instrument is the **Scanning Electron Microscopy** (SEM) which apart from measuring the shape and size of the particles and topography of the surface can be used to determine the composition of elements and compounds the sample is composed of (Fig.4). In SEM the specimen surface is scanned with a high energy electron beam. The electrons in the beam interact with atoms in the specimen and interactions are detected using detectors.

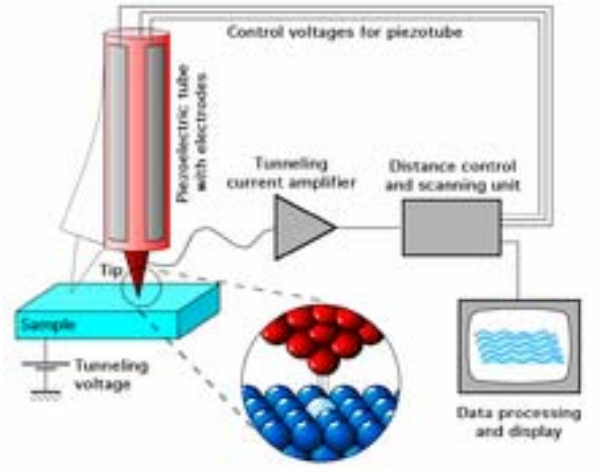

Fig. 3. *Diagram of Scanning Tunneling Microscope*

The interactions produced are back scattering of electrons, transmission of electrons, secondary electrons etc. To remove high angle electrons magnetics lenses are used. Scanning electron microscopy (SEM) instruments primary electron columns. Separate detectors are required for secondary and backscattered electrons.

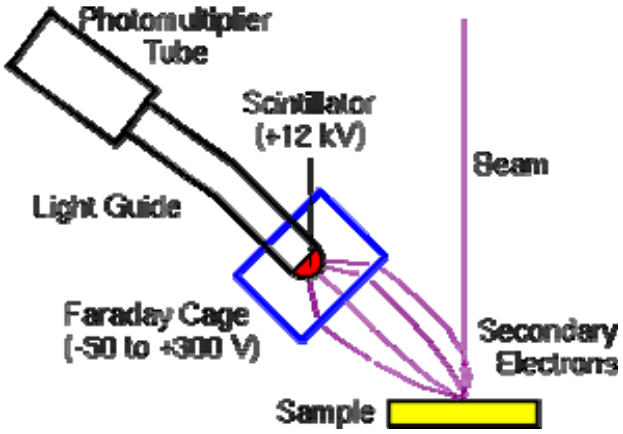

Fig. 4. *Diagram of Scanning electron microscopy*

To produce images, these electron signals are measured as a function of primary beam position while the beam is scanned in a raster pattern over the sample. The scintillator-photomultiplier electron detector (called an Everhart-Thornley detector, after its inventors) measures the secondary electrons. Higher voltages on the Faraday cage draw in more secondary electrons with more diverse trajectories. Off-axis detector placement favors secondary electrons with trajectories leading toward the detector. This provides the topographical information characteristic of secondary electron images [4].
The assembly of nanocrystals onto the CNT array is demonstrated by scanning electron microscopy (SEM) images (Fig.5). As a comparison, figure show the SEM images of as-grown, vertically-aligned CNTs on an Si wafer. The CNTs were about 10 µm in length and 150

nm in diameter. The average spacing between nanotubes was about 500 nm, with an estimated areal density of 4×10^8 tubes/cm^2.

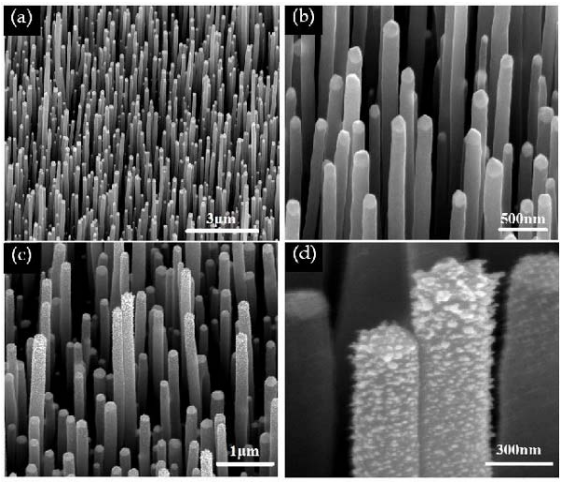

Fig. 5. SEM images of as-grown CN [5]

The backscattered electrons are usually measured with a solid state detector located on the primary beam pole piece. The detector consists of a diode with a thin gold conductor across the front surface. Backscattered (but not secondary) electrons have sufficient energy to pass through the front surface and produce electron hole pairs which produce a current in the diode.

A **Coordinate Measuring Machine** (CMM) that works at the nanoscale would have a smaller frame than the CMM used for macroscale objects (Fig.6). This is so because it may provide the necessary stiffness and stability to achieve nanoscale uncertainties in x,y and z directions. The probes for such a machine need to be small to enable a 3-D measurement of nanometre features from the sides and from inside like nanoholes.

Fig. 6. Dimensional metrology using CMM

There are a variety of nanostructures. The most common way to classify nano structures is by their dimensions (Table 1).

Dimensions	Criteria	Examples
Zero dimensional (0-D)	The nanostructure has all dimensions in the nanometer range.	Nanoparticles, quantum dots, nanodots
One Dimensional (1-D)	One dimension of the nanostructure is outside the nanometer range.	Nanowires, nanorods, nanotubes
Two Dimensional (2-D)	Two dimensions of the nanostructure are outside the nanometer range.	Coatings, thin-film-multilayers
Three Dimensional (3-D)	Three dimensions of the nanostructure are outside the nanometer range.	Bulk

Table 1. Dimensional classification

Also for accuracy laser interferometers need to be used. NIST has developed a surface measuring instrument, called the **Molecular Measuring Machine** (Fig 7). This instrument is basically an STM. The x- and y-axes are read out by laser interferometers. The molecules on the surface area can be identified individually and at the same time the distance between any two molecules can be determined. For measuring with molecular resolution, the measuring times become very large for even a very small surface area.

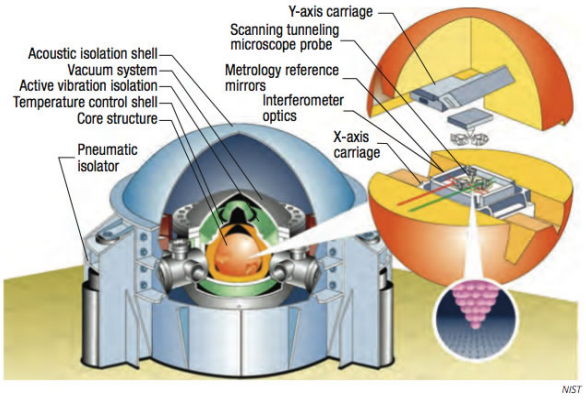

Fig. 7. Cut-away view of the Molecular Measuring Machine. Illustration NIST

X-ray diffraction (XRD) is a versatile, non-destructive technique that reveals detailed information about the chemical composition and crystallographic structure of

natural and manufactured materials. Line profile analysis is a diffraction technique used to obtain microstructural information of the sample averaged over the diffraction volume. Nanometrology tools are essential to reveal, verify and control the dimensions and structures in nanomaterials. X-ray analytical techniques are ideally suited for this purpose, making use of radiation with a short wavelength (typically around a tenth of a nanometer) and due to the high penetration depth of X-rays in many kinds of materials.
MEMS/NEMS (Micro/Nano Electro-Mechanical Systems) is a rapidly growing field building upon the existing silicon processing infrastructure to create micron/nano-scale machines. These devices are widely used in aerospace, automotive, biotechnology instrumentation, robotics, manufacturing and other applications and our gateway into coming nano-technology devices and systems. Unlike conventional integrated circuits, these devices can have many functions, including sensing, communication, and actuation. Just like microelectronics, MEMS/NEMS technology will permeate our everyday lives in the coming decades. The specific experience in this area allows to achieve excellent pratical results especially when machining hard materials where ultraprecision turning may be used as an alternative to fine grinding.
Nanobiotechnology addresses the development of nanometrology related to biomedicine, bioscience and bio-technology. This is of particular importance for the pharmaceutical industry, health care applications, clinical diagnostics, and medical devices (e.g. implants), as well as for food safety. Measurement challenges in this rapidly developing area include the measurement of dimensions of biological structures, measurement of relevant levels of biologically important substances (such as drugs, biomarkers, and toxins), and the biological variability of systems. Characterising soft and wet materials at the scale of nanometers remains a challenging task to this community. During the past decade, atomic force microscopy (AFM) has been increasingly used to image and manipulate biomolecules and cell surfaces in their native environment. In this application note, we show how the power of AFM force spectroscopy with tips bearing biologically active molecules can be utilized to explore the dynamics of the interaction between individual bacterial adhesions and their receptors as well as to map single adhesins directly on living bacteria.

3. CONCLUSIONS

There exist close interactions between precision metrology and newest industrial and technological developments in the field of precision machining. Quality control and quality management are far more than practical application of precision measurement technique but it is not possible to achieve high quality, precision and reliability of technical products without appropriate and intelligent metrology.
The need for dimensional micro and nano metrology is evident, and as critical dimensions are scaled down and geometrical complexity of objects increased the available technologies appear not sufficient. Major research and development efforts have to be undertaken in order to answer these challenges. The developments of course have to include new measuring principle and instrumentation.

4. REFERENCES

[1] Nakayama, K., Tanaka, M., Shiota, F., Kuroda, K.: *Metrologia*, 28(6), 483–502, 1992.
[2] Carneiro, K.: *The need for measurement and testing in nanotechnology*, High Level Expert Group on Measurement and Testing Under the European Framework , 2002.
[3] Škorić, B., Kakaš, D., Gostimirović, M., Miletić, A.: *Nanoscale Modification of Hard Coatings with Ion Implantation*, Materials and technology 45 4,pp.69-72, 2011.
[4] Goldstein, J., I., Newbury, D., E., Echlin, P., Joy, D., C., Fiori, C., Lifshin, E.: *Scanning Electron Microscopy and X-Ray Microanalysis*, Plenum Press, New York.
[5] Lu, G., H., Zhu, l., Y., Wang, P., X., Chen, J., H., Dikin, D., A., Ruoff, R., S., Yu, Y., Ren, Z., F.: *Electrostatic-force-directed assembly of Ag nanocrystals onto vertically aligned carbon nanotubes*, J. Phys. Chem. 48, pp.17919-17922, 2007.

Authors: **Prof. Dr. Branko Škorić,** University of Novi Sad, Faculty of Technical Sciences, Department for Production Engineering, Trg Dositeja Obradovica 6, 21000 Novi Sad, Serbia, Phone.: +381 21 485 2342, Fax: +381 21 454-495.
E-mail: skoricb@uns.ac.rs
Univ.-Prof. Roman Schrittwieser, Institute for Ion Physics and Applied Physics Leopold-Franzens University of Innsbruck, Technikerstr. 25, A-6020 Innsbruck, Austria
Prof. PhD Albano Cavaleiro, University Coimbra, Grupo de Materiais, Pinhal de Marrocos, 3030-201 Coimbra, Portugal.

Journal of Production Engineering
Vol.16 No.2

Original Scientific Paper

Narayan C. Nayak, Antaryami Mishra

DEVELOPMENT AND MECHANICAL CHARACTERIZATION OF PALMYRA FRUIT FIBER REINFORCED EPOXY COMPOSITES

Received: 01 November 2013 / Accepted: 29 November 2013

Abstract: *In recent years, lingo cellulosic fibers are increasingly used as reinforcements in many thermoset and thermoplastic matrices for the production of low-cost and lightweight materials. Composites of Palmyra fruit fiber and epoxy have been prepared with various fiber volume fractions and tested. It is observed that with increase in fiber content there is considerable increase in strength. Similarly composites of different fiber weight fractions were prepared and epoxy as matrix material. Water absorption tests were performed to assess their performances. With the increase of fiber size water absorption capability of composites were increased due to the hydrophilic nature of fibers.*

Key words: *Palmyra fruit fiber, Epoxy, Composites, Strength, Water absorption*

Razvoj i mehanička karakterizacija epoksi kompozita ojačanih palmira vlaknom. *U poslednjih nekoliko godina, celulozna vlakna se sve više koriste za ojačanje mnogih termoset i termoplastičnih matrica za proizvodnju jeftinih i lakih materijala. Kompoziti od epoksi i Palmira vlakana su pripremljeni sa različitim jačinama frakcije vlakana i testirani. Primećuje se da sa povećanjem vlakana u sadržaju postoji značajno povećanje snage. Slično tome su pripremljeni kompoziti sa različitim težinama frakcije vlakana i epoksi kao materijala matrice. Za procenu njihovih performansi urađeni su testovi apsorpcije vode. Sa povećanjem veličine vlakana kompozita mogućnosti apsorpcije vode su povećane zbog hidrofilne prirode vlakana.*

Ključne reči: *palmira vlakno, epoksi, kompoziti, jačina, apsorpcija vode*

1. INTRODUCTION

In today's engineering world many classes of composite materials have emerged, including fiber reinforced Plastics (FRP), natural fiber composites, metal matrix composites (MMC) and ceramic matrix composites (CMC). During the last few years, a series of works have been done to replace the conventional synthetic fiber with natural fiber composites. Sisal, jute, cotton, flax and broom are the most commonly fibers used to reinforce polymers. In addition, fibers like jute, oil palm, bamboo, wheat and flax straw, waste silk and banana have been proved to be good and effective reinforcement in the thermoset and thermoplastic matrices. A number of investigations have been conducted on several types of natural fibers such as kenaf, hemp, flax, bamboo and jute to study the effect of these fibers on the mechanical properties of composite materials. In recent composite technology research and development, efforts have focused on new out-of-autoclave material forms, and automated processes that can markedly increase stiffness, toughness, ambient & high temperature strength production efficiencies.

2. REVIEW OF LITERATURE

In order to exploit the excellent attractive mechanical properties of Empty Fruit Bunch (EFB) fibers, enormous effort is being made by the researchers to develop the EFB-reinforced polymer matrix composites. Korenis et al. [1] assessed the performance where aspects of suitability for the candidate elements in terms of mechanical properties are analyzed. Ahmed et al [2] studied the physical and mechanical properties of oil palm empty fruit bunch fiber reinforced with polypropylene. They observed that tensile strength has considerably increased with oxidized fiber reinforcement and water absorption capacity is optimum till 25 wt. % of fiber. Beyond this water absorption capacity has increased. Nicollier and Mutasher [3] investigated mechanical properties of banana-fiber-cement composites. Thermal, mechanical and morphological properties of fruit bunch fiber reinforced epoxy composites were examined by Jawaid et al. [4]. Fractures surfaces were also studied by scanning microscopy. Rao et al. [5] studied the wear behavior of coir fiber reinforced epoxy composites with the Taguchi method. Toutanji et al. [6] studied the fiber reinforced polymer composites (FRPC) and established an effective mean for the repair and rehabilitation of infrastructure. Razak and Kalam [7] studied the effect of OPEFB size on the mechanical properties and water absorption behaviour of OPEFB/PP nanoclay/PP hybrid Composites. The EFB laminates were tested for thermal and mechanical properties. Thermal shock and thermal insulation performance of the EFB laminates were evaluated under high powered IR heating lamps simulating a high heating rate and high heat flux environment for about 70^0 C. Velumurugan et al. [8] conducted tensile tests and finite element analysis for palmyra fruit fiber reinforced epoxy composites to determine the tensile strength and fracture properties. The influence of fibre length on wear behavior of

borassus fruit fibre reinforced epoxy composites was studied by Boopathi et al. [9]. It was seen that 5 mm length of fiber reinforced composite exhibited better wear properties sliding against steel. Ogbuagu et al. [10] investigated pulp and paper making potential of borassus fruit fibers in acidic and alkali media. Fibers treated in alkali medium had lower yield than treated in acidic medium. However better mechanical properties were observed from alkali treated fibers.

3. SCOPE

The objective of the present research is to explore the possible use of Palmyra fruit fiber wastes as reinforcement in a polymer matrix for making composites and

a. The fibers are to be cut and crushed to micron sizes for proper mixing with the matrix of epoxy to develop composites
b. Hand moulding technique is employed to fabricate the tensile test bars etc. by developing suitable dies in house
c. Mechanical characterization of these specimens in terms of tensile strength, tensile modulus etc. by standard methods using Tensometer or available equipments.
d. Water absorption capacity of the specimens by weight gain method as per ASTM standards
e. Out of different types of composites so prepared the best one under above tests may be found out.

4. MATERIALS AND METHODS

4.1 Palmyra Fruit Fiber (PFB)

Palmyra fruit bunch fiber is a lingo cellulosic source which is available as substrate in cellulose production. The application of cellulose to produce bio-ethanol (alternative source of fuel) is handicap by high cost. The use of fruit bunch, wastage from Palmyra will reduce the cost of enzyme production comparable to other sources. Advantages of Palmyra fruit bunch fibers are its availability, renewability, low cost and high strength. These materials have been collected from local areas available in plenty in Odisha at Talcher in Angul district (Fig.1)

4.2 Epoxy Resin

Epoxy resin (CY-230 and Hardener-HY 951 were collected from Hindustan Ceiba Geigy Ltd, India) for preparation of the composite and investigation. Properties of epoxy resin in use are, Density = 1200 kg/m^3, Young's modulus of elasticity = 20 GPa, Tensile strength = 75 MPa.

4.3 Preparation of Composite

4.3.1 Alkali Treatment of Fibers

The PFB fibers were taken out with specified dimensional size as mentioned earlier. The fibers were soaked in 1% NaOH solution at room temperature for 24 hours. Then, the fibers were taken out and washed with distilled water for 7 times to remove excessive alkaline solution. The fibers were dried in an oven at 80°C for 8 hours. This has been done for proper wetting of fibres with polymer matrix and has better strength than untreated fibers.

4.3.2 Specimen preparation

Palmyra fibers of 2-3 mm length and 0.5 mm diameter were cut for mixing with epoxy to prepare test bars of ASTM D 638 standards for tensile test. These fibers were further crushed to particle sizes. The particles of different diameters have been selected passing it through sieve shaker. Particulate composites of different weight fractions i.e 5, 10 and 15 % respectively for three different fiber sizes (106µm, 150µm, and 212µm) (Fig.2,3 and 4) were prepared.

The compounding process was performed in a dispersion mixer at 180ºC which follows the standard of thermoplastic temperature with rotating speed of 50 rpm and PFB particles were poured into the mixer after 20 min. Compounding process is continued further at same speed for 10 to 15 min, to ensure the PFB particles mix thoroughly with the matrix before the compound was poured in a box type steel die for making sheets. The composite sheet was prepared after curing at room temperature for three days. Further these sheets were cut into 50x13x5 mm rectangular sizes for water absorption tests.

4.4 Die Design for Tensile Testing

A wooden die (Acacia wood) has been prepared suiting to the requirements of ASTM D 638 Standard as shown in Fig. 5. The limiting dimensions have been given in Table 1. The photograph of the mould is also shown in Fig.6.

Fig. 1 Palm Fiber (0.5 mm)

Fig. 2 212µm fiber

Fig. 3 150µm fiber

Fig. 4 106µm fiber

Table 1 Specimen dimensions as per ASTM Standard

Specimen	l_1	l_2	l_3	l	w_1	w_2	w_3	w_4	w_5	w_6	w_7	t_1	t_2	t_3
Standard	42	100	42	204	25	25	13	13	13	25	25	-	-	-

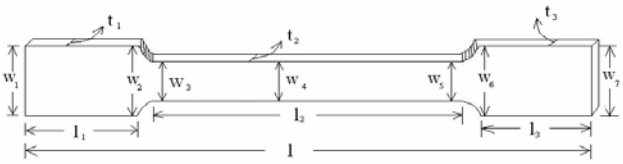

Fig.5: Standard tensile test specimet

Fig. 6: Wooden Die block for tensile test

5. RESULTS AND DISCUSSION

5.1 Tensile Test

A standard specimen is prepared as shown in figure 5. The test process involves placing the test specimen in the Tensometer and applying tension to it until it fractures. During the application of tension, the elongation of the gauge section is recorded against the applied force. The Tensometer and the specimens under test have been shown in Fig.7 and 8 respectively. Tensometer has been supplied by MIKROTECH (A Kudale Enterprise based at Pune, India) in the year 1992. Capacity – 2000 Kgf (20 KN), Loading ranges are – 2000,1000, 500, 250,125.62.5,31.25, 16 and 8 Kgf, Vice type grips were used. Overall dimension-965x235x230 mm. A load range of 16 Kgf was set for the experiment.

Fig.7 The Tensometer

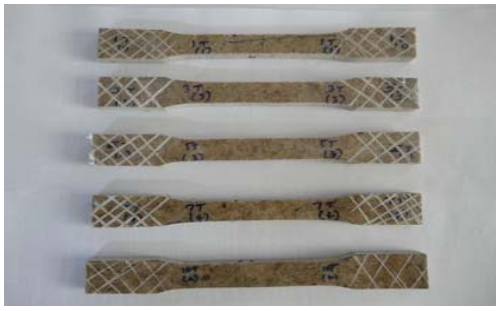

Fig.8 Test specimens

Figures (9-12) show the effect of volume fraction of Palmyra fiber on mean tensile strength, mean tensile modulus, specific tensile strength and specific tensile modulus respectively. In Fig. 9, mean tensile strength decreases up to volume fraction of 0.18 and then increases. In Fig. 10, mean tensile modulus increases with the increase in volume fraction. Specific tensile strength decreases up to 0.11 and then increases with the increase in volume fraction in Fig. 11. Specific tensile modulus increases with the increase in volume fraction in Fig. 12.

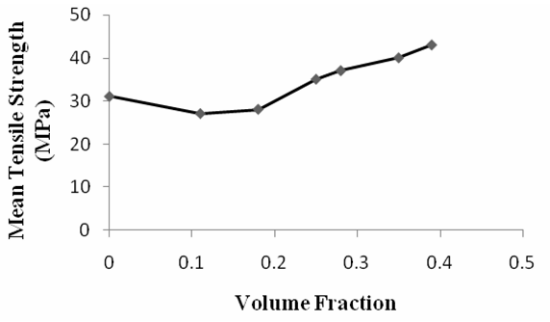

Fig. 9: Vol. Fraction vs. Mean Tensile Strength

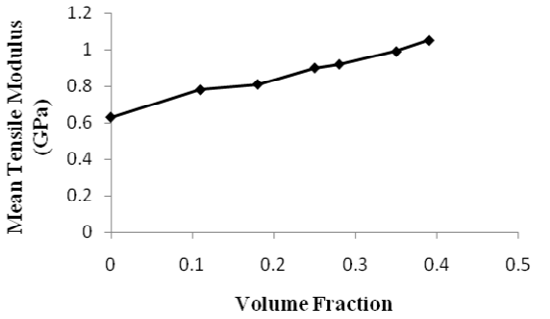

Fig. 10 Vol. Fraction vs. Mean Tensile Modulus

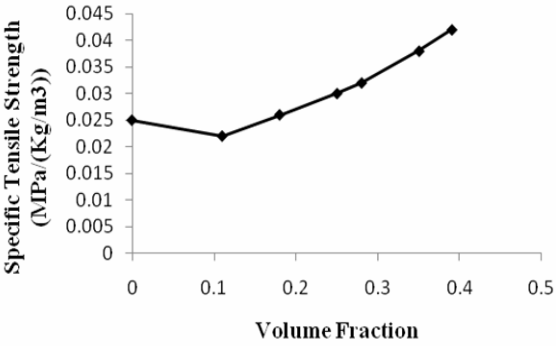

Fig.11 Vol. Fraction vs. Specific Tensile Strength

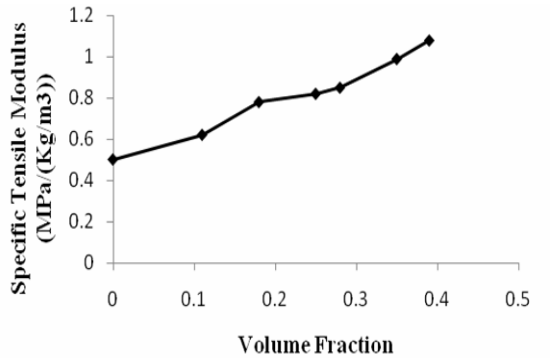

Fig. 12 Vol. Fraction vs. Sp. Tensile Modulus

5.2 Water Absorption Test

Water absorption (ASTM D570) is used to determine the amount of water absorbed under specified conditions. For this test, the specimens prepared are (50

mm x 13 mm with thickness of 5 mm) dried in an oven for a specified time and temperature and then placed in desiccators to cool. The specimens are weighed in electronic balance having least count of 0.001gm. The material is then soaked in water, often at room temperature for 24 hours. The final weight is taken in electronic balance and thus the difference between initial weight and final weight gives the water absorption capacity of the material. This test is necessary because various polymeric materials are susceptible to water absorption during its life exposure. The specimens tested under such conditions exhibited the gain in weight as indicated in Table 2.

6. CONCLUSIONS

It is observed from the tensile tests that the tensile strength and modulus increases with the increase in volume fraction of fibers. Of course with less fiber reinforcement (10% or so) there is slight decrease in strength which might have occurred due to higher amount of matrix material. Further it is seen that at around 40 % of fiber content highest strength and modulus has been achieved for this type of composite. This is in near agreement with the work of earlier researchers [8] where 5 mm length of fibers showed tensile strength around 22 MPa where as in this case it is found to be around 40 MPa. This might have been obtained due to lesser length of fibers i.e. 2-3 mm. The water absorption tests indicate that for 106 micron and 212 micron sizes of fibers with 10% weight fraction of fibers are less susceptible to moisture absorption than for 150 micron size of fibers. However it can be concluded that these composites absorb water much more than specified as per standard and not suitable for application in wet environment. Probably the hydrophilic nature of these fibres contributes to such properties. But these composites can be very well suitable for structural applications in dry environment due to higher strength.

Table 2 Percentage of water absorption by various composites

Fiber size in micron	Fiber Weight fractions of the composite	Initial weight in gms	Final weight in gms	Percentage absorption
106	5	4.312	7.532	74.68
	10	5.102	7.005	37.31
	15	5.450	7.512	37.83
150	5	5.212	7.023	38.20
	10	4.823	6.80	40.99
	15	4.684	6.223	32.86
212	5	4.003	6.543	63.45
	10	5.220	6.450	23.56
	15	5.231	7.231	38.23

7. REFERENCES

[1] Koronis. G., Silva. A., Fontul. M. “Green composites. A review of adequate materials for automotive applications,” International Journal of Mechanical Sciences, Vol.52 (2010), pp.874–891.

[2] Ahmed, A.S., Alam, M.A., Piee, A., Rahman, M.R. and Hamdan, S. “Study of Physical and Mechanical Properties of Oil Palm Empty Fruit Bunch Fiber Reinforced Polypropylene Composites,” Jou. of Energy and Environment, Vol.2, (2010) , pp.16-21

[3] Nicollier, C., and Mutasher, S.A. “Failure prediction on advanced grid stiffened composite cylinder under axial compression,” Composite Structures, Vol.93 (2011), 1939–1946.

[4] Jawaid, M., Abdul Khalil, H.P.S.,Bhat, A.H., and Abu Baker, A. “ Impact Properties of Natural Fiber Hybrid Reinforced Epoxy Composites,” Advanced Material Research, Vol.264-265, (2011) , pp.688-693.

[5] Rao. C.H., Kundalwal. S.I. and Ray, M.C. “Sensing of Damage and Healing in Three-dimensional Braided Composites with Vascular Channels,” Composites Science and Technology, Vol.72 (2012), pp. 1618–1626.

[6] Toutanji. H, Li. F. and Cheng. H.M. “Effective Properties of a Novel Continuous Fuzzy-fiber Reinforced Composite Using the Method of Cells and the Finite Element Method,” European Journal of Mechanics of Solids, Vol. 36 (2012), pp. 191-203.

[7] Razak, N. W. A. and Kalam, A. “Effect of OPEFB Size on the Mechanical Properties and Water Absorption Behaviour of OPEFB/PP nanoclay/PP Hybrid Composites,” Procedia Engineering Vol.41 (2012) pp.1593 – 1599.

[8] Velumurugan, G., Vadivel, D., Aravind, R., Vengatesan, S.P. and Mathizhagan, A. “Tensile Test Analysis of Natural Fibre Reinforced Composites,” Int. Jou. of Mechanical and Industrial Engineering, Vol.2, Issue-4, 2012, pp.56-60.

[9] Boopathi, L, Sampath, P.S., Mylsamy, K. “ Influence of Fiber Length in the Wear Behaviour of Borassus Fruit Fibre Reinforced Epoxy Composites,” Int. Jou. of Engineering Science and Technology, Vol.4, Sept. 2012, pp. 4119-4129.

[10] Ogbuagu, A.S., Ekpunobi, U.E., Onwuka, T.N., and Okeye, N.H., “Pulp and Paper Making Potential of Palmyra Fruit Fiber Borassus Flabelifar,” Der Chemica Sinica, Vol. 4, (2013), pp. 19-24.

***Authors*: Phd Narayan C. Nayak, Phd Antaryami Mishra,** Mechanical Engineering Department, Indira Gandhi Institute of Technology, Sarang, Odisha, India.
E-mail: nayak.iem@gmail.com
antaryami_igit@ yahoo.com

Journal of Production Engineering
Vol.16 No.2

Original Scientific Paper

Abhimanu Singh, Datta, C. K.

LOSS MINIMIZATION POLICY FOR A PRODUCTION LINE WITH IMMEDIATE FEEDBACK AND MULTI SERVER FACILITY AT ALL PROCESSING UNITS

Received: 7 April 2013 / Accepted: 09 May 2013

Abstract: *In this paper, we have derived mathematical expressions for the loss caused by ill processing of items or jobs at various processing units in a production line. On the basis of the expressions, we concluded a policy for minimization of the loss caused by ill processing of jobs or items at various processing units. In the production line, each of the processing units has multi-server facility. Arrivals to the first processing unit are according to Poisson distribution. Service times at each of the processing units are exponentially distributed. At each of the processing units, we have taken into account immediate feedback and the rejection possibility. Considering the processing cost at each of the processing units, the average loss to the system due to rejection, caused by ill processing at various processing units, is obtained.*

Keywords: *Queuing Network, Processing Units, Production Line, multi-server, Immediate Feedback*

Politika minimizacije gubitka za proizvodnu liniju sa trenutnom povratnom vezom u multi serverskom okruženju za sve proizvodne jedinice. *U ovom radu je izveden matematički izraz za gubitak usled neadekvatne obrade delova ili radnih pozicija na različitim proizvodnim jedinicama na proizvodnoj liniji. Na početku experimenta je usvojena politika minimizacije gubitka usled neadekvatne obrade delova ili radnih pozicija na različitim proizvodnim mestima. Na proizvodnoj liniji svaka proizvodna jedinica ima multi serversko postrojenje. Dolazak do prvih proizvodnih jedinca se odvija shodno Poasonovoj raspodeli. Servisna vremena na svakoj proizvodnoj jedinici su eksponencionalno raspoređena. Na svakoj proizvodnoj jedinici je uzeta u obzir trenutna povratna sprega i moguće odbacivanje. Uzimajući u obzir troškove obrade na svakoj proizvodnoj jedinici, prosečan gubitak sistema usled odbacivanja, usled neadekvatne obrade na različitim proizvodnim jedinicama, je održan.*

Ključne reči: *čekajuća mreža, proizvodne jedinice, proizvodna linija, multi server, trenutna povratna sprega*

1. INTRODUCTION

A production line as shown in fig.1 is a sequence of a finite number of processing units arranged in a specific order. At each of the processing units, service may be provided by one person or one machine that is called single- server facility, or it can be provided by more than one persons or more than one machines that is called multi-server facility at the respective processing units. In this paper we have considered multi-server facility at each of the processing units. At each of the processing units, a specific type of processing is performed i.e. at different processing units material is processed differently. At a processing unit, the processing times of different jobs or items are independent and are distributed exponentially around a certain value, called mean processing time.

In a production line the processing of raw material or a job starts at the first processing unit. It is processed for a certain time interval at the first processing unit and then it is transferred to the second processing unit for other type of processing, if its processing is done correctly at the first processing unit. This sequence is followed until the processing at the last processing unit is over. In a production line raw material is processed at a series of processing units one after the other and finally it is transformed into finished goods ready for use.

End of processing at each of the processing units give rise to the following three possibilities:

(a) Processing at a unit is done correctly and the job or material is transferred to the next processing unit for other type of processing.

(b) Processing at a unit is not done correctly but can be reprocessed once more at the same processing unit.

(c) Processing at a unit is neither done correctly nor it can be reprocessed at the same processing unit i.e. this job or material is lost, in this situation the job or material is rejected and put into the scrap.

We are applying Queuing Theoretical approach to study the production line and hence to derive the policy for minimization of the said loss. Several researches have studied the queues in series having infinite queuing space before each servicing unit. Specifically, J. R. Jackson [1] had studied network of waiting lines, R.R. P. Jackson [2] studied finite and infinite queuing space with phase type service taking two queues in series. In, K.L. Arya [3] has found that the steady state distribution of queue length taking two queues in the system, where each of the two non- serial servers is separately in service. O.P. Sharma [4] studied the stationary behavior of a finite space queuing model consisting of queues in series with multi-server service facility at each node.

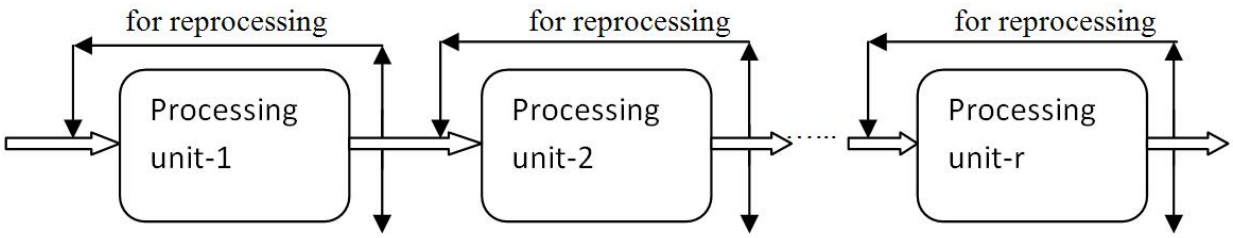

Fig. 1. A production line

2. MODELING

We consider a production line as shown in fig.2 consisting of an arbitrary number(r) of processing units arranged in a series in a specific order. Each of the processing units has multi- server facility and immediate feedback.

Let

λ = Mean arrival rate to the first processing unit from an infinite source, following Poisson's rule.

μ_i = Mean service rate of an individual server at the i^{th} processing unit having exponentially distributed service times.

s_i = Number of servers at the i^{th} processing unit.

n_i = Number of unprocessed jobs before the i^{th} processing unit waiting for service, including one in service, if any, at any time t.

$p_{i,i+1}$ = Probability that the processing of a job or material at the i^{th} processing unit is done correctly and it is transferred to the $(i+1)^{st}$ processing unit.

$p_{i,i}$ = Probability that the processing of a job or material at the i^{th} processing unit is not done correctly but it can be reprocessed once more, so, it is transferred to the same processing unit for processing once more.

$p_{i,o}$ = Probability that the processing of a job or material at the i^{th} processing unit is neither done correctly nor it remains suitable for reprocessing.

C_i = Processing cost per unit at the i^{th} processing unit.

L = Average loss per unit time, to the system due to rejection of items at various processing units due to ill-processing.

$P(n_1, n_2, ...n_r, t) =$ Probability that there are n_1 jobs waiting for processing before the first processing unit including one in service, if any, n_2 jobs before the second processing unit waiting for service including one in service, if any, and so on, n_r jobs before the r^{th} processing unit waiting for service including one in service ,if any at time t, with $n_i \geq 0 (1 \leq i \leq r)$, and $P(n_1, n_2, ...n_r, t)$=0, if some n_i <0 (because number of jobs cannot be negative).

The above production line can be represented by a serial network of queues in which each processing unit is equivalent to a queue with the same number of similar servers and the same numbers of jobs waiting for service.
In the above serial network of queues, each queue has immediate feedback. To analyze this serial network of queues firstly we remove the immediate feedback.

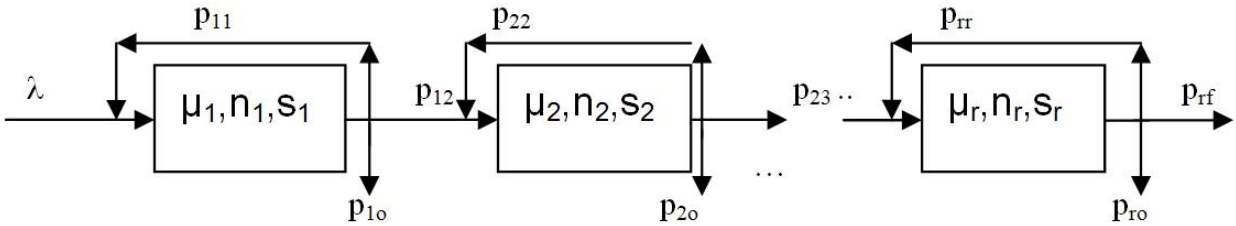

Fig. 2. Proposed production line

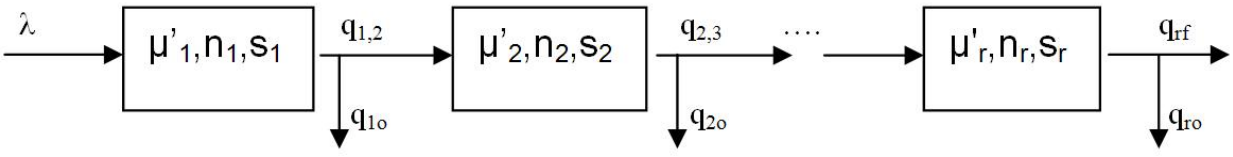

Fig.3. Equivalent serial network of queues

After the removal of immediate feedback the above serial network of queues is replaced by one, as shown in Fig. 3.

Here $\mu_i^{'} = \mu_i(1-p_{i,i})$, where $\mu_i^{'}$ is the effective service at the i^{th} processing unit after the removal of the immediate feedback [5].

And the respective probabilities become as follows

$$q_{io} = \frac{p_{io}}{(1-p_{ii})}, q_{ii+1} = \frac{p_{ii+1}}{(1-p_{ii})} \qquad (1)$$

3. EQUATIONS GOVERNING THE QUEUING SYSTEM

Under the steady state conditions, we have [6, 7, 8] :

$$\left[\lambda + s_1\mu_1^{'} + s_2\mu_2^{'} + ... + s_r\mu_r^{'}\right].$$

$$\mathrm{P}(n_1, n_2, ...n_r) = \lambda \mathrm{P}(n_1 - 1, n_2 n_3, ...n_r) +$$

$$\sum_{i=1}^{r} s_i\mu_i^{'}.q_{i,i+1}.P(n_1, n_2, ...n_i + 1, n_{i+1} - 1, ...n_r) +$$

$$\sum_{i=1}^{r} s_i\mu_i^{'}.q_{i,o}.P(n_1, n_2, ...n_i + 1.n_{i+1}, ...n_r) \qquad (2)$$

4. SOLUTION FOR INFINITE QUEUING SYSTEM

Under the steady state conditions all the queues behave independently and thus the solution of steady state equation in product form is given by [9,10]

$$\mathrm{P}(n_1, n_2, ...n_r) = \prod_{i=1}^{r}(1-\rho_i)\rho_i^{n_i}, \quad \text{where}$$

$$n_i \geq 0 (1 \leq i \leq r) \text{ and } \rho_i < 1 \ (1 \leq i \leq r) \qquad (3)$$

If any $\rho_i \ (1 \leq i \leq r) > 1$ then the stability is disturbed and the behavior of the system will not remain stationary consequently solution will not be given by Eq. (3).

Here, we have

$$\rho_i = \frac{\lambda_i}{s_i\mu_i'},$$

Where $\lambda_i = \lambda \prod_{k=1}^{i} \frac{p_{k-1,k}}{(1-p_{k-1,k-1})}, \ p_{0,0} = 0$

Thus

$$\rho_i = \frac{\lambda}{s_i\mu_i} \prod_{k=1}^{i} \frac{p_{k-1,k}}{(1-p_{k,k})}, \qquad (4)$$

With $p_{0,1} = 1$

It is observed that

$$\sum_{i=1}^{r} \lambda_i.q_{i,o} + \lambda_r.q_{r,f} = \lambda \qquad (5)$$

5. EVALUATION OF AVERAGE LOSS:

Let c_1 be the processing cost at the first processing unit, c_2 the processing cost at the second processing unit and so on $\ldots c_r$, the processing cost at the r^{th} processing unit.

If an item is rejected just after its processing at the first processing unit is over, then it causes a loss c_1 to the system. If an item is rejected just after its processing at the second processing unit is over, then it causes a loss (c_1+c_2) to the system. Thus, in general if an item is rejected just after its processing at the r^{th} processing unit is over, then it causes a loss $(c_1+c_2+c_3+\ldots+c_r)$ to the system.

L, the average loss per unit time to the system due to rejection of items just after the processing at various processing units due to ill-processing (processing of an item is neither done correctly nor it can be reprocessed) is

$$\mathrm{L} = c_1 \ \lambda \ q_{1,o} + (c_1 + c_2) \ \lambda \ q_{1,2} \ q_{2,o} + \ldots$$

$$+ (c_1 + c_2 + ...c_r) \ \lambda \ q_{1,2} \ q_{2,3} \ldots q_{r-1,r} \ q_{r,o}$$

$$= \sum_{i=1}^{r} (c_1 + c_2 + ...c_i) \ \lambda \ q_{1,2}.q_{2,3}...q_{i-1,i}q_{i,o},$$

With $q_{0,1} = 1$

$$= \sum_{i=1}^{r} (c_1 + c_2 + ...c_i) \ \lambda \quad \frac{p_{1,2}}{1-p_{1,1}} \frac{p_{2,3}}{1-p_{2,2}} \ldots$$

$$\frac{p_{i-1,i}}{1-p_{i-1,i-1}} \frac{p_{i,o}}{1-p_{i,i}},$$

$$= \lambda \sum_{i=1}^{r} (c_1 + c_2 + ...c_i) \prod_{k=1}^{i} \left(\frac{p_{k-1,k}}{1-p_{k-1,k-1}} \right).$$

$$\frac{p_{i,o}}{(1-p_{i,i})}$$

With $p_{0,0} = 0, and \quad p_{0,1} = 1$ (6)

On the basis of the above expressions, it is clear that later the stage of rejection of an item from the assembly line greater the loss to the system.

6. POLICY TO MINIMIZE THE LOSS

There are two types of losses.

1. First Type-

one-when the processing of an item or job is not done correctly and it is reprocessed at the same production line. In this type the time spent by the machine goes waste and creates loss to the system.

2. Second Type-
when the processing of an item or job at a processing unit is not correctly as well as it can not be reprocessed once more, it then is put into the scrap. In this type, the cost of bringing the item or job into the present form goes waste. This loss includes the cost occurred due to processing at the earlier stages and the cost occurred on the material in making it suitable for processing at the first processing unit.

In this study, we are considering the second type loss caused as the cost occurred due to processing at the earlier stages

Average loss i.e. the sum in equation (6), can be minimized by minimizing the individual terms. This we can do in three ways:

(i) It is obvious from the equation (6) that if an item (or a job) is rejected from the production line at a later stage it causes more and more loss to the system. Thus, emphasis should be given to install comparatively much efficient machines at later stages.
(ii) The sum in equation (6) can be minimized by minimizing the term $P_{io.}$. Thus loss can be minimized by installing machines with minimum rejection rate.
(iii) The sum in equation (6) can be minimized by maximizing the term $(1-P_{ii})$ i.e. by minimizing P_{ii}. Thus, loss can be minimized by installing machines with minimum reprocessing rate.

7. ACKNOWLEDGEMENT

The corresponding author is thankful to Prof. C.K. Datta, [Formerly Professor at Delhi Technological University], and Prof. B.D. Acharya, [Formerly Sci.'G' & Senior Advisor to Govt. of India, DST, New Delhi], for encouragement. I am thankful to the management of BPIT, Rohini, Delhi, also, for providing creative and learning environment in the institute and my colleagues for cooperation and support they extended all the time

8. REFERENCES

[1] Jackson, J. R., (1957), "*Networks of waiting lines"*, Oper. Res.,5, pp. 518-521.
http://or.journal.informs.org/content/5/4/518.full.pdf
[2] Jackson, R.R.P.,(1954**)** "*Queueing Systems with Phase Type Service***,"** Operations Research Quarterly, 5(2), pp. 109-120.
[3] Arya,K. L., (1972*), Study of a Network of Serial and Non-serial Servers with Phase Type Service and Finite Queueing Space*, Journal of Applied Probability [online] 9(1), pp198-201.
http://www.jstor.org/stable/3212649
[4] Sharma, O.P., (1973), *A Model for Queues in Serie*s. Journal of Applied Probability [Online] 10(3), pp. 691-696.
http://www.jstor.org/stable/3212791
[5] J. Walrand*, An Introduction to Queueing Networks*, Prentice Hall, Englewood Clifs, New Jersey, (1988), ch 4, pp. 160.
[6] Saaty, T. L., *Elements of Queueing Theory*, McGraw-Hill, New York, 1961, ch. 12, pp. 260.
[7] Gross ,D. and Harris, C. M., *Fundamentals of Queueing Theory*, John-Wiley New York, 1985, ch. 4, pp. 220-226
[8] Guy, L., Curry. Richard M. Feldman*, Manufacturing System*, Springer-Verlag, Berlin Heidelberg, 2011, ch. 3, pp. 77-80.
[9] Bhat, U.N.*, An Introduction to Queueing Theory*, Birkhäuser, Boston, 2008, ch. 7, pp 144-147.
[10] Kishor.S.Trivedi., *Probability & Statistics with Reliability, Queuing and Computer Science Applications*. Wiley India (P.) Ltd., 4435/7, Ansari Road, Daryaganj, New Delhi, (2002), ch. 9, pp. 564

***Authors*: Mr. Abhimanu Singh**, Assistant Professor, Applied Mathematics, BPIT, Sector-17, Rohini, Delhi, India**, Prof., Dr., C. K. Datta**, Deptt. of Mechanical Engineering, PDM College of Engineering, Bahadurgarh, Haryana, India(Formerly Professor in Production Engineering at Delhi Technological University, Delhi, India).
65.
E-Mail: asingh19669@yahoo.co.in

Journal of Production Engineering
Vol.16 No.2

Preliminary Note

Senderská, K., Ižol, P., Mareš, A.

DIGITAL MILING LABORATORY

Received: 23 September 2013 / Accepted: 14 October 2013

Abstract: *The presented article focuses on the digital milling laboratory creation based on the digital factory concept. Realized 3D model of the laboratory lay-out contains 3D model of all machines and laboratory equipments. The realized ergonomics analysis provides RULA analysis results as a base for optimal laboratory arrangement. The created machine kinematics simulation enables to obtain mistake-free and more safety milling procedure.*

Key words: milling laboratory, digital factory, machine kinematics simulation, ergonomic

Digitalna laboratorija glodanja. *Predstavljen rad se fokusira na ostvaranje digitalne laboratorije glodanja na temelju koncepta digitalne fabrike. Realiziran 3D model rasporeda laboratorija sadrži 3d modele strojeva i opremu laboratorija. Ostvarena ergonomska analiza daju rezultati RULA analize kao osnov za optimalni raspored laboratorija. Ostvarena simulacija kinematike stroja omogučava dobjanje sigurnijeg procesa glodanja,bez grešaka.*
***Ključne* reči:** *laboratorija glodanja, digitalna fabrika, simulacija kinematike mašina*

1. INTRODUCTION

Information technologies progress has stimulated the development of various computational methods enabling to perform realistic simulation of various phenomena and processes, including the manufacturing processes [1,2,3]. Virtual manufacturing systems enable to try the proposed changes without interrupting the actual production process, without consumption of materials and energy and with a considerable benefit also in the area of security. The development has been taking the direction towards the use of the Digital Factory and/or Digital Manufacturing concepts where it is possible to realistically model and simulate all components of the manufacturing system starting with the machining simulation through moving parts in the workplaces, workers' movements and activities at the workplace up to the machinery and equipment maintenance [4]. In an effort to get closer to this trend the concept of digital milling laboratory has been gradually built at the authors' work site, which would enables virtual simulation and verification of all work activities and operations carried out at the workplace after its completion. The created digital laboratory is based on an existing workplace, which is located at the authors' work site.

2. DIGITAL MILLING LABORATORY CONCEPT

The Digital Factory concept covers the entire product life cycle from the development through the production up to the final disposal at the end of the life cycle. Since this is a very extensive range of activities, the different parts of this concept are gradually created and integrated within the process of building the digital milling laboratory concept. To date the models have been created and virtual activities tested relative to the machining simulation within which modifications and supplements were made in order to eliminate problems associated with the collision states in machining and with the simulation of the machine operation.

2.1 Milling laboratory

As mentioned above, the concept development is based on the existing laboratory (Fig. 1). The basis of the milling laboratory is the Emco Concept MILL 155 milling machine with three controlled axes and the possibility of control system exchange. There are Heidenhain TNC 426 and Sinumerik 840D available. The size of a semi-finished product is limited by the clamping surface with the dimensions of 520 x 250 mm and the distance of 280 mm between the spindle face and the table. The total weight of the workpiece and the clamping device must be less than 20 kg, which represents the maximum table load. The machine can execute all common milling and drilling operations. Examples of milled parts may include parts of the drawing tools (punch, die), chain or gear wheels and models for molding. Further there are also different types of flanges, brackets, bearing beds, device bodies and the like. The NC programs are created either directly in the control system (simple components, semi-products, etc.) or by CAM systems and their postprocessors (parts with complicated shapes).

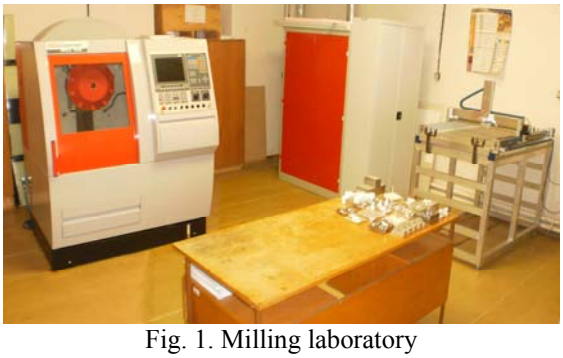

Fig. 1. Milling laboratory

The laboratory also includes a 3-axis engraving machine designed for cutting out of sheets and engraving.

The laboratory is certainly also equipped with cabinets, a worktable and other equipment.

The laboratory is used both, for research and education with focus to educate students such way, that they will be well prepared for praxis [5].

2.2 Laboratory digital model

The basis of a digital milling laboratory is constituted by a digital milling machine model, as well as other components and equipment located in the laboratory. A model of the engraving and milling machine shown in Fig. 2 and 3 was created in CATIA V5R17.

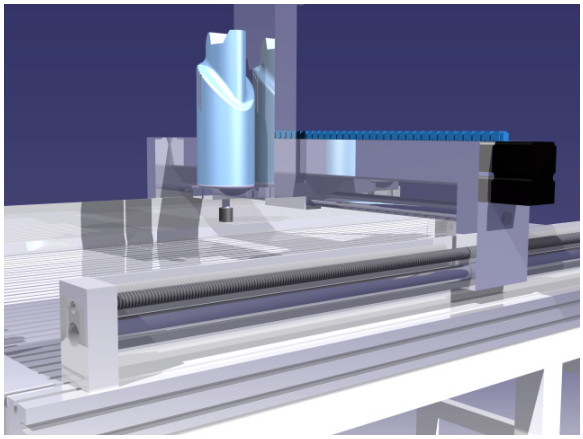

Fig. 2. 3D CAD model of the engraving machine created in the Catia V5 [6]

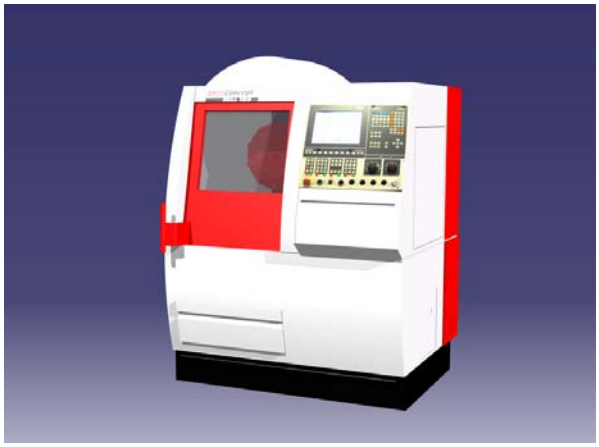

Fig. 3. Milling machine 3D CAD model created in the Catia V5 [6]

At the same time, 3D models where created of all other components located in the laboratory, i. e. working desks, a computer desk, a tool trolley, a workbench and a 3D model of the actual laboratory with building elements, doors, etc. Based on these models fully corresponding to the real objects it was possible to create the laboratory layout as shown in Fig. 4. It is certainly possible to create other variants of the laboratory layout and/or to create a new design in case of a change and/or enhancement of the laboratory.

After creating this virtual laboratory it was possible to proceed to the selection and simulation of the activities within the concept of digital milling laboratory.

Fig. 4. Milling laboratory digital model [6]

2. 3 Ergonomics

One of the simulated activities was the operation of a machine by a human (Fig. 5) and the overall worker activity at the work site, as well as the evaluation of their ergonomics. The mentioned analyses were performed in the CATIA V5R17 environment, which offers – besides the possibility to create 3D model – a variety of other useful support modules [7,8]. One of these is the ergonomics analysis module.

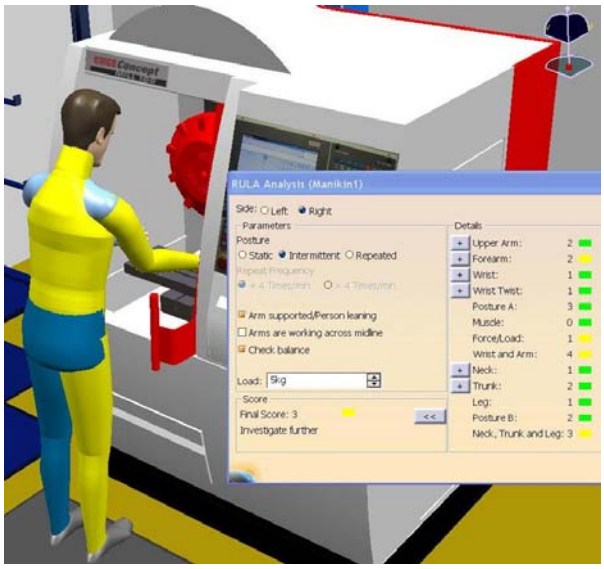

Fig. 5. Ergonomic analysis of manual machine operating - printscreen from Catia [6]

There was performed a reach analysis and also the RULA analysis of worker's position. The results were used for the evaluation of the laboratory layout, as well as the individual actions. They were also helpful in the optimization of the arrangement of kits, tools, jigs – in order to achieve the condition in which they are within the reach area.

2.4. Machine kinematics simulation

Another activity that was subject to the simulation were the operations associated with the machining. Conventional simulation of the machining process, performed in the control systems or CAM systems displays the process in a simplified manner from the point of view kinematics. The workpiece is fixed

(stationary) and all movements are executed by the tool. These simulations are essential for creating and debugging the NC program.

In case of machining under standard conditions, this level of verifying the generated tool paths is often fully sufficient. Programming systems also enable to make the simulation realistic by the use of clamping device models and models of tools and tool clamps. The simulation at this level enables to detect the collision of the tool with the workpiece or a clamping device. This can significantly prevent troubles that might occur during production. However, the collisions do occur in the real operation of a machine. It is due to the limited possibilities of these simulations.

At the described three-axis milling machine with a drum magazine for tools placed directly in the machine workspace there is a quite frequent occurence of collision states, where tools or even the drum run into the clamping devices. This happens most often during machining with small tools and short overhanging. The short tool overhanging requires that the drum come to the immediate proximity of the part and the clamping devices. Other collision situations occur in case of dense tool placement at the drum (tools are clamped in every position). There can occur also a crash of the tools adjacent to the working tool in the clamping device. This can occur especially during a short tool operation with a long tool being in the adjacent position. There have also been collisions of large size workpieces with workspace covers.

CAM systems also enable to realize a detailed simulation of the manufacturing process on the basis of a prepared NC program. The simulation shows the production machine, while relevant machine parts execute the working movements. In a three-axis milling machine the workpiece clamped on the machine table moves in a horizontal plane and the tool clamped in the spindle moves in the vertical direction. To avoid the above mentioned collisions it is necessary to create an enhanced simulation. The first step in the implementation of such a simulation is the creation of CAD models of the machine parts. The machine moving parts – longitudinal and transverse slide, machine table, drum magazine for tools – are modelled in detail. The parts that are not directly related to the machine kinematics can be modelled in a simplified way (e.g. machine cover).

The second step is to define the machine in the CAM environment, consisting of an assembly of machine part models and the definition of their movements. It begins by inserting the machine body as a stationary base. When inserting the moving part, it is first necessary to select the required axes (X, Y or Z) and then to determine the type of a movement (translational or rotational) and its range (maximum and minimum value). Only then a respective assembly of machine parts is to be assigned to this movement. When inserting the movable parts it is necessary to proceed logically in such a way as to consider interdependence of the respective assemblies of machine parts. In this step the clamp device and workpiece models are added to the assembly. To prevent the assembly from becoming exploded during the simulation it is necessary to define the coordinate system of each modelled machine part relative to the machine zero point M – Fig. 6.

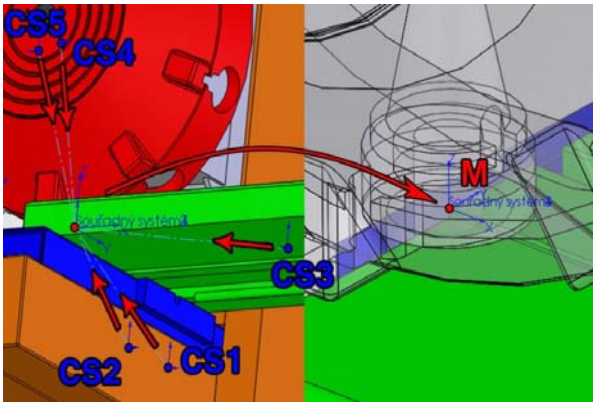

Fig. 6. Defining position of each modelled part coordinate system relative to the machine zero point M [9]

The machine definition is completed by the identification of the machine parts that will be mutually controlled for possible collisions. The using of the machine model is to be enabled and configured in the CAM system settings.

The environment for controlling the machine kinematics simulation is shown in Fig. 7. The figure shows the toolbars marked as “a” to “g” used for machine kinematics simulation control, e.g. toolbars “a” and “g” are used for starting, forwarding and for speed regulation, toolbar c enables to zoom the specified simulation element (tool, workpiece).

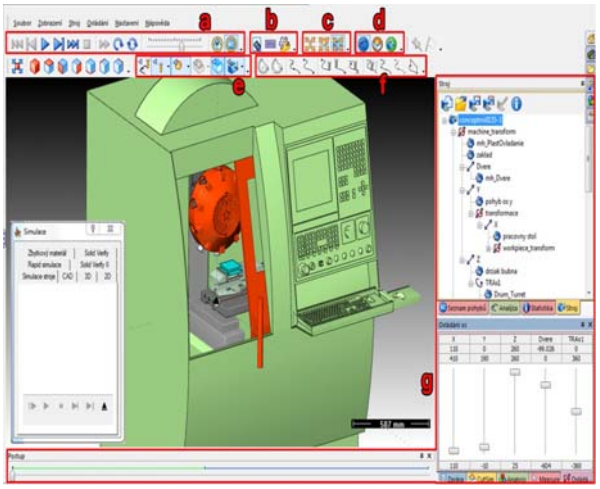

Fig. 7. Simulation environment with highlighted control toolbars [9]

Activation of the kinematics simulation is carried out by the selection of the *Machine simulation* command. A necessary precondition for this is a prepared NC program. The system indicates the identified collision by changing the colour of the appropriate elements and stopping the simulation. The Fig. 8 shows a collision state between a tool and the clamping device – both elements highlighted. The respective line in the NC program, the code of which is

displayed on the right side of the screen, is also highlighted.

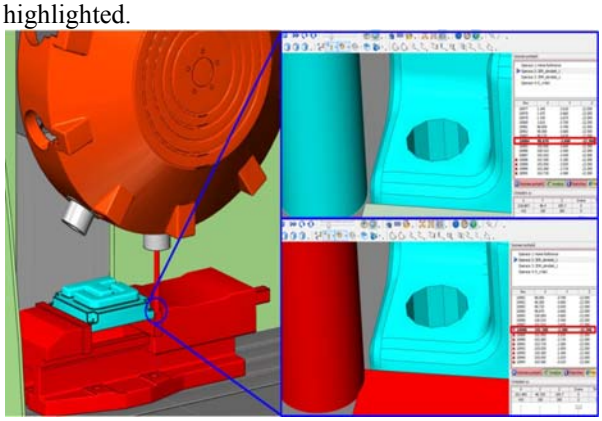

Fig. 8. Collision between tool and the clamping device [9]

3. CONCLUSION

The created digital model of milling laboratory and the activities tested within the concept of Digital Manufacturing up to now enable to obtain practical experience and knowledge in the application of that concept. Simulation and evaluation of the human movement ergonomics at the work site enable to optimize the entire workplace layout and arrangement of its elements in order to avoid the worker's overload. The aim of the described simulation of the CNC machine kinematics was to find the collisions that may occur during the machine operation [10]. When defining the potential collision situations, the knowledge and experience from present operation of the modelled machine were used. This simulation does not replace other simulations necessary for creating and debugging of the NC program, but it is a useful enhancement contributing to the trouble free production.

Simulations are one of the effective and economical ways of improving the production quality and reducing the costs. The application is of a wide range – from optimizing the manufacturing process itself through the analysis of the impact of changes on the manufacturing process, up to the virtual testing of the new kinematics principles and construction elements of the proposed machines.

ACKNOWLEDGEMENTS: This contribution is the result of the project implementation: Center for research of control of technical, environmental and human risks for permanent development of production and products in mechanical engineering (ITMS: 26220120060) supported by the Research & Development Operational Programme funded by the ERDF and project VEGA 1/0500/12 „Research on Quality Improvement when Milling Formed Surfaces by Advanced Coated Tools".

4. REFERENCES

[1] Cvetkovič, S.: *Modeliranje i upravljanje logističkim sistemom.* In. "VIII međunarodna naučno-stručna konferencija MMA 2003. Novi Sad, 2003. ISBN 86-85211-96-4

[2] Daneshjo, N., Olejník, F., Korba, P., Iľaščíková, L.: *CAx systémy v leteckom priemysle*. Košice : TU, 2011, 253 p. ISBN 978-80-553-0692-6

[3] Spišák, E., Fabian, M.: *Strojárske technológie s CAx podporou.* 1. vyd. Košice : Elfa, 2010, 379 p. ISBN 978-80-8086-136-0

[4] Rudy, V., Kováč, J.: *Innovation methods of model design of structures of production systems*. In: Oraldyn, fylym žaršycy. Vol. 15, no. 7, 2008, pp. 47-51. ISSN 1561-6908

[5] Gonda, J.: *Modely strojov a simulácia ich kinematiky v CAM systémoch.* Diplomová práca, SjF TU v Košiciach, 2012

[6] Šutľák, P.: *Navrhovanie výrobných pracovísk v Catii*. Diplomová práca, SjF TU v Košiciach, 2012

[7] Molnár, V., Fedorko, G.*: Catia - základy projektovania 2*. Košice - FBERG TU v Košiciach, 2007, 106 p. ISBN 978-80-8073-804-4

[8] Monková, K., Monka, P.: *Tvorba konštrukčného uzla s počítačovou podporou. 1*. Vyd. Prešov : Apeiron, 2012, 91 p. ISBN 978-80-89347-13-1

[9] Soták, V., Kuník, M., Soták, R.: *Theora and practice in the area of teaching and deployment of CAD/CAM systems.* In: Journal of Technology and Information Education. Vol. 3, num. 1, 2011, pp. 49-54. ISSN 1803-537X

[10] Pokorný, P., Peterka, J., Václav, Š.: *The task of 5-axis milling.* - ITMS 26220120013. - registrovaný: Web of Science, Master Journal List, Scopus. In: Tehnički Vjesnik - Technical Gazette. - ISSN 1330-3651. - Vol. 19, No. 1 (2012), s. 147-150

Authors: Ing. Katarína Senderská, PhD., Ing. Peter Ižol, PhD. , Ing. Albert Mareš, PhD. Technical University of Košice, Faculty of Mechanical Engineering, Department of Technologies and Materials, Masiarska 74, 04001 Košice, Slovakia.
E-mail: katarina.senderska@tuke.sk
peter.izol@tuke.sk
albert.mares@tuke.sk

Journal of Production Engineering
Vol.16 No.2

Preliminary Note

Šebo, J., Fedorčáková, M.

ECONOMIC OPTIMIZATION OF RECYCLING ORIENTED DISASSEMBLY OF CONSUMER ELECTRONICS: THE CASE STUDY OF MOBILE PHONE

Received: 15 September 2012 / Accepted: 21 January 2013

Abstract: *The planning of disassembly of consumer products is a complex process. Different aspects as product design, secondary material prices, possibilities of disassemble automation, labor costs and others play a role in selection of optimal disassembly strategy and sequence. In our article we present the case study of mobile phone disassembly sequence optimization based on hierarchical end-of-life decision model. By application of the model we identify which connection to dismantle and which leave intact, and which strategy of two (recycling or disposal) to apply for each component of mobile phone, to be economically optimal.*
Key words: *Disassembly, recycling, mobile phone, optimization.*

Ekonomska optimizacija demontaže pri reciklaži potrošačke elektronke: slučaj mobilni telefon. *Planiranje demontaže potrošačkih proizvoda je složen proces. Različiti aspekti kao što su dizajn proizvoda, cene sekundarnih sirovina, mogućnosti automatizacije demontaže, troškovi rada itd., imaju ulogu pri izboru optimalne strategije demontaže. U ovam radu je predstavljen je model optimizacije redosleda demontaže mobilnog telefona na bazi hijerarhije životnog veka. Primenom modela je identifikovano koja od dve strategije (reciklaža ili odlaganje) može da se primeni za svaku komponentu mobilnog telefona, a da je ekonomski optimalno.*
***Ključne* reči:** *Demontaža, reciklaža, mobilni telefon, optimizacija.*

1. INTRODUCTION

Currently a number of environmental aspects influence the decisions in manufacturing industry. The concepts like Environmentally Conscious Manufacturing, Closed Loop Supply Chain and others have developed to cope with these aspects. Disassembly has an important role in these concepts. The determination of optimal disassembly sequence and end-of-life (EOL) options for product and its individual components are well-known problems in respective literature.

2. METHODOLOGY

Lee [1] define EOL option decision problem as to choose the EOL option that maximizes profit. Based on the hierarchical representation of the product, the optimal EOL option for each level is determined in his model. He finds the optimal EOL option by integrating two steps: maximize the economic value of EOL component options and minimize the disassembly cost, i.e. maximizes {Profit - Disassembly Cost}. In the model, because of remanufacturing strategy perspective, it is assumed that either the Remanufacturing (r) or Disposal (n) option should be selected for each subassembly or component. He uses following determination of the profits for each option [Gonzales and Adenso-Diaz (2005) in 1]:

Remanufacturing Profit $P_{r,i} = R_{r,i} - C_{r,i}$

$R_{r,i}$: the revenue obtained when the remanufacturing option is applied

$C_{r,i}$: the cost incurred when the remanufacturing option is applied

Disposal Profit $P_{n,i} = R_{n,i} - C_{n,i}$

$R_{n,i}$: the revenue obtained when the disposal option is applied

$C_{n,i}$: the cost incurred when the disposal option is applied.

For n components in the same layer, the EOL option decision model is formulated by integer programming, as shown in Equation (1) [1]:

$$z(x,y) = \sum_{i=1}^{n}\{P_{n,i}(1-x_i) + P_{r,i}x_i\} - \sum_{i=1}^{n}\sum_{j=i+1}^{n} y_{ij}d_{ij}a \quad (1)$$

subject to $2y_{ij} \geq x_i + x_j$ for all i = 1,2,...,n and j = 1,2,...,n

x_i = 1, if component i is remanufactured
0, if component i is disposed

y_{ij} = 1, if components i and j are disconnected
0, otherwise

d_{ij}= cost incurred if components i and j are disconnected.

The bottom-up approach is used to determine the EOL options for the entire product [1].

In the article we apply above described model to optimize disassembly of mobile phone (MP) Nokia 7250i. Unlike the original model, we do not consider remanufacturing but we think about recycling as a second alternative to disposal. When applying the model we start with composition of Bill of Material (BOM) and Connection diagram. Then, based on real

data and calculations we arrange a table of profits/losses for the individual components and sub-assemblies for both alternatives. Based on the measured disassembly times and unit disassembly costs we compute disassembly costs for each connection identified by a connection diagram. Then we use formula (1) for finding the optimal EOL option. By using the formula we calculate the profits for all evaluated sub-assemblies (for each sub-assembly all EOL option combinations of individual components). Based on the calculation and diagrams we make the final table with economically optimal (maximum profit, respectively minimum loss) options for the treatment of individual components and sub-assemblies. Also, we identify the most appropriate disassembly sequence (i.e., which connections to maintain and which to disconnect).

2. MODEL CALCULATION

2.1 Graphical representation of the MP Nokia 7250i

As a basis for below calculations and final identification of the optimal EOL option and disassembly sequence we first draw a BOM (Fig. 1) and connection diagram (Fig. 2).

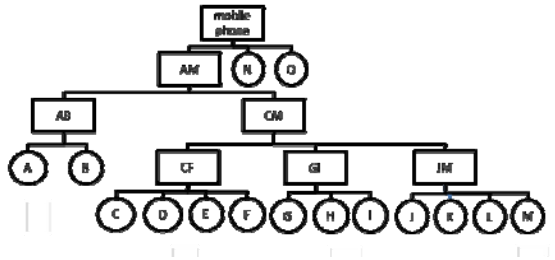

Fig. 1. BOM of MP Nokia 7250i

2.2 Profits/losses from the disassembly of individual components and subassemblies of MP Nokia 7250 for recycling and disposal option

Summary of profits/losses (and the revenues and costs) for individual components for recycling and disposal options are listed in Table 1. Below is a detailed description of the calculation of the revenues and costs based on actual data, such as purchase prices of secondary materials, weight and material composition of components and subassemblies of examined mobile phone, transport costs etc. Due to the need to include distance in the calculation we assume that the hypothetical disassembly operation is located in the Technical University campus.

Determination of revenues and costs for the individual components for recycling alternative

Revenues in this alternative is the sale of discarded parts (or materials) as a secondary raw material. In calculating the revenues of individual components we use material composition and weight of each component [2] and the actual purchase prices for 1 kg of secondary raw materials [3,4].

As the costs for recycling alternative we consider transportation costs to buyer of secondary materials (in our considered case is 2 km from hypothetical disassembly operation) in the mass-transport container. The costs are 0.0003186 €/kg (or 0.00003186 eurocents /g) [5]. It is a very low number so these costs we consider to be zero. We assume also that the costs of recycling of batteries are covered by the recycling fee (Recycling fee for 1 kg of batteries marketed in Slovak Republic is equal to 1.49 €/kg (see e.g.[6])), so in our calculation we consider also them to be zero.

Determination of revenues and costs for the individual components for disposal alternative

In the disposal alternative of the disassembled components are revenues equal to zero, as the companies that dispose of waste collect a great variety of secondary raw materials free of charge. In our considered case the waste company Kosit (Kosice) take without charge these secondary raw materials: paper and cardboard, glass, plastics, metals, bulky waste (washing machines, refrigerators, sinks, cabinets, ...), green waste, textiles, electronic waste (TV, monitor ...), tires, a small building waste (to 1 m3), waste oils, paints and thinners.

Regarding costs for this alternative, we consider again only transport costs (calculated above), which are very low and therefore we consider them equal to zero.

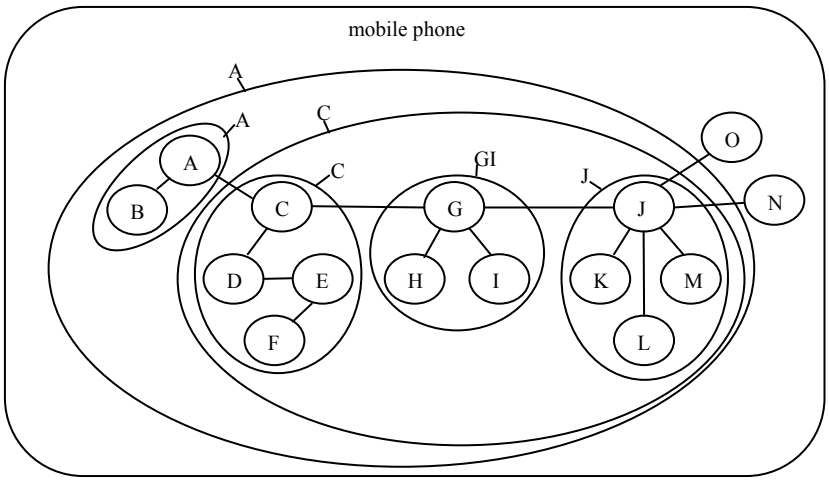

Fig. 2. Connection diagram of MP Nokia 7250i

Component/sub-assembly	Label	R r,i	C r,i	P r,i = R r,i - C r,i	R n,i	C n,i	P n,i= R n,i - C n,i
Frame of LCD	C	0,02508	0	0,02508	0	0	0
Display cover	E	0,03876	0	0,03876	0	0	0
Contact area of keyboard	D	2,77704	0	2,77704	0	0	0
Display	F	0	0	0	0	0	0
Keyboard	B	0	0	0	0	0	0
Front cover	A	0	0	0	0	0	0
Camera cover	I	0,0057	0	0,0057	0	0	0
Camera module	H	0,1218	0	0,1218	0	0	0
Mother board	G	16,3212	0	16,3212	0	0	0
Back cover	N	0	0	0	0	0	0
Internal plastic cover	J	0	0	0	0	0	0
GSM signal module	K	0	0	0	0	0	0
Power connector	L	0	0	0	0	0	0
Vibration engine	M	0,00931	0	0,00931	0	0	0
Battery	O	0	0	0	0	0	0
Sub-assembly	CF				0	0	0
	GI				0	0	0
	JM				0	0	0
	CM				0	0	0
	AB				0	0	0
	AM				0	0	0
Product	Mobile p.				0		

Table 1. Profits/losses from the disassembly of individual components and subassemblies of MP Nokia 7250 for recycling and disposal options

2.3 The cost of disassembly of the connections between components of MP Nokia 7250i

When calculating the cost of disassembly of each connection we assume, that the studied MP is manually disassembled with the normal tools (e.g. screwdriver). For manual disassembly is the dominant cost - total cost of labor. Other costs are negligible, hence in our calculations equal to zero. Total cost of labor we calculate from the average wage of employees in industry in Slovak republic in 2011 [7] and is equal to 1114,048 €. If the annual working time fund equals to 2000 hours (i.e. 7.2 million seconds), the resulting total labor cost of a working second is equal (rounded) to 0.1857eurocents/second. The final costs of the disassembly of connections, identified by a connection diagram, are shown in Table 2.

2.3 Disassembly optimization of MP Nokia 7250i

Based on the formula (1) we compute gradually profits/losses for each sub-assemblies and combinations of EOL alternatives (recycling or disposal) of parts of these sub-assemblies. For example for sub-assembly CF with 4 parts C, D, E, F we have created 16 combinations (Table 3).

Connections	Disassembly time (sec)	Disassembly costs (eurocent)
JN	5	0,9285
JO	2	0,3714
AC	10	1,857
GJ	51	9,4707
CG	7	1,2999
CE	11	2,0427
EF	4	0,7428
CD	19	3,5283
AB	4	0,7428
GH	4	0,7428
GI	6	1,1142
JK	4	0,7428
JL	4	0,7428
JM	6	1,1142

Table 2. The cost of disassembly of the connections between components of MP Nokia 7250i [own measurements and calculations on the base of 8 and 2]

Combination example: component C is disposed, component D is recycled, components E is recycled and component F is disposed - notation CnDrErFn. (Note: for each component A, B, C .... O in subsequent calculations index n represents a disposal alternative and index r recycling alternative.) For each combination we calculate profit/loss and we identify the optimal combination for a given sub-assembly, which is that with highest profit (or lowest loss). Thus, for example in the case of sub-assembly CF is the most advantageous combination (the one that brings the highest profit from particular EOL options for individual components) CnDnEnFn (Table 3) so it means disposal of all four components respectively all subassembly CF.

The individual sub-assemblies were identified based on a hierarchical representation of the MP (Fig. 3). The hierarchical representation we draw based on information in above BOM (Fig. 1) and connection diagram (Fig. 2). The calculation of individual sub-assemblies proceeds bottom-up in the hierarchical representation of the MP. Most profitable combinations for individual sub-assemblies are presented in Table 4. Table 5 represents the transformation of the previous calculations summarized in Table 4 to the optimal (profit maximizing) EOL alternatives (recycling or disposal) for individual components and sub-assemblies of MP. Note: In the case of indifference of alternatives we state „Dispose/Recycle“.

Based on calculations in previous tables and connection diagram we determine the optimal disassembly sequence (Table 6), so we define which connections to disconnect and which to maintain.

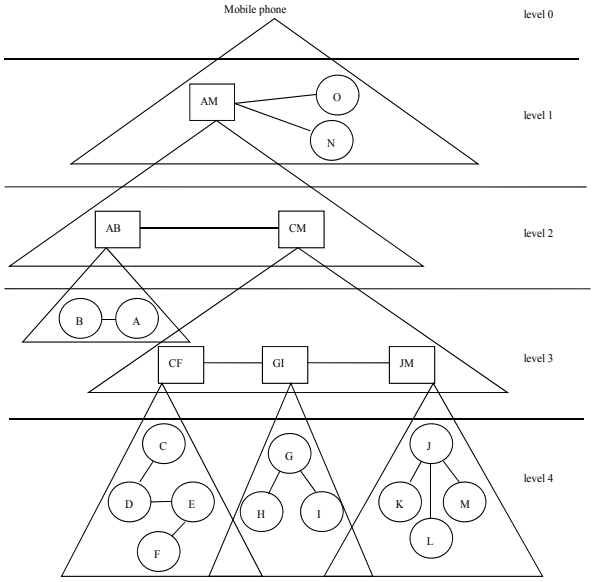

Fig. 3. The hierarchical representation of the MP Nokia 7250i

profit(	CrDrErFr	)=(	0,02508	+	2,77704	+	0,03876	+	0	)-(	3,5283	+	2,0427	+	0	+	0	+	0	+	0,7428	)=	-3,47292
profit(	CrDrErFn	)=(	0,02508	+	2,77704	+	0,03876	+	0	)-(	3,5283	+	2,0427	+	0	+	0	+	0	+	0,7428	)=	-3,47292
profit(	CrDrEnFr	)=(	0,02508	+	2,77704	+	0	+	0	)-(	3,5283	+	2,0427	+	0	+	0	+	0	+	0,7428	)=	-3,51168
profit(	CrDrEnFn	)=(	0,02508	+	2,77704	+	0	+	0	)-(	3,5283	+	2,0427	+	0	+	0	+	0	+	0	)=	-2,76888
profit(	CrDnErFr	)=(	0,02508	+	0	+	0,03876	+	0	)-(	3,5283	+	2,0427	+	0	+	0	+	0	+	0,7428	)=	-6,24996
profit(	CrDnErFn	)=(	0,02508	+	0	+	0,03876	+	0	)-(	3,5283	+	2,0427	+	0	+	0	+	0	+	0,7428	)=	-6,24996
profit(	CrDnEnFr	)=(	0,02508	+	0	+	0	+	0	)-(	3,5283	+	2,0427	+	0	+	0	+	0	+	0,7428	)=	-6,28872
profit(	CrDnEnFn	)=(	0,02508	+	0	+	0	+	0	)-(	3,5283	+	2,0427	+	0	+	0	+	0	+	0	)=	-5,54592
profit(	CnDrErFr	)=(	0	+	2,77704	+	0,03876	+	0	)-(	3,5283	+	2,0427	+	0	+	0	+	0	+	0,7428	)=	-3,498
profit(	CnDrErFn	)=(	0	+	2,77704	+	0,03876	+	0	)-(	3,5283	+	2,0427	+	0	+	0	+	0	+	0,7428	)=	-3,498
profit(	CnDrEnFr	)=(	0	+	2,77704	+	0	+	0	)-(	3,5283	+	0	+	0	+	0	+	0	+	0,7428	)=	-1,49406
profit(	CnDrEnFn	)=(	0	+	2,77704	+	0	+	0	)-(	3,5283	+	0	+	0	+	0	+	0	+	0	)=	-0,75126
profit(	CnDnErFr	)=(	0	+	0	+	0,03876	+	0	)-(	0	+	2,0427	+	0	+	0	+	0	+	0,7428	)=	-2,74674
profit(	CnDnErFn	)=(	0	+	0	+	0,03876	+	0	)-(	0	+	2,0427	+	0	+	0	+	0	+	0,7428	)=	-2,74674
profit(	CnDnEnFr	)=(	0	+	0	+	0	+	0	)-(	0	+	0	+	0	+	0	+	0	+	0,7428	)=	-0,7428
profit(	CnDnEnFn	)=(	0	+	0	+	0	+	0	)-(	0	+	0	+	0	+	0	+	0	+	0	)=	0

Table 3. Profit (+)/loss (-) for various combinations of EOL options (recycling and disposal) of individual components that make up sub-assembly CF

profit(	CnDnEnFn	)=(	0	+	0	+	0	+	0	)-(	0	+	0	+	0	+	0	+	0	+	0	)=	0
profit(	JnKnLnMn	)=(	0	+	0	+	0	+	0	)-(	0	+	0	+	0	+	0	+	0	+	0	)=	0
profit(	GrHrIr	)=(	16,3212	+	0,1218	+	0,0057			)-(	0,7428	+	1,1142	+	0							)=	14,5917
profit(	CFrGIrJMr	)=(	0	+	14,5917	+	0			)-(	1,2999	+	0	+	9,4707							)=	3,8211
profit(	AnBn	)=(	0	+	0					)-(	0											)=	0
profit(	ABrCMr	)=(	0	+	3,8211					)-(	1,857											)=	1,9641
profit(	AMrNrOr	)=(	1,9641	+	0	+	0	+		)-(	0,9285	+	0,3714	+	0							)=	0,6642

Table 4. Most profitable (or least loss) combinations for all subassemblies

Component/sub-assembly	Label	Optimal alternative
Frame of LCD	C	Dispose
Display cover	E	Dispose
Contact area of keyboard	D	Dispose
Display	F	Dispose
Keyboard	B	Dispose
Front cover	A	Dispose
Camera cover	I	Recycle
Camera module	H	Recycle
Mother board	G	Recycle
Back cover	N	Dispose/Recycle
Internal plastic cover	J	Dispose
GSM signal module	K	Dispose
Power connector	L	Dispose
Vibration engine	M	Dispose
Battery	O	Dispose/Recycle
Sub-assembly	CF	Dispose/Recycle
	GI	Recycle
	JM	Dispose/Recycle
	CM	Recycle
	AB	Dispose/Recycle
	AM	Recycle
Product	Mobile phone	Recycle

Table 5. Optimal EOL alternatives (recycling or disposal) for individual components and sub-assemblies of MP Nokia 7250i [8]

Connection	Disassembly operation
JN	disconnect
JO	disconnect
AC	disconnect
GJ	disconnect
CG	disconnect
CE	maintain
EF	maintain
CD	maintain
AB	maintain
GH	disconnect
GI	disconnect
JK	maintain
JL	maintain
JM	maintain

Table 5. Optimal disassembly sequence of MP Nokia 7250i

3. CONCLUSION

On the base of the application the model on the mobile phone case, we can conclude that this model is relatively easy calculable for this complexity level products. The output of the model in a form of EOL option and disassembly sequence seems to be reasonable and consistent with generally known and practiced sequences in the case of mobile phones, it means to dispose almost all parts of mobile phone excluding printed circuit board which is suitable for recycling. In the case of battery which is suitable for special recycling/disposal, the model gives indifferent result „Dispose/Recycle“. In real case this would not be a complication because EOL option for battery is usually set by environmental legislation.

4. ACKNOWLEDGEMENT

This contribution has been supported by research grant VEGA 1/1320/12 (Inovačné koncepcie agilných podnikových systémov dynamicky reagujúcich na trhové podmienky).

5. REFERENCES

[1] Lee H.B., Cho N.W., Hong Y.S.: A hierarchical end-of-life decision model for determining the economic levels of remanufacturing and disassembly under environmental regulations, Journal of Cleaner production, 18 (2010), p.1276-1283.
[2] K. Dóry: Technicko-ekonomické hodnotenie demontáže mobilných telefónov, diploma work, Technical university of Košice, 2012.
[3] Plzeňský skart a.s (online). Plzeň : 2012 [cit. 2012-04-14] http://www.plzenskyskart.cz/vykupni-cenik-maloobchodni#kategorieCeniku_397.
[4] P+K s.r.o. (online), http://www.p-k.sk/?content=sluzby&subcontent=vykup-zelezneho-srotu-a-farebnych-kovov.
[5] Kosit a.s. Košice, cenník služieb.
[6] SLOWMAS, http://www.slovmas.sk/pdf/cennik_2012.pdf)
[7] Statistical Office of Slovak Republic, www.statistics.sk.
[8] How to replace mobile phone LCD. Demonstration of how to replace mobile phone LCDs for Nokia 6110, 6110i, 7250, 7250i (online) www.youtube.com.

Authors: **Ing. Juraj Šebo, PhD., Ing. Monika Fedorčáková, PhD.**, Technical University of Košice, Faculty of Mechanical Engineering, Department of Industrial Engineering and Management, Nemcovej 32, 04200 Košice, Slovak Republic, Phone.: +421 55 6023241
E-mail: juraj.sebo@tuke.sk

Journal of Production Engineering
Vol.16 No.2

Preliminary Note

Fedorčáková, M., Šebo, J.

THE RESULTS OF APPLICATION OF WASTEWATER BY NEW DEVELOPING ELECTROLYTIC FLOTATION METHODS

Received: 9 October 2012 / Accepted: 15 November 2012

Abstract: *Cyanobacteria are during the summer months in stagnant water fundamental threat to water workers, vacationers who use the polluted waters and fishermen. High production of cyanobacteria adversely affects water quality and threatening aquatic animals and plants living in the affected area. We are constantly looking for and improve the methods, techniques and hydrological interventions to limit this phenomenon. Post points to the utility and availability of new developing electrolytic flotation wastewater methods for a particular case study carried out in selected Slovak site.*

Key words: *Electro flotation, Cyanobacteria, Stagnant Water.*

Rezultati primene i razvoj elektrolitičkih flotacionih metoda na otpadne vode. *Cijanobakterije tokom letnjih meseci u stajaćoj vodi predstavljaju osnovnu pretnju po radnike, turiste, ribare koji koriste zagađene vode. Visoka produkcija cijanobakterije negativno utiče na kvalitet vode i preti životinjama i biljkama koje su nastanjeni u zagađenoj oblasti. Konstantna je potraga za poboljšanje metoda, tehnika i hidroloških intervencija da bi se ograničo ovaj fenomen. Korisnost i dostupnost novih elektrolitičkih flotacionih metoda na otpadne vode za određenu studiju slučaja su sprovedena Slovačkoj.*

Ključne reči: *Elektroflotacija, cijanobakterija, stajaća voda.*

1. INTRODUCTION

The occurrence of cyanobacteria in excessive standing water is a global problem. As a result of proliferation of cyanobacteria is the process of eutrophication, which causes excessive nutrient enrichment of water [1]. Overgrowths of cyanobacteria create a water bloom. Ability of the water is blue-green algae bloom in the chemical and physical properties of water and release dangerous toxins. These toxic substances are hazardous to human health as well as for individual dwelling organisms in the environment. Water prevents flower water, fish culture, leisure and continuing use of stagnant water.

2. DISPOSAL METHOD OF CYANOBACTERIA

Nowadays are available many methods for the disposal of cyanobacteria. Methods and techniques of disposal and removal of water by the Flower [2] based on mechanical, chemical, biological and electrolytic principle. Mechanical equipment used to remove sediments show low efficiency and their application is expensive [3]. The chemical disposal is undesirable amount of chemical concentrations of disadvantage, as this may cause a negative impact on other organisms and its use also by [4] only a limited amount of cyanobacteria. The shortcomings of these methods eliminates the electrolytic method of disarming, whose principle is electro flotation.

3. APPLICATION METHOD ELECTRO FLOTATION WATER DISPOSAL

The disposal of cyanobacteria in 14 pooled samples of water from the study sites were used electro flotation method. The principle of physical-chemical process is the separation of suspended solids in the sample, the observed surface water or directly in standing water and subsequent mechanical removal, more in [5].

Description of the monitored location

Analysis was carried out and microscopic evaluation of water samples containing water blooms of Slovak Kačato Lake, located on the outskirts of Roznava. Surrounded by a wooded area of deciduous trees. The right side consists of marshy shore. There is an agricultural area, the area under oilseed rape, on the left side.

Due to the use of chemical sprays and artificial fertilizers, water quality can be affected by increased nitrogen content. The size of the water body is 0.3 hectares and a depth of 4 m. Spring is springing near the pond inlet to the water body. Outflow from the pond flows into the left-hand tributary of Slana River, the river Čremošná. Fauna consists mainly carp, frogs, as well as wild ducks. The pond is used as a fishing ground Rožňava district [6,7].

4. PROCESS ELECTRO FLOTATION

To realize the experiment based on electro flotation method to obtain samples of the above locations. The sample is poured into a 6 l glass jar. The containers were placed electrodes necessary for the conduct of electro flotation 10 x 10 cm with a distance of 10 mm. The electrodes were connected to the battery Progress 20, the voltage was set at 24 V, the effective charging

current was on average 10 to 15 A. Contaminated water was placed between the electrodes.

The effect of current implied a dissolving anode, which is formed due to coagulation agent, which gradually was mixed with contaminated water. Electro flotation was carried out within a period of 15 minutes. During the measurements to monitor the emergence of floating bubbles generated on the surface of samples and subsequent deposition on the surface fleet.

Accumulated fleet from surface samples collected mechanically. After realization of electro flotation sample was taken and the water just after the application of electrolysis is also sampled fleet. Water without fleets showed the clarity with pinkish tinge.

Fig.1. Illustrate process electro flotation

Battery	description
Manufacturer	HELVI
Model	Progress 20
Voltage	230 V 50/60 Hz
Battery voltage	12 – 24 V
Dimensions	280x285x470 mm
Mass	12,2 kg

Table 1. Description of battery Progress 20

5. MICROSCOPIC ANALYSIS AND EVALUATION

The samples were subjected to microscopic analysis in the laboratory at the Technical University in Kosice, Department of Environmental Science. Microscopic analysis also looked at the content of suspended solids during the whole measurement.

The analysis showed a positive effect electro flotation. After the withdrawal of mechanical sedimentary fleet was seen near the water clear, pinkish color. This phenomenon was caused due to rusty electrodes. However, no threat to water quality after flotation. Water Fig. 2 showed the occurrence of cyanobacteria, which created the fleet, and despite the effect of electro flotation method of micro life has survived without signs of damage.

The method of electro flotation is constantly under development. It looks different proportions and design of electrolytic devices for the most efficient elimination of cyanobacteria, which while not harming other organisms.

The main advantages of using electro flotation methods include respect for the environment, harmless to other organisms, simplicity, and ease of access through the solution.

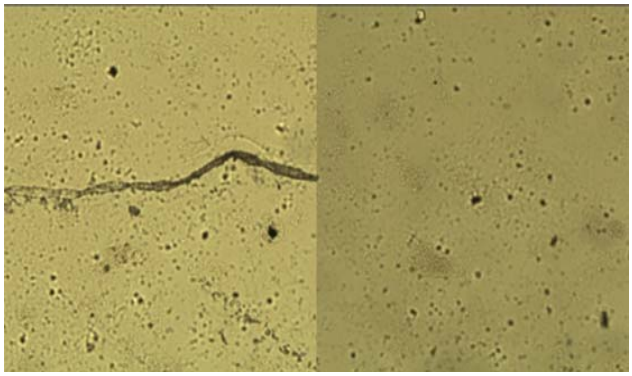

Fig. 2. Images of water samples by electro flotation, observed under the microscope

The disadvantage is power consumption as needed for electrolysis, but this eliminates the use of solar cells. At this point it is not possible to comment on the life of the electrolytic device located on the surface of stagnant water, there are only estimates and carry out the experiments. Within the project "Implementation and modification of technology to reduce the occurrence of cyanobacteria in Stagnant Waters" ITMS: 26220220028, supported by the Research & Development Operational Programe funded by the ERDF, to verify the long-term operation of the plant on a large standing water [8, 9].

6. SUMMARY

The problem of eutrophication is complex and specific conditions for individual lakes. Disposal of water blooms is one way to prevent damage to the environment and human health. The best available method of disposal of water flowers shows today use electro flotation wastewater in the presence of a combination of methods and other methods. The effect, which is achieved after only a few minutes of standing water in the sample taken from Lake Kačato was remarkable. Exposure to the electrodes on the sample water cyanobacteria were paralyzed and fleets in a thin layer on the surface. It can be said that electro flotation method is highly effective cleaning method of surface water by cyanobacteria, which requires the effective application of extensive polluted waters. The method of electro flotation is constantly under development.

7. ACKNOWLEDGEMENT

This contribution is the result of the project implementation: Implementation and modification of technology to reduce the occurrence of cyanobacteria in stagnant waters ITMS: 26220220028 supported by the Research & Development Operational Programme funded by the ERDF.

8. REFERENCES

[1] Nariadenie vlády SR č. 242/1993 Z. z., ktorým sa ustanovujú ukazovatele prípustného stupňa znečistenia vôd, (in Slovak).
[2] Komárek, J.: *Cyanoprokaryota*, Teil 1., Nachdruck, 1998, 548s., ISBN 978-3-8274-2111-1.
[3] Holoda, E., Pistl, J.: *Všeobecná mikrobiológia a genetika mikroorganizmov.* Praktické cvičenia, Katedra mikrobiológie a imunológie UVL, Košice, 2001, 161s., ISBN 978-80-889-8562-4, (in Slovak).
[4] Vysoká škola báňská – Technická univerzita Ostrava. *Ekologické aspekty*. Metódy obnovi eutrofizovaných nádrží. [online] [cit 2012-02-20]. Dostupné na internete:<http://hgf10.vsb.cz/546/Ekologicke%20aspekty/cviceni/cviceni_lenticky/obnovy_eutro_nadrzi.htm>, (in Czech).
[5] Fedorčáková, M., Šebo, J., Malega, P.*: Koncept implementácie technológie na znižovanie výskytu siníc,* 2010. In: Trendy a inovatívne prístupy v podnikových procesoch : 13: Košice, december 2010. - Košice : TU, SjF, 2010. - ISBN 978-80-553-0570-7, (in Slovak).
[6] Šebo, D., Fedorčáková, M.: *Vývoj technológie na znižovanie eutrofizácie stojatých vôd* , 2010.In: TOP 2010 : Technika ochrany prostredia : zborník prednášok : 15.-17. jún 2010, Častá - Papiernička. - Bratislava : STU, 2010 S. 365-368. - ISBN 978-80-970438-0-3, (in Slovak).
[7] Sinice – vodné cyanobaktérie. *Zneškodňovanie siníc.* [online] [cit 2012-01-11]. Dostupné na internete: <http://sinice.webnode.sk/zneskodnovanie-sinic/>, (in Slovak).
[8] Slovenská agentúra životného prostredia. Odborná organizácia Ministerstva životného prostredia SR. Metódy sanácie vôd ex situ. [online] [cit 2012-02-25]. Dostupné na internete: <http://charon.sazp.sk/Envirozataze/AtlasSanMetod/Jar/default.htm?turl=WordDocuments%2Fflotcia.htm>, (in Slovak).
[9] Centre for ecological sciences. Energy. Limnology. [online] [cit 2012-02-20]. Dostupné na internete: <http://ces.iisc.ernet.in/energy/monograph1/Limpage4.html>.

Authors: **Ing. Monika Fedorčáková**, **PhD.**, Technical University of Kosice, Faculty of Engineering, Park Komenského 5, 040 01 Kosice, monika.fedorcakova@tuke.sk,
Ing. Juraj Šebo, PhD., Technical University of Kosice, Faculty of Engineering, Park Komenského 5, 040 01 Kosice.

INSTRUCTIONS FOR CONTRIBUTORS

No. of pages:	4 DIN A4 pages
Margins:	left: 2,5 cm
	right: 2 cm
	top: 2 cm
	bottom: 2 cm
Font:	Times New Roman
Title:	Bold 12, capitals
Abstract:	Italic 10
Headings:	Bold 10, capitals
Subheadings:	Bold 10, small letters
Text:	Regular 10
Columns:	Equal column width with 0,7 cm spacing
Spacing:	Single line spacing
Formulae:	Centered and numerated from 1 in ascending order. Equations must be typed in Equation Editor, with following settings: Style>Math – Times New Roman Size>Full 12pt, Subscript/Superscript 7pt, Symbol 18 pt
Figures:	High quality, numerated from 1 in ascending order (e.g.: Fig.1, Fig. 2 etc.); Figures and tables can spread over both two columns, please avoid photographs and color prints
Tables:	Numerated from 1 in ascending order (e.g..: Tab. 1, Tab. 2, etc.)
References:	Numerated from [1] in ascending order; cited papers should be marked by the number from the reference list (e.g. [1], [2, 3] ...)
Submission:	**Papers prepared in MS Word format should be e-mailed to: pkovac@uns.ac.rs, savkovic@uns.ac.rs**
Notice:	**Papers are to be printed in Journal of Production Engineering** Sample paper with detailed instructions can be found at: **http://www.jpe.ftn.uns.ac.rs/**

FOR MORE INFORMATION, PLEASE CONTACT:

Prof. Pavel Kovač, PhD, MEng.
Borislav Savković, *MSc. Assistant*
FACULTY OF TECHNICAL SCIENCES
Department for Production Engineering
Trg Dositeja Obradovica 6
21000 Novi Sad
Serbia
Tel.: (+381 21) 485 23 24; 485 23 20 ; 450 366;
Fax: (+381 21) 454 495
E-mail: pkovac@uns.ac.rs, savkovic@uns.ac.rs
http://www.jpe.ftn.uns.ac.rs/